Bart Peerdeman

Development of an underactuated hand prosthesis with compliant control

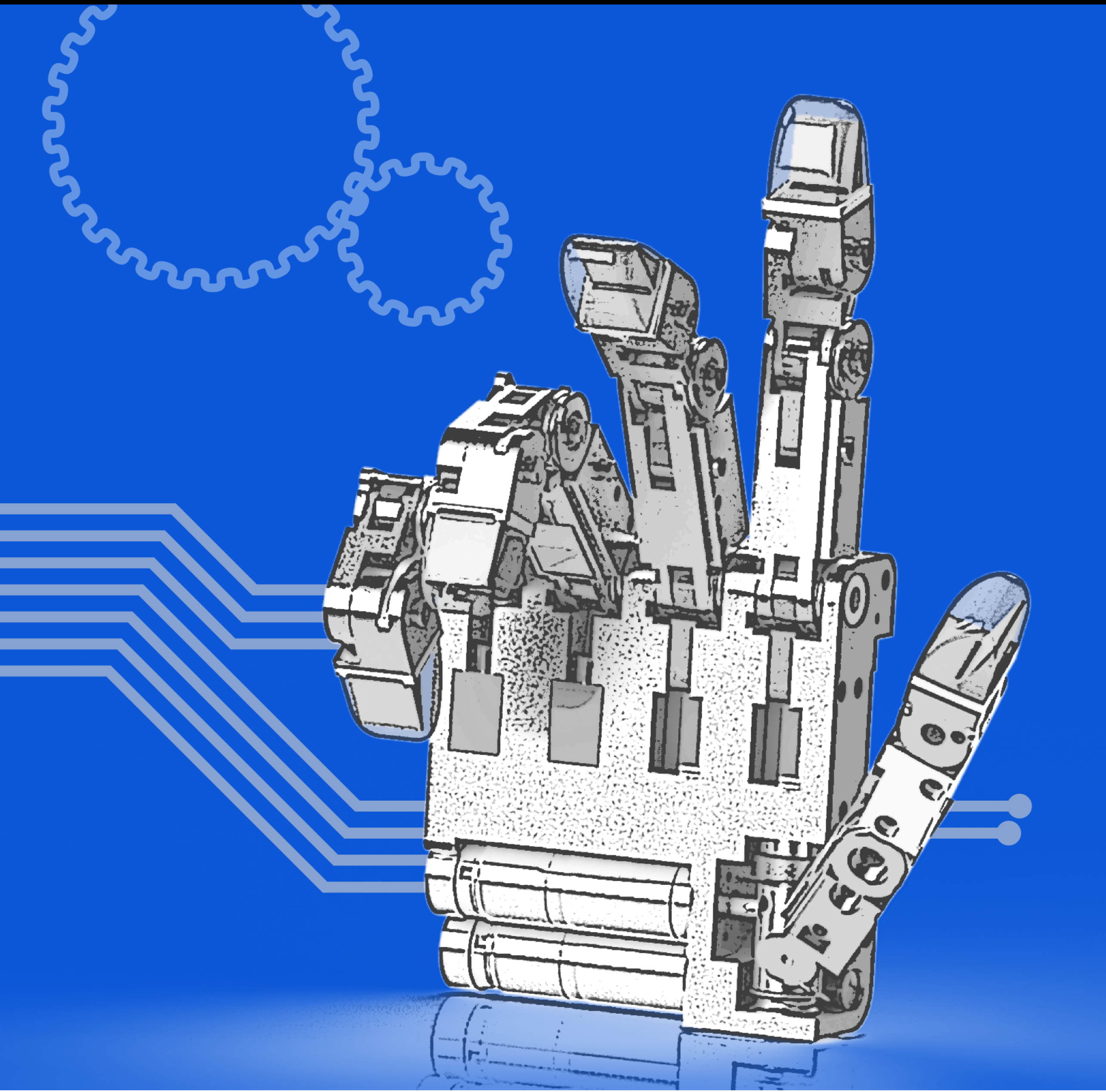

Development of an underactuated hand prosthesis with compliant control

Bart Peerdeman

Graduation committee

Chairman and secretary
Prof.dr. P.M.G. Apers — University of Twente, Enschede, The Netherlands

Promotor
Prof.dr.ir. S. Stramigioli — University of Twente, Enschede, The Netherlands

Assistant promotor
Dr. S. Misra — University of Twente, Enschede, The Netherlands

Members

Prof. dr. ir. H.F.J.M. Koopman	University of Twente, Enschede, The Netherlands
Prof. C. Melchiorri	University of Bologna, Bologna, Italy
Dr. ir. D.H. Plettenburg	Delft University of Technology, Delft, The Netherlands
Prof. dr. J.S. Rietman	University of Twente, Enschede, The Netherlands
	Roessingh Research and Development, Enschede, The Netherlands
Prof. dr. ir. P.H. Veltink	University of Twente, Enschede, The Netherlands

This research has been conducted at the Robotics and Mechatronics group of the University of Twente, within the Myopro project. The research was funded by the Dutch Ministry of Economic Affairs and the Province of Overijssel, within the Pieken in de Delta (PIDON) initiative.

Cover: Hjalmar Haagsman & Bart Peerdeman
Author: Bart Peerdeman
E-mail: b.peerdeman@gmx.com
ISBN: 978-90-9028264-0
Printed by Wöhrmann Print Service.

DEVELOPMENT OF AN UNDERACTUATED HAND PROSTHESIS WITH COMPLIANT CONTROL

PROEFSCHRIFT

ter verkrijging van
de graad van doctor aan de Universiteit Twente,
op gezag van de rector magnificus,
prof.dr. H. Brinksma,
volgens besluit van het College voor Promoties
in het openbaar te verdedigen
op donderdag 22 mei 2014 om 16:45 uur

door

Bart Peerdeman
geboren op 21 september 1984
te Venhuizen, Nederland

Dit proefschrift is goedgekeurd door:

Prof.dr.ir. S. Stramigioli, promotor
Dr. S. Misra, assistent-promotor

Summary

User abandonment of modern myoelectric hand prostheses is a significant problem, as around two thirds of the prostheses issued eventually go unused. A major factor in this is insufficient functionality and controllability; therefore, the goal of this research is to develop a mechanical design that is capable of a variety of relevant grasping motions, and a control system that provides the user with intuitive access to these motions.

The functionality of modern hand prostheses is mainly limited by the size and weight of their actuators. To address this, many hand prostheses feature underactuation: multiple joints connected to a single actuator. However, such systems reduce the individual controllability of the joints, and limit the number of motions the hand can perform. The ability to control these joints separately can be preserved by using miniature locking mechanisms which fit inside the fingers and palm. To keep these mechanisms as small as possible, their design must require minimal actuation force and still have a high resistance to torque. In this research, locking components have been developed that only require contact to be established to block all joint motion. The resulting mechanisms fit inside the individual phalanges of the fingers, providing increased controllability while adding negligible size and weight.

A combination of underactuation and joint locking has been implemented to control the fingers of a new anthropomorphic prosthesis prototype: the UT Hand I. With 15 degrees of freedom and only 3 main actuators, the UT Hand I allows the user to perform various grasps relevant to daily living. To provide the user and the control system with feedback during grasping, the hand contains position sensors in the finger joints; additionally, each fingertip contains a set of four force sensors coated in rubber.

The control of myoelectric hand prostheses is based on electrical impulses produced by the activation of the user's remaining forearm muscles. With these signals the user can indicate the desired motions of the hand, but they can be difficult to reliably start, stop, and maintain. The interface developed for the UT Hand I reduces the amount of activity required from the user by allowing the selection, opening and closing of a grasp to be done with a minimal number of signals.

The grasp itself is performed automatically by the hand's low-level control system; the user retains the ability to influence the speed and force of the grasp at any time. The development of the low-level controller focused on ensuring compliance in contact with the environment. Several versions were evaluated, both in

simulation and on various testbeds; the resulting controller directly monitors the energy applied by the motors, in order to maintain a stable grasp and ensure safe interaction with objects and people at all times.

The completed UT Hand I system demonstrates several innovative mechanical design and control techniques, which improve the functionality and controllability of modern myoelectric hand prostheses.

Samenvatting

Het afwijzen van moderne myoelektrische handprotheses door gebruikers is een significant probleem; meer dan twee derde van alle toegekende protheses wordt uiteindelijk niet meer gebruikt. Een belangrijk onderdeel hiervan is het tekort aan functionaliteit en controleerbaarheid. Het doel van dit onderzoek is daarom het ontwikkelen van een mechanisch ontwerp dat een aantal gevarieerde grijpbewegingen kan uitvoeren, en een controlesysteem dat de gebruiker voorziet van een intuitieve manier om deze bewegingen aan te sturen.

De functionaliteit van moderne handprotheses is hoofdzakelijk gelimiteerd door de omvang en het gewicht van hun actuatoren. Om dit te verhelpen gebruiken veel handprotheses het principe van onderactuatie: het verbinden van meerdere gewrichten aan een enkele actuator. Zulke systemen verminderen echter de individuele aanstuurbaarheid van de gewrichten, en limiteren het aantal bewegingen dat de hand uit kan voeren. De mogelijkheid om de gewrichten apart aan te sturen kan bewaard gebleven worden door miniature gewrichtsblokkeringen die verwerkt worden in de vingers en palm. Om deze mechanismes zo klein mogelijk te houden, moet hun ontwerp een zo laag mogelijke actuatiekracht vereisen en toch weerstand bieden tegen hoge gewrichtskrachten. In dit onderzoek zijn onderdelen ontwikkeld waartussen alleen contact nodig is om alle gewrichtsbeweging te blokkeren. Het hieruit voortkomende mechanisme past geheel in de vingerkootjes van de hand, en voorziet de hand van verbeterde controleerbaarheid zonder deze noemenswaardig groter of zwaarder te maken.

Een combinatie van onderactuatie en gewrichtsblokkeringen is gebruikt om de vingers van een nieuw handprothese-prototype, de UT Hand I, aan te sturen. De UT Hand I bevat 15 graden van vrijheid met slechts 3 actuatoren, en stelt de gebruiker in staat om verscheidene greepbewegingen uit te voeren die relevant zijn in het dagelijks leven. Om de gebruiker en het aansturingssysteem tijdens een greep van terugkoppeling te voorzien bevat de hand positiesensoren in de gewrichten van de vingers; elke vingertop bevat eveneens een set van vier in rubber gegoten krachtsensoren.

De aansturing van myoelektrische handprotheses is gebaseerd op elektrische impulsen die geproduceerd worden bij activatie van de onderarmspieren van de gebruiker. Met deze signalen kan de gebruiker de gewenste bewegingen van de hand aangeven, maar het kan moeilijk zijn om ze betrouwbaar te starten, stoppen, en aan te houden. De interface die ontwikkeld is voor de UT Hand I vermindert de hoeveelheid benodigde activiteit van de gebruiker door voor het selecteren, openen en sluiten van een greep zo weinig mogelijk signalen te vereisen.

De greep zelf wordt automatisch uitgevoerd door het controlesysteem van de hand; de gebruiker blijft altijd in staat om de snelheid en kracht van de greep te beïnvloeden. De ontwikkeling van dit controlesysteem is gefocust op meegaand contact met de omgeving. Verscheidene versies ervan zijn zowel in simulatie als op verschillende testplatformen geëvalueerd; de hieruit voorkomende controller beheert direct de energie die door de motoren toegevoerd wordt, zodat een stabiele greep behouden blijft en de veiligheid van interactie met objecten en mensen te allen tijde gewaarborgd wordt. Het voltooide UT Hand I systeem demonstreert een aantal innovatieve technieken voor mechanisch ontwerp en aansturing, welke de functionaliteit en regelbaarheid van moderne myoelektrische handprotheses verbeteren.

Contents

Chapter 1

Introduction

This section contains parts adapted from “Myoelectric forearm prostheses: State of the art from a user-centered perspective" [1].

1.1 Hand prostheses

Throughout history, the loss of functionality and wholeness associated with the lack of a hand or arm has caused people to devise artificial replacements. In early history, such prostheses were mostly solid cosmetic reproductions of the lost limb made out of wood, leather, and metal. More functional shapes such as hooks were also used.

During the Middle Ages more advanced prostheses were developed; these artificial hands were often designed by skilled armorers and watchmakers. Knights

Figure 1.1: An articulated hand prosthesis from the 16th century (Figure adapted from [2]).

who commissioned these hands would still go to battle with their new prosthesis, so they were fitted with ingenious articulation mechanisms capable of not only grasping shields and swords, but even precisely holding a quill. However, due to the state of medicine at the time, the mortality rate for amputations was still very high. Between the 16th and 19th century more advanced methods of anesthesia and amputation were discovered, but the mortality rate would remain high until the late 1800s.

Large wars such as the American Civil War and World War I led to a significant increase in amputees. During these wars, the number of amputees rose by the tens or hundreds of thousands, leading to government initiatives to promote the development of new prosthetics. Around 1915-1920, the first externally powered prostheses were developed [3]. These electric or pneumatic hands were controlled mechanically, as electronic prosthesis control was not developed until 1940-1950. In the 1960s, myoelectrically (ME) controlled hand prostheses were available commercially for the first time. These systems record, filter, and amplify the electric signals generated by the activation of the remaining muscles in the forearm. Electromyographic (EMG) sensing has been developed further until this day, and is currently the most common form of externally actuated hand prosthesis control.

Current commercially available hand prostheses can be divided into three main categories:

Passive prostheses cannot move or perform grasps, and are optimized for either appearance or functionality: cosmetic prostheses are made to resemble the human hand as closely as possible, and practical prostheses can mount a variety of tools for specific tasks. Users are generally unable to perform many activities of daily living with these prostheses alone.

Body-powered prostheses are mechanical systems that use the movement of another body part (typically the opposite shoulder) to operate the hand. While these hands often do not have more than one degree of freedom (DOF) and require some effort to use, the mechanical connection does provide the user with direct sensory feedback.

Externally powered prostheses have their own power supply, and can act autonomously. The most common variety of externally powered prosthesis is electrically powered, with a combination of batteries and direct current (DC) motors for actuation. However, since the actuation of an externally powered hand is no longer directly connected to the body, it also requires signals to be provided for control of the hand. One example of such a hand is the Otto

Bock MyoHand.

Otto Bock MyoHand

(Figure adapted from [4])
The Otto Bock MyoHand is one of the most common currently commercially available myoelectric hand prostheses. It has 1 DOF and is controlled by a pair of EMG electrodes.

In the last few decades, the structure of commercially available myoelectric prostheses has moved from a simple claw to more closely resembling the human hand. The combination of EMG sensing and DC motor actuation provides the user with a way of controlling the motions of such a multifunctional prosthesis. However, around two thirds of the people that are given a myoelectric prosthesis eventually stop using them [5], with users citing reasons such as non-intuitive control, lack of feedback and insufficient functionality.

1.2 Myopro

The Myopro project has been set up to address these shortcomings directly, by developing a myoelectrically controlled prosthesis that restores the signal flow to and from the user. Control signals are obtained through an EMG sensing system capable of detecting several activation patterns. These signals are used to adjust the behavior of the hand's control system, which also measures relevant information and sends it back to the user via a tactile feedback system. Figure 1.2 shows the signal flow through the able hand, as well as how the combination of the aforementioned systems works to restore it. Three research groups have been working on these systems as part of the Myopro project:

Roessingh Research and Development has been involved in developing the improved EMG sensing system, to be able to isolate a larger number of control signals than current commercially available systems.

The Biomedical Signals and Systems group of the University of Twente

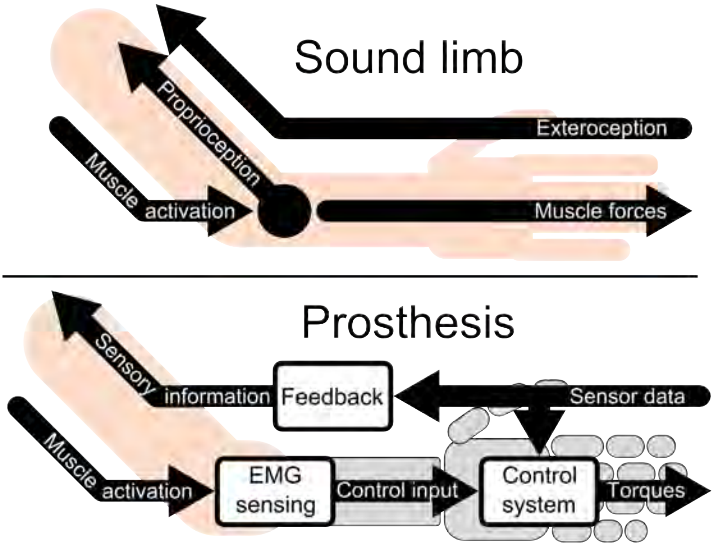

Figure 1.2: The signal flow in the human forearm, and the structure of a myoelectric prosthesis system to restore this signal flow to the user.

has been working on a new tactile feedback system capable of supplying the user with both force and position information.

The Robotics and Mechatronics group of the University of Twente has been responsible for developing the mechanical design of the new prosthesis system, as well as its control system; the culmination of this work is the subject of this thesis.

Additionally, several companies have taken part in the Myopro project. TMSi, Re-lion and IMS have supported the development of the EMG detection system, created a virtual training environment, and overseen systems integration, respectively.

Developing a new myoelectric prosthesis that can address the current systems' lack of usability calls for a set of requirements to be determined. These requirements should be based on the needs of the users, combined with the knowledge of clinicians and engineers.

1.3 Requirements

To determine the requirements for a modern ME hand prosthesis, a workshop was organized. In this workshop the properties of the ideal forearm prosthesis with regard to its subsystems (see Figure 1.2) and mechanical design were discussed. Combining information from literature [5, 6, 7] and the results of the workshop, functional requirements for ME forearm prostheses were derived.

To develop a user-accepted ME forearm prosthesis, both users and technicians should be involved in the design process [8]. However, directly involving users in the design process may be difficult, due to differences in terminology and methodology [9]. In this case, user representatives (i.e. clinicians with first-hand experience) can provide a useful alternative. As someone who has regular contact with many forearm prosthesis users, a user representative has a high familiarity with the opinions and wishes of their patients. Therefore, the workshop participants comprised a multidisciplinary group of several user representatives and engineers from multiple centers throughout the Netherlands. All participants had interests and expertise in the area of upper-extremity amputation and prostheses. The user representatives were two occupational therapists, three rehabilitation medicine physicians, two physiotherapists, a certified prosthetist/orthotist, and a movement scientist. Six researchers and four engineers constituted the academic contributors.

Concrete representations of ME prosthesis use are necessary to facilitate good user-designer communication [10]. Therefore, activities of daily living that are relevant for forearm prosthesis users formed the starting point of the needs assessment. In preparation of the workshop, the participants were shown an educational video about different prosthetic options and user opinions. Combined with the first-hand knowledge of occupational therapists and physiotherapists (representing end-users), important aspects of the daily use of forearm prostheses were investigated.

A plenary discussion led to a selection of five activities in which the important aspects of upper-extremity prosthesis use are well represented. A refined version of the list of instrumental activities of daily living of Bookman et al. [11] - which was formed using these aspects as criteria - was used as a starting point. Three different aspects of these activities were examined, focusing on the three prosthesis subsystems. Each activity was analyzed using a structured worksheet especially designed for this workshop, which contained a set of six predefined wrist movements and seven grasps. Multidisciplinary groups were each asked to divide one activity into sub-tasks. For every aspect, the worksheet contained several questions to be answered for each sub-task of the activity. After the analysis in small groups, the needs for all aspects were validated and refined in a plenary discussion to reach consensus.

The results of the workshop can be summarized into the following set of requirements for the mechanical design and control of a transradial myoelectric prosthesis:

1. The design should resemble the human hand.

2. The size and weight of the hand should be minimized.

3. The cylindrical, tripod, and lateral grasp types should be available.

4. The grasp execution time should not disturb the user.

5. The hand's pose and external forces should be measured.

6. The user should be able to directly control the speed and force of grasping.

7. The prosthesis should automatically continue holding a grasped object.

In the following sections, these requirements will be discussed in detail.

1.3.1 Anthropomorphism

The required functionality of the prosthesis' mechanical design is based on its role in activities of daily living. The prosthesis should resemble the human hand for both cosmetic and functional reasons, and this resemblance should be present both at rest and when in motion.

With regard to prosthesis design, the most significant features of the human hand are its weight, size, and DOFs. The weight and size strongly limit the mechanisms that can be integrated into the palm, most significantly the number of actuators. The weight of the average human hand is around 400 g [12]. However, a hand prosthesis is usually fitted to a socket surrounding the stump. This socket is not rigidly connected to the stump, which leads to a lever arm which increases the force exerted on the stump. Because of this lever arm, the weight of the prosthesis should be around 2/3 of the able hand's weight, or around 250 g. For the purposes of developing a prosthesis prototype, the average size of an adult male hand will be used.

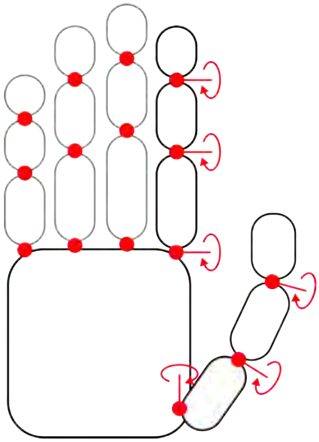

Figure 1.3: Degrees of freedom for an anthropomorphic hand prosthesis.

The human hand has about 21 DOFs [13]. The most important DOFs for general grasping tasks are the three flexion DOFs of the fingers, the two flexion DOFs of the thumb, and the opposition of the thumb. The opposition of the thumb is normally a combination of the various carpometacarpal (CMC) thumb DOFs, but can be approximated by a single rotation DOF. To accomplish this, the thumb should be placed at a 45 degree angle to the other fingers, and be rotated an additional 45 degrees around its own axis towards the palm. The thumb can then rotate around an axis aligned with the extended index finger. With this configuration, the hand will have a structure as shown in Figure 1.3, which is capable of performing the required grasping motions while limiting the number of DOF that need to be actuated.

1.3.2 Grasping

The majority of transradial amputations is unilateral [5]. With a unilateral amputation, the user generally uses the prosthesis in a supporting role, grasping or supporting objects to be manipulated with the able hand. With this in mind, the design of the prosthesis should be optimized to robustly grasp a variety of objects.

Objects of many different shapes and sizes will be encountered during activities of daily living. Establishing a proper grasp on each of these objects is difficult to achieve with a single grasping motion; therefore, the grasping behavior of the hand has been divided into different grasp types.

A grasp type can be seen as the combination of an initial configuration of the fingers and thumb, and coordinated flexion and extension of the fingers. These two main phases are designated as preshaping, in which the fingers and thumb

Figure 1.4: The different grasp types the hand should be able to perform (from left to right): the lateral grasp, the cylindrical grasp, and the tripod grasp.

are moved into position, and execution, where the active fingers and/or thumb are flexed around the object. In between these phases, the user can freely position the hand around the object. Three main grasp types have been determined by the participants of the needs assessment workshop (See Figure 1.4):

- The cylindrical grasp is used to surround relatively large objects with all fingers and the thumb. To preshape the grasp, the extended thumb is moved in opposition to the four extended fingers; the grasp is executed by flexing the four fingers simultaneously, followed by flexion of the thumb.
- The lateral grasp involves holding a flat object such as a card or key between the side of the index finger and the thumb. Preshaping consists of flexion of all four fingers and extension of the unopposed thumb, and execution of the grasp is performed by flexing the thumb.
- The tripod grasp is used to accurately pick up smaller objects between the index finger, middle finger, and the thumb. To preshape the tripod grasp, the ring and little finger are fully flexed, the index and middle finger are extended, and the extended thumb opposes the index and middle fingers. Execution consists of flexing the index and middle fingers and thumb simultaneously.

1.3.3 Sensing

Accurate knowledge of the prosthesis' state is important to both the user and the prosthesis controller itself. For interaction with the environment, the main physical quantities that need to be measured are the angles (and angular velocities) of the joints, and external forces on the hand. From these values, other data can be derived, such as the relative pose of the fingers and the stiffness of a grasped object. Also, the energy injected into the system needs to be monitored; to accomplish this, the motor's force/torque and position/velocity should be measured as well.

Primary data: angles and forces Measuring the joint angles requires the presence of sensors near or on each joint shaft. Given the structure of the joint, this angle can be determined by measuring the rotation of the joint shaft directly, or by measuring the distance or angle between points on either side of the joint.

To determine the forces exerted on the prosthesis by the environment (and vice versa), a series of sensors should be integrated with the contact surfaces of the hand. While ideally these sensors would be placed in various places on the fingers and palm, the fingertip forces are relevant in most grasp types, and will therefore be focused on.

Secondary data: pose and stiffness Knowing the dimensions of the hand, the position and orientation of all fingers can be calculated as a function of the joint angles. As the fingers only operate in a plane, their kinematics are relatively straightforward. The thumb is at an angle with regard to the extended fingers, and is rotated around its longitudinal axis. Depending on its actuation and the position of its joints, the thumb's kinematics might require more attention.

Given the external forces on the finger and the changes in its position over time, the stiffness of a grasped object can also be determined. This information could be used to supply the user with tactile feedback on the object.

Motor: force/torque and position For DC motor actuators, the torque provided by the motor can be determined by measuring the current through it. Alternative methods of actuation would require a force sensor in between the actuator and the fingers and thumb. Additionally, the actuators should contain sensors that indicate their position, and from which their velocity can be derived.

1.3.4 Control system

The main focus of the workshop discussion on prosthesis control was selecting the functions that should be automatically controlled by the prosthesis. Generally, the initiation of actions was considered to be best controlled by the user, whereas the actual execution of those actions can be performed automatically. Grasp type selection and initiation of grasp execution were mentioned as decisions that should be performed by the user.

In the opinion of the workshop participants, the prosthesis should automatically continue holding an object once grasped. This allows the user to focus on moving the object with arm and wrist movements, and manipulate it with the able hand. Preventing slip is also a high priority in this case, but the availability of such a system depends on the quality of the hand's force sensors.

Direct user control of the speed of grasping or the force applied to a grasped object were found useful in several activities. The control system should be able to allow the user to control both intuitively. To implement this, a measure of the desired grasping power is required. The average amplitude of the EMG activity from all electrodes can be taken as a measure of the grasp's intensity [14], and will therefore be used to control grasp force and speed.

Given that the prosthesis should control interaction with the environment automatically, the control system should be designed to remain stable with regard to any disturbances. During grasping, a compliant behavior of the fingers is essential to performing activities of daily living in a safe and natural way. While this can partially be obtained through the mechanical design of the prosthesis, the control system should also be centered around the idea of compliance.

1.4 Contributions

In the course of this project, the following research papers were published in international journals or conference proceedings:

- “A Modeling Framework for the Development of Myoelectric Hand Prosthesis Control Systems" [15], published in: *Proceedings of the International Conference of the IEEE Engineering in Medicine and Biology Society (EMBC)*, 2010.

- “Myoelectric forearm prostheses: State of the art from a user-centered perspective" [1], published in: *Journal of Rehabilitation Research & Development (JRRD)*, 2011.

- “Design of Joint Locks for Underactuated Fingers" [16], published in: *Proceedings of the IEEE International Conference on Biomedical Robotics and Biomechatronics (BioRob)*, 2012.

- “Development of Prosthesis Grasp Control Systems on a Robotic Testbed" [17], published in: *Proceedings of the IEEE International Conference on Biomedical Robotics and Biomechatronics (BioRob)*, 2012.

- “Evaluation of Pneumatic Cylinder Actuators for Hand Prostheses" [18], published in: *Proceedings of the IEEE International Conference on Biomedical Robotics and Biomechatronics (BioRob)*, 2012.

- “Development of Underactuated Prosthetic Fingers with Joint Locking and Electromyographic Control" [19], published in: *Mechanical Engineering Research*, 2013.

- “UT Hand I: A Lock-Based Underactuated Hand Prosthesis" [20], accepted for publication in: *Mechanism and Machine Theory*, 2014.

- “EMG-Based Grasp Control of the UT Hand-I" [21], submitted for publication in: *Bionic Engineering*, 2014.

These papers make up many of the chapters and sections in this thesis. They have been included mostly unedited; this may lead to some overlap in descriptions of the systems that have been developed.

1.5 Outline

This thesis covers the development of the mechanical design and control system of the UT Hand I prosthesis prototype, based on the requirements put forth in Section 1.3. The structure of this thesis is as follows:

Chapter 2: State of the art Taking examples from literature and commercial prostheses, this chapter covers common elements and considerations in the design and control of modern hand prostheses.

Chapter 3: Mechanical systems design The development of various subsystems for actuation, underactuation and sensing of hand prostheses is discussed in this chapter.

Chapter 4: Two-fingered prototype development This chapter describes the development and evaluation of the initial two-fingered prototype, designed to evaluate the newly developed actuation mechanisms and make the first strides towards development of an integrated prosthesis control system.

Chapter 5: Mechanical design of the UT Hand I In this chapter, the mechanical design of the UT Hand I anthropomorphic prosthesis prototype is examined in detail.

Chapter 6: Myoelectric prosthesis control During the development of a control system for myoelectric hand prostheses, research has been done on biomechanical modelling of the hand, evaluation of interaction control methods, and the control system implemented on the UT Hand I. The results of this research are shown in this chapter.

Chapter 7: Discussion This chapter covers the results of the UT Hand I's development, and contains recommendations for future research in this area.

Chapter 2

State of the art

To develop a new hand prosthesis system, the current state of the art in hand prosthesis design and control should be evaluated. Various companies and research groups worldwide have devoted themselves to developing new prosthetic hands and systems to control them. By making a thorough inventory of their developments and design decisions, a system can be compiled that will fulfill the requirements put forth in Section 1.3. Additionally, by looking at the problems that these groups have encountered, research can be focused on compensating for the shortcomings of existing systems.

The most significant aspect of the mechanical design of multifunctional hand prosthesis is their actuation. Therefore, most attention will be focused on the actuation methods that are currently employed in research prototypes, as well as ways to circumvent the restrictions that these actuation methods impose.

The control systems of modern hand prostheses feature a variety of methods to use EMG signals for task selection, and to control the hand's interaction with the environment. To achieve intuitive control, these systems need to work reliably and cooperate seamlessly, but also provide the user access to the functions of the system in a way that is easily learned and understood.

This chapter contains elements from "Myoelectric forearm prostheses: State of the art from a user-centered perspective" [1], "A Modeling Framework for the Development of Myoelectric Hand Prosthesis Control Systems" [15], and "Evaluation of Pneumatic Cylinder Actuators for Hand Prostheses" [18].

2.1 Actuation

Perhaps the most limiting factor in the design of multifunctional hand prostheses is their actuation. Ideally, each degree of freedom would be actuated by a separate actuator, able to provide speeds and forces equal to those of the able hand. However, the main reason this is currently unfeasible is that all of the prosthesis' actuators need to fit inside the hand itself, whereas the human hand is mostly actuated by muscles in the forearm. Also, the actuators usually represent a significant part of the prosthesis' weight, which should be less than the hand's natural weight (400 g) to allow for comfortable continued use. In the case of DC motor actuation, these limitations generally allow around 4 actuators to be used, whereas a fully anthropomorphic hand would have to support 21 DOFs. In this section, common actuator types used in hand prosthesis prototypes are evaluated.

2.1.1 DC motors

CyberHand

(Figure provided by author of [22])

The CyberHand [22] is a prototype anthropomorphic hand prosthesis with 16 DOFs. It contains 6 DC motors: one for each finger, and two for the thumb. The fingers are underactuated by means of a tendon-pulley system.

Modern externally powered prosthetic hands are almost exclusively actuated by DC motors, which are readily commercially available. DC motors are easily controllable, and can be powered by increasingly efficient rechargeable battery packs. Unfortunately, these motors only provide rotational motion and generally have a relatively high mass and size. Also, because prosthesis actuation requires high torques, a transmission is required; the associated gear ratios can reduce the motor's speed to below an acceptable level. Some DC motors used in prosthesis applications include the Maxon EC 13 (Southampton Hand [23]), the Faulhaber 2224 U 006 SR (CyberHand [22]), and the Faulhaber 1727 U 006 C (MANUS Hand [24]).

2.1.2 Pneumatic actuators

Pneumatic actuators are an alternative to DC motors offering a high power-to-mass ratio and convenient energy storage in the form of disposable gas cartridges [25]. In the field of pneumatic prosthesis actuation, two main approaches have been used to some success: pneumatic cylinders, and pneumatic artificial muscles (PAMs) [26]. Recent research in pneumatics for robotic and prosthetic hands often involves PAMs (e.g. [27, 28, 29, 30]), while cylinder actuators are rarely encountered. However, recent research suggests that properly dimensioned pneumatic cylinders offer advantages in mass, size, and power-to-mass ratio when compared to common PAMs [31].

2.1.3 Other

Possible alternatives to either DC motor or pneumatic actuation are also being developed for use in hand prostheses:

Shape memory alloys are materials that change their shape when exposed to heat. A wire of such a material can be made to contract when heated, providing an actuation force. While the resulting motion is difficult to control and the wires are sensitive to environmental conditions, an actuation system with SMA wires can be very small and is mechanically simple.

Hydraulic actuation is technically not a separate actuation system, as it transmits force but does not generate it. However, it allows the force of a main pump motor to be directed to multiple smaller pistons. Such a system has been developed for the Fluidhand [32].

Fluidhand

(Figure provided by author of [32])
The Fluidhand [32] is a hand prosthesis prototype with hydraulic actuation. It uses a single electric pump motor to actuate 8 hydraulic chambers on the joints of the fingers and thumb.

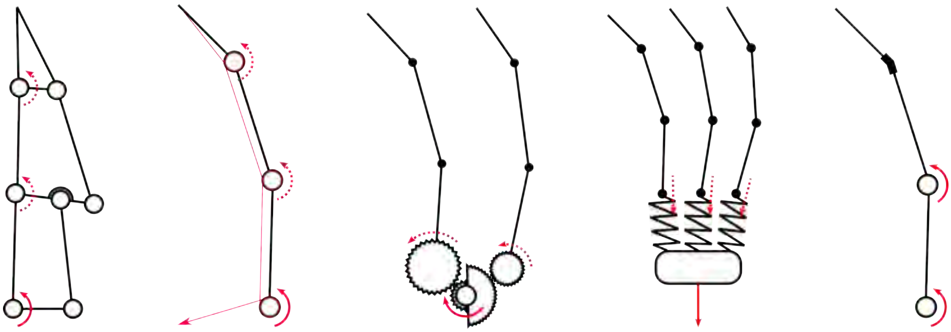

Figure 2.1: Various methods of underactuation. From left to right: Mechanical linkage, tendon-pulley system, intermittent actuation, compliant coupling, and passive joints.

2.2 Underactuation

The strong limitations on a hand prosthesis' weight and size, combined with the desire for increased functionality, often result in designs featuring a large number of DOFs which are connected to a small number of actuators. This principle is known as underactuation. To achieve underactuation, the prosthesis' DOFs need to be connected in some way. The following subsections show various ways in which this is accomplished in research prototypes and commercial prostheses.

2.2.1 Mechanical linkage

Mechanical linkages are a common way of transmitting bidirectional motion. A mechanism such as that seen in Figure 2.1 will move the distal and intermediate joints of the finger when the proximal joint is rotated. A series of coupled four-bar linkages will also automatically adapt its shape to that of an object being grasped, as obstructed phalanges do not prevent the other phalanges from moving. An example of a mechanical linkage for finger underactuation can be found in the AR Hand III [33].

Southampton-Remedi Hand

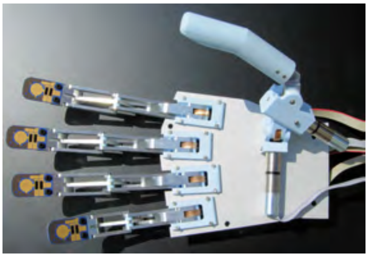

(Figure provided by author of [23])
The Southampton-Remedi hand prosthesis [23] is a lightweight with 6 actuators and 14 DOFs. The joints of each finger are mechanically linked and connected to a DC motor via a worm gear transmission.

2.2.2 Tendon-pulley system

Another method of underactuation involves the use of a freely rotating pulley on each joint, and one or more tendons connected to an actuator. Tension in the tendon will be transmitted to each of the joints, the ratio depending on the relative radii of the pulleys and external forces [34]. A drawback of a tendon system is that it is unidirectional, and tension on the tendons should be maintained. To compensate for this, elastic elements are often used in opposition to the tendons.

A tendon system can also be designed to function without pulleys, by using specially designed tendon sheaths [35, 36]. These systems mimic the actuation of the human hand more closely and allow for more control over the flexion motion, but the sheaths may lead to increased friction on the tendon.

VU Bionic Hand

(Figure adapted from [37])
Developed at Vanderbilt University [37], this hand uses sheathed tendons to connect its 9 DOFs to 4 DC motors. A single motor actuates the 6 DOFs of the ring, middle and little fingers.

2.2.3 Intermittent actuation

The motion of a single actuator can also be distributed over two or more DOFs intermittently, often using a combination of specially designed gears. A mechanism similar to a Geneva drive is implemented to alternate between opposition and flexion of the MANUS-HAND's thumb [24].

MANUS-HAND

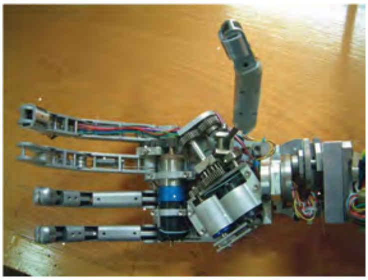

(Figure adapted from [24])
The MANUS-HAND [24] combines several different underactuation techniques: The index and little fingers are coupled by tendons and pulleys, the thumb is actuated intermittently by a Geneva drive, and the ring and little fingers are passive.

While such actuation is mechanically robust, only a single DOF can move at any given time, and control over which DOFs can be actuated is limited.

2.2.4 Compliant coupling

The joints of the hand can also be connected by springs or other elastic elements. Such systems have the advantage of adding compliance to the grasp, which is desirable in interaction with the environment.

TBM Hand

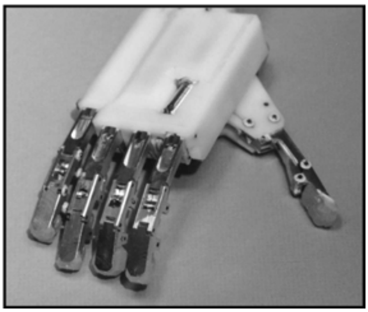

(Figure adapted from [38])
The TBM Hand [38] has 5 fingers that each contain linkages to couple their joints. A single actuator moves a central actuation body, to which all fingers are connected by preloaded springs.

When the central body is moved, the springs flex the individual fingers; if one of the fingers contacts an object, it will stop moving while its connecting spring extends, allowing the other fingers to continue flexing. This system provides underactuated compliant grasping to any number of fingers, though grasps not involving all fingers can become momentarily unstable as the other fingers continue flexing.

2.2.5 Passive joints

Some prostheses also replace less important joints with passive elements to reduce the effective number of DOFs. These can simply be fixed at a certain angle, or be movable by the able hand to adjust a grasp. The distal finger joints and thumb opposition are often implemented in this way.

I-limb Hand

(Figure adapted from [39])
The i-limb is a commercially available EMG-controlled hand prosthesis. Its fingers are individually motorized, and have two compliantly coupled DOFs each. The distal joint of each finger is passive.

2.3 Control

Control systems for ME prostheses combine the output signals of the EMG sensing system with data from internal and external sensors to generate the hand motions intended by the user. Control of the hand can be divided into two levels: high-level control, the user controlled part that determines the hand's desired grasping behavior; and low-level control, the automatically controlled part that interacts with the environment.

2.3.1 High-level control

The high-level control of the hand should allow the user to access all the functions of the hand as intuitively as possible. Two main methods of grasp control are found in literature: A selection of discrete grasp types to be executed, or the direct control of one or more fingers. The MANUS-HAND contains an example of grasp type control [40]: the user enters a code of three EMG signals, which have three possible intensity levels (one of which is 'no activity'). This code therefore allows up to 18 possible hand actions to be selected, as 'no activity' signals are not detected first. The Southampton-Remedi Hand's control system [41] is based on a state machine structure. The states represent the desired automated behaviors of the hand, and the user's EMG signals or external signals can switch between these states to change the hand's behavior.

AR Hand III

(Figure adapted from [33])
The AR Hand III [33] is strongly underactuated, with 15 DOFs connected to 3 DC motors by mechanical linkages. Up to 18 different combined motions of the fingers and thumb can be controlled by EMG input.

The user can also be given direct control over the movement of the fingers. In the AR Hand III [33], the flexion and extension of the thumb, index finger and (combined) other three fingers are separately controlled by EMG input. This system gives the user increased control over the hand, but may reduce the intuitiveness of grasping. Research into the movements of the human hand during grasping [42] has led to the discovery that in around 80% of cases, the motion of the hand can be described as a linear combination of two 'synergies': specific combinations of the hand's DOFs moving in concert. If these synergies can be actuated by carefully designed underactuation or precise control of the hand's DOFs, coupling them to EMG input could lead to an intuitive method of directly controlling hand motion.

2.3.2 Low-level control

Research on myoelectric control of modern hand prostheses often focuses on the interpretation of EMG signals and efficiently accessing the various functions of the hand. However, the automated control systems of the hand are often limited to a straightforward position controller, with optional force control in case contact is detected. This approach is simple to implement and control, but will not guarantee any stable interaction with the environment. Interaction control approaches are more common in robotic hand control applications, but some groups have tried to implement them for prosthesis use as well.

Proportional control applies a force to the fingers proportional to the difference between the actual and desired positions of the finger. It is analogous to connecting a mechanical spring with zero rest length between the fingertip and the desired end position. The MANUS Hand [40] uses proportional control to move its active fingers into position. The addition of a derivative term to the control action results in damping on the finger, reducing sudden changes in motion. Such an approach has been proposed in research on control systems for the Cyberhand [43].

2.4 EMG sensing

EMG sensing is the current standard in the non-invasive control of externally powered prostheses. Myoelectric signals are the electrical expression of the neuromuscular activation generated by skeletal muscles [44]; they are rich in information regarding the user's intent and can therefore serve as an effective control input. With these signals the user's intended hand movements can be detected and reproduced by the prosthesis.

EMG sensing uses surface electrodes to detect the myoelectric signals. However, the potential arriving at the electrodes is very small in comparison to other detected signals, e.g. cardiac-related noise, environment noise and motion artifacts. Therefore, amplification and a filtering method must be applied to reduce these noise signals [45, 46]. In most current EMG systems, the signal data is then segmented into small intervals of which features (i.e. characteristic parameters related to user intent) are extracted. Several parameters in the time, frequency, and time-frequency domains can be used as features, such as the root mean square, mean absolute value, mean frequency, and wavelet transform coefficients.

Detection of a certain number of intended actions requires the same number of unique muscle activity patterns. Each pattern is described by a specific set of features that are entered into a classifier, which determines the movement intended by the user [46, 47, 48]. Examples of frequently used classifiers in literature are linear discriminant analysis [49] and artificial neural networks [50].

Chapter 3

Mechanical systems design

After evaluating the current state of the art of the mechanical design of myoelectric hand prostheses, some avenues of research were found to be important in the development of a new prosthesis. First of all, almost all reviewed hands opt to use significant underactuation to move a large number of DOFs with a strongly limited number of actuators. However, the use of underactuation comes at the cost of removing the controllability of individual DOFs. This often causes the motion of the finger to depend solely on internal frictions and stiffnesses or external forces on the hand, which are difficult to control. A mechanism that can selectively engage or disengage a number of these DOFs at will would not only allow for a single actuator to move any number of fingers simultaneously, but also to change the flexion motion of a single finger to better fit a certain type of grasp. Section 3.1 documents the initial search for ways to implement such a mechanism.

The use of DC motor actuation is dominant in both commercially available and research prototype hands, despite their low torque and relatively high size and mass. Pneumatic actuation is often presented as an alternative to DC motors, though almost entirely in the form of pneumatic artificial muscles (PAMs). In Section 3.2, the application of miniature pneumatic cylinders is investigated as a way of harnessing the speed and power of pneumatic actuation in a small and extremely light package.

Section 1.3.3 listed the types of information that need to be provided to the user and control system of the hand. The angles of the hand's joints and forces exerted on and by the hand should be measured without adding to the hand's size and weight. Several systems to accomplish this are implemented and evaluated in Section 3.3.

3.1 Joint locking

This section was published as “Design of Joint Locks for Underactuated Fingers" [16].

3.1.1 Introduction

Modern electrically powered hand prostheses [51, 52, 53] emulate the structure of the human hand for both cosmetic and practical reasons. The human hand has over 20 degrees of freedom (DOFs), but imposes strong restrictions on the size and weight of an anthropomorphic prosthesis.

DC motors are currently the preferred method of actuation for both commercial and prototype hand prostheses [1]. These actuators are versatile, easily controlled, and readily available. However, the size and weight of the motors and their transmissions allow only a few to be placed inside the prosthesis. This limitation is circumvented by modern prostheses in various ways, shown in Figure 3.1.

These underactuation techniques all allow a single motor to actuate multiple DOFs. However, they also reduce the individual controllability of these DOFs. Mechanisms to transfer the actuation torque of a single motor to different joints have been implemented to remedy this [54], though this approach is limited to small numbers of DOFs. Alternatively, some robotic and prosthetic hands have included passive mechanisms to block joints or entire fingers when certain external forces or torques are applied [55, 56].

The ability to actively lock and release joints can be used to change underactuated fingers' flexion trajectory, or to selectively actuate combinations of fingers with a single actuator. In this paper, novel miniature locking mechanisms are developed to actively control individual joint movement in tendon-pulley underactuated fingers. These mechanisms can fit inside of the phalanges, leading to the development of smaller and lighter multifunctional hand prostheses.

The locks' requirements are derived in Section 3.1.2. Section 3.1.3 describes the different concepts that were explored for both joint locking and actuation. The testing of the various concepts is discussed in Section 3.1.4, and in Section 3.1.5 the test results are shown. In Section 3.1.6, these results are discussed; Section 3.1.7 concludes the paper and provides directions for future work.

3.1.2 Requirements

Implementation of joint locks in a modern multifunctional hand prosthesis leads to a number of requirements which have to be fulfilled. These requirements will

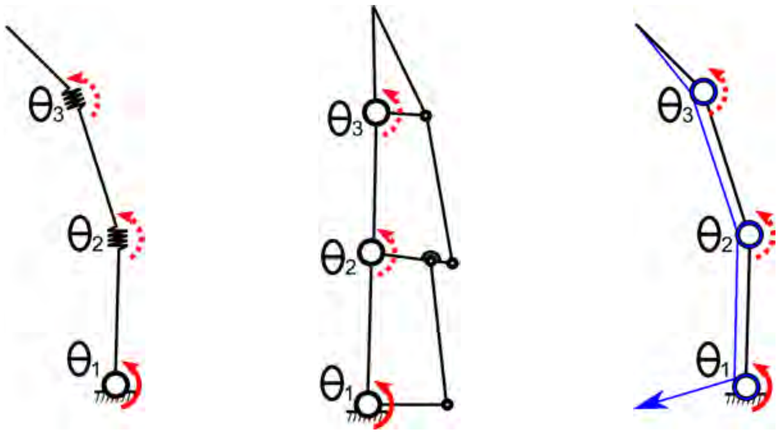

Figure 3.1: Various implementations of underactuation in prosthetic hands: (a) passive elements replacing actuated joints [24], (b) mechanically linked joints/fingers [23], and (c) tendon-pulley mechanisms [22]. The joint angles θ_1, θ_2, and θ_3 are passively connected; actuation of the proximal joint (or in (c), the blue tendon) causes the other joints to move. The actuated joints are represented by solid red arrows, while the passive joints are indicated by dashed red arrows.

be used to evaluate the lock concepts.

First of all, the joint locks have to be fitted inside a human-sized hand. The smallest finger joint to be individually controllable is the proximal interphalangeal (PIP) joint, which has an average depth and width of approximately 17 mm [57]. Any other mechanisms should fit inside of the proximal phalanx, the average length of which is approximately 30 mm, excluding the joints [58]. Because of this, the joint locks should be designed to be operable with as little force and stroke as possible. An important property to accomplish this is self-locking, or the ability of a locked, actuated joint to remain locked without applying force to the lock. This significantly reduces the required lock actuation force.

The locks also need to withstand the torque exerted on them by the main actuator. This locking torque is highest when the locks are engaged while grasping an object, which occurs during the tripod grasp. In many modern prostheses, the grasp force for precision grasping lies between 5-10 N [23, 22, 32]. With an average finger length of 100 mm [58], this amounts to a maximum locking torque of 1 Nm on the most proximal finger joint.

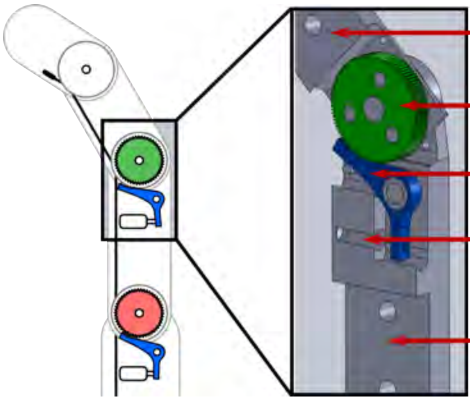

Figure 3.2: Gear locking concept. Rotating the toothed pawl locks the joint by blocking the gear wheel connected to the distal phalanx.

3.1.3 Concepts

The concepts for joint locking mechanisms can be divided into two main approaches: constraining the joint movement by locking elements; and canceling out the joint torque with an opposing friction force [59]. Each approach has its own drawbacks and advantages, and therefore a mechanism has been designed for each of these approaches.

Gear locking

To constrain joint motion, a gear can be rigidly connected to the joint, and movement of the gear can be obstructed by a toothed block. This gear locking concept has been further developed into the mechanism of Figure 3.2. It consists of a radially toothed gear wheel connected to the distal phalanx of the joint and a toothed pawl connected to the proximal phalanx. This pawl can be rotated around its shaft to either lock or release the wheel. In order to avoid overloading of the mechanism and prevent problems with releasing the lock, the teeth do not completely block the motion of the gear; however, the toothed pawl is designed for a high ratio between locking torque and actuation force.

A possible shortcoming of this concept is the indexing resolution caused by the limited number of teeth on the gear wheel. An added requirement of an indexing resolution under 5 degrees was added to the gear concept for this reason.

Design For the design of the gear wheel and toothed pawl, several properties need to be considered: the number of teeth should be maximized to reduce the

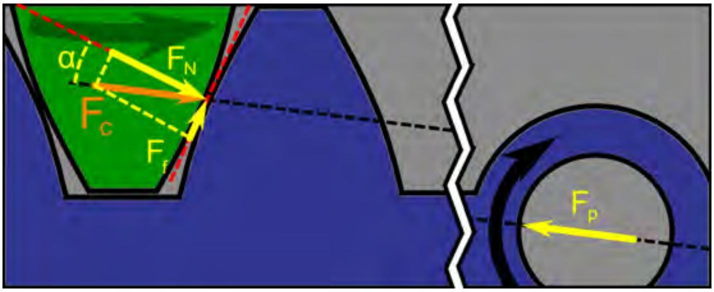

Figure 3.3: Gear locking concept free body diagram, illustrating the contact angle α and the forces on the toothed pawl: the friction force F_f, normal force F_N, total contact force F_c, and pawl shaft force F_p. Curved arrows indicate the parts' direction of motion before locking.

indexing resolution, the shape of the teeth should enable self-locking to reduce the required actuation force, and the gear teeth should be strong enough to withstand the maximum joint torque.

At least 72 teeth are required for an indexing resolution below 5 degrees. In this concept 100 teeth were used, which leads to a resolution of 3.6 degrees. Due to manufacturing restrictions, the minimal module for this number of teeth was 0.2 mm, which led to a gear diameter of 20 mm. Though this exceeds the lock size requirement, it provides a proof of concept; a 75-tooth gear fulfills both requirements.

In order to enable self-locking, the teeth should have a contact angle α such that the friction force F_f between the gear wheel and the pawl keeps the teeth together when a constant joint torque is applied (see Figure 3.3). The static friction depends on the normal force on the pawl F_N as follows:

$$F_f \leqq \mu F_N \tag{3.1}$$

with μ being the friction coefficient between the pawl and gear. Given a static equilibrium condition, both F_N and F_f can be derived from the pawl shaft force F_p:

$$F_N = -\cos(\alpha)F_p \ ; \ F_f = -\sin(\alpha)F_p \tag{3.2}$$

This leads to the following relationship for F_f and F_N:

$$F_f = \tan(\alpha)F_N \tag{3.3}$$

Combining (3.1) and (3.3) leads to the conclusion that the pawl should be self-locking if $\tan(\alpha)$ is less than or equal to μ. The contact is steel-on-steel, and a

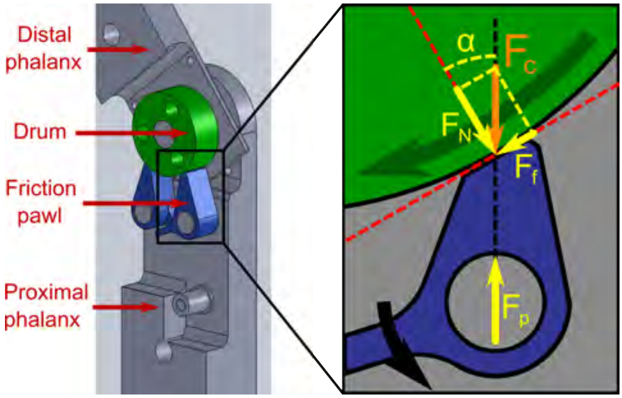

Figure 3.4: Friction amplification concept. Once the friction pawl touches the drum, the joint becomes locked. The forces acting on the pawl are illustrated; curved arrows indicate the parts' direction of motion before locking.

value for μ of approximately 0.4 is expected. In this case, a contact angle of 20 degrees or less should be sufficient to achieve self-locking in most circumstances.

The force on the gear lock is limited by the maximum bending stress on a single tooth. The Lewis equation [60] is a simple method of determining the maximum bending stress on a gear tooth in a static situation. The bending stress σ_b can be determined as follows:

$$\sigma_b = \frac{F_c}{b \cdot m \cdot Y} \tag{3.4}$$

Here, F_c is the contact force on the tooth in N, b is the tooth width in mm, m is the gear module in mm, and Y is the Lewis Form Factor, which for 100 involute teeth at 20 degrees is 0.447 [60]. For F_c, b, and m being 100 N, 4 mm, and 0.2 mm respectively, σ_b is calculated to be 278 MPa. An allowable bending stress can be estimated at one third of a material's ultimate tensile strength; therefore, hardened tool steel (45NiCrMo16, ISO 1.2767) with an ultimate tensile strength of around 1500 MPa has been selected.

Friction amplification

The joint torque can also be opposed by a friction-based locking mechanism, which uses rotating friction pawls to block the motion of a drum connected to the distal phalanx. This friction amplification (FA) mechanism can be seen in Figure 3.4. When one of the friction pawls is moved into contact with the rotating central drum, the friction between them pulls the pawl further along. This increases the contact force between drum and pawl, and thereby the friction. It

Table 3.1: Toothed pawl parameters.

Pawl	T1	T2	T3	T4
Number of teeth	10	2	10	2
Tooth angle (deg)	20	20	20	15
Gear module	0.2	0.2	0.2	0.5
Indexing resolution (deg)	3.6	3.6	3.6	9
Tooth shape	Involute	Involute	Pointed	Straight

should be noted this locking principle is unidirectional; two friction pawls would be needed to enable joint locking in both directions.

Design The free body diagram describing the forces acting on the pawl during self-locking is shown in Figure 3.4. If the friction pawl is self-locking, it becomes a two-force member, meaning the line of the pawl shaft force F_p lies through both the rotation point and the contact point. This can only be the case if the angle α between this line and the normal force F_N is smaller than the friction angle $(\arctan(\mu))$. Similar to the gear concept, the contact angle should therefore be 20 degrees or lower.

Given the 1 Nm maximum joint torque and a drum diameter of 15 mm, the maximum friction force F_f will be approximately 133 N; at a 20 degree contact angle, this leads to a contact force F_c of approximately 365 N.

To determine the maximum contact stress, the pawl and drum are modeled as parallel cylinders. This leads to the following equations for the maximum Hertzian contact stress σ_{Hmax} [61], where F_c is the contact force, E is the Young's modulus of the material, ν is the Poisson ratio of the material, b is the width of the contact area, and ρ is based on the contact surfaces' radii of curvature ρ_1 and ρ_2:

$$\sigma_{Hmax} = \sqrt{\frac{1}{2\pi \cdot (1-\nu^2)} \cdot \frac{F_c \cdot E}{b \cdot \rho}} \ , \tag{3.5}$$

$$\text{where } \rho = \frac{\rho_1 \cdot \rho_2}{\rho_1 + \rho_2} \tag{3.6}$$

Given steel-on-steel contact and a flat pawl surface, this results in a maximum contact stress of approximately 597 MPa. The hardened tool steel mentioned in Section 3.1.3 has an allowable contact stress of several thousand MPa, so this should not be a problem.

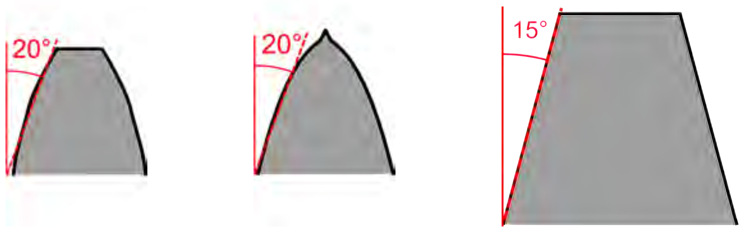

Figure 3.5: Pawl tooth variations: (a) Involute teeth, used in pawls T1 and T2; (b) Pointed teeth, used in pawl T3; (c) Straight teeth, used in pawl T4. The tooth angle is indicated in red.

Actuation

Various methods of electrically powered small-scale actuation are currently available. The following have been investigated: piezo elements, shape memory alloy, and solenoids.

Many varieties of piezoelectric actuator are available, based on the deformation of certain materials when exposed to an electric field. A $5 \times 5 \times 18$ mm^3 piezoelectric stack actuator can provide forces in excess of 800 N, though its stroke is limited to around 0.015 mm [62]. This stroke can be raised to 1 mm by implementing a piezo bending actuator, which reduces the actuation force to a maximum of 0.5 N [63].

Shape memory alloy (SMA) is a material that when deformed can return to a previous shape when exposed to a change in temperature. This effect can be used in actuation, and requires only a wire of SMA material and an electrical current to heat it. The drawbacks of a SMA wire of sufficient size are a cooldown time of up to several seconds [64] and hysteresis in the transformation characteristic [65].

Solenoid actuators use an electromagnetic field to move a ferromagnetic armature. A solenoid actuator with a diameter of 11.3 mm and a length of $13.3\ \mathrm{mm}$ can exert impulse forces of up to 4.5 N with a stroke of 2 mm [66]. However, a higher stroke or longer operation time reduces the maximum force.

When comparing the above actuators, the solenoid actuator provides the best combination of actuation force and stroke. Therefore, for further evaluation of the lock concepts solenoid actuation will be used.

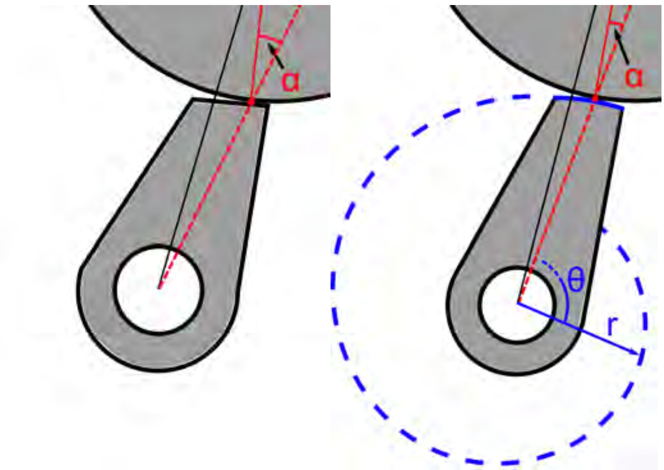

Figure 3.6: Friction pawl variations: (a) Short pawl with flat contact surface, used in pawls F1, F2, and F3; (b) Long pawl with spiraled contact surface, used in pawls F4, F5, and F6. The contact angle α is indicated in red; the spiral's radius r and angle θ are indicated in blue.

Table 3.2: Friction pawl parameters.

Pawl	F1	F2	F3	F4	F5	F6
Length (mm)	8.6	8.6	8.6	22.9	22.9	22.9
Contact angle (deg)	24	18	8	13	10	7
Contact surface	Flat	Flat	Flat	Spiral	Spiral	Spiral

3.1.4 Testing

To allow for uncertainties in the design parameters, several variations of each concept have been developed. In this section, these variations are described, followed by a test protocol based on the requirements.

Concept variations

The gear locking concept features four different gear wheel/pawl combinations (T1 through T4), with variations in the number of teeth on the pawl, tooth shape, and tooth size.

For the FA concept, six friction pawls have been made (F1 through F6) with varying contact angle α (see Figure 3.4). Also, two different implementations of the friction pawls' contact area have been tested: in addition to the default flat profile, a logarithmic spiral surface has been designed. The radius of these pawls' contact surface r depends on the angle θ as follows: $r = a \cdot e^{b\theta}$. At any point on this surface, the angle ϕ between the tangent and the radial line is constant and given by $\phi = \arctan(\frac{1}{b})$. This reduces the effect of play, as the pawl can accommodate variations in distance to the drum with minimal effect on the contact angle α. This concept is illustrated in Figure 3.7.

The respective parameters for each of the pawls can be found in Table 3.1 and Table 3.2, and are illustrated in Figure 3.5 and Figure 3.6.

Test protocol

For each of the systems described in Section 3.1.4, the following tests are performed:

Self-locking First, the lock's self-locking properties are tested; the joint lock is actuated with a force of 10 N, and an external torque of 1 Nm is applied to the joint. As soon as the joint is successfully locked, the actuation force is removed. If the joint remains locked, it can be considered self-locking.

Torque ratio If the lock is not self-locking, the ratio of maximum locking torque to actuation force will be determined. This is done by measuring the maximum torque the lock can withstand without slipping or releasing for different actuation forces.

Actuation and release The pawl stroke required to engage and release the lock is evaluated, and if the lock is self-locking, the force required to release the lock is measured.

The test setup used for the gear locking and FA concepts can be seen in Figure 3.8.

3.1.5 Results

Summaries of the test data for both concepts are shown in Table 3.3 and Table 3.4. For each test, the results are discussed separately.

Self-locking

No self-locking was observed for any of the gear-locking concepts. The FA concepts showed self-locking at contact angles of 10 degrees and lower, though the

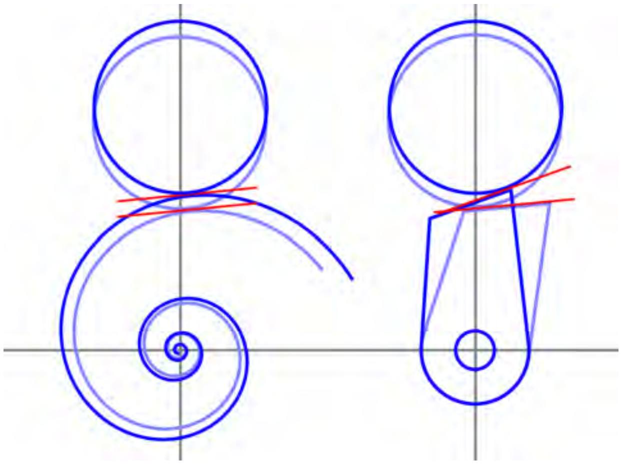

Figure 3.7: A diagram illustrating the effect of play on the contact angles of a logarithmic spiral and a straight pawl.

property was inconsistent when testing the 10 degree FA pawl (pawl F5). The self-locking FA concepts (pawls F3, F5, and F6) were able to handle joint torques up to 2.0 Nm without any problems.

Torque ratio

For the non-self-locking pawls, the ratio between the maximum locking torque and actuation force was measured. These can be seen in Table 3.3 and Figure 3.9 for the gear concept, and Table 3.4 for the FA concept. The gear concept showed an almost linear ratio, independent of movement direction or joint angle. During testing of the non-self-locking FA concepts, the torque ratio proved almost negligible. At the 10 degree contact angle (pawl F5), the self-locking property was observed to be dependent on joint orientation and applied actuation force, as seen in Figure 3.10.

Actuation and release

The gear wheel's actuation and release stroke depends on the geometry of the teeth, and the number of teeth on the pawl. For the two-toothed pawls, the stroke is equal to the tooth length; the ten-toothed pawls require a slightly larger stroke to clear the gear. As none of the toothed pawls are self-locking, no release force was measured.

Although the FA concept has almost zero actuation stroke, a significant

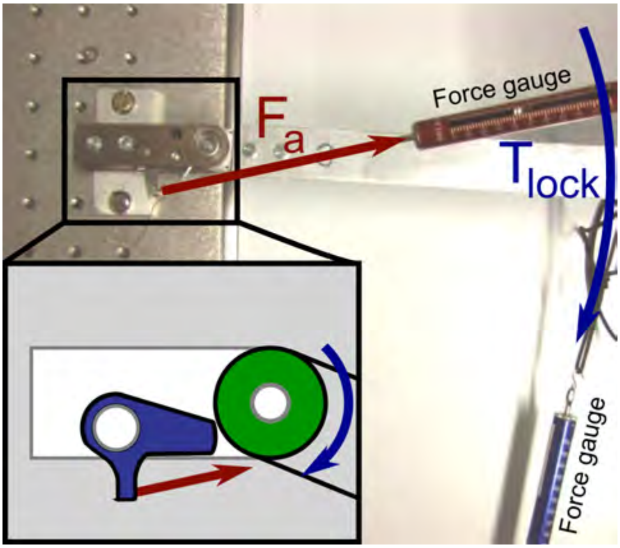

Figure 3.8: Joint lock test setup, with a diagram of the internal mechanism of the FA concept. Actuation force (F_a), locking torque (T_{lock}), and the force gauges used to measure these are indicated.

amount of joint compliance was found with the spiraled self-locking pawls (F5 and F6); this caused up to 11 degrees of additional joint deflection at 1 Nm. Because of their low contact angle, any deformation or play in the lock components results in a large rotation of the locked joint; additionally, the spiraled surface of the pawls causes a slower buildup of force in the lock, leading to a lower rotational stiffness.

After removing the joint torque, the force required to release the self-locking FA systems was found to be approximately 0.3 N.

3.1.6 Discussion

In this section, the differences in performance of the concept variations are discussed. Afterward, the concepts will be evaluated by comparing the test results to the appropriate requirements.

Concept variations

Gear locking The decrease in tooth angle had a positive effect on the torque ratio. Also, reducing the number of teeth from 10 to 2 made it more likely for the pawls to lock into the gear wheel. Increased tooth size showed no obvious

Table 3.3: Gear locking concept test results. Since no self-locking occurred, no release forces were measured.

Pawl	T1	T2	T3	T4
Self-locking	No	No	No	No
Torque ratio (Nm/N)	0.03	0.045	0.077	0.125
Actuation/release stroke (mm)	0.8	0.7	0.8	1.2

Table 3.4: Friction amplification test results. (*) indicates conditional self-locking.

Pawl	F1	F2	F3	F4	F5	F6
Self-locking	No	No	Yes	No	Yes*	Yes
Torque ratio (Nm/N)	~0	~0	N/A	0.006	0.015	N/A
Release force (N)	N/A	N/A	0.2	N/A	0.3	0.3

benefits, whereas the higher indexing resolution is a significant drawback. The pointed shape of the teeth on pawl T3 initially resulted in a higher locking torque, though the shape was worn down after several rounds of testing.

Friction amplification For the FA concept, the variations in contact angle and contact surface shape were most influential. The locks' performance was almost exclusively reliant on the occurrence of self-locking, and the required contact angle for self-locking proved to be much lower than expected. The spiraled contact surface ensured that any play caused by the high normal forces had no effect on the contact angle, though it also resulted in an increase in compliance of the locked joint. Increasing the pawls' length also diminished the relative effects of play in the shafts and bearings.

Concept evaluation

Mechanism size and weight The gear locking concept's gear wheel exceeded the stated joint size requirement by 3 mm. However, reducing the number of teeth to 75 could lower the diameter to 15 mm without exceeding 5 degrees of indexing resolution.

The thicknesses of the gear wheel and FA drum were 4 and 5 mm, respectively, which allows for the placement of actuation pulleys and extension springs in the joint.

An early prototype of the FA concept with solenoid actuator implemented in a $15 \times 17 \times 60$ mm^3 phalanx can be seen in Figure 3.11. The total weight of all lock components and the solenoid actuator is 17.2 g for the gear concept, and 13.4 g

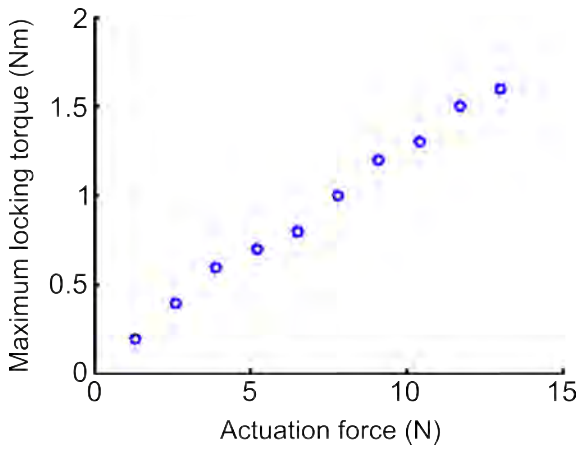

Figure 3.9: Maximum locking torque as a function of actuation force for the gear locking concept, pawl T4.

for the FA concept.

Actuation force and stroke As mentioned in Section 3.1.3, the selection of a solenoid actuator limits the actuation force to 4.5N. The test results show that none of the tested gear locking concepts would fulfill this requirement, as the minimal actuation force needed to meet the joint torque requirement of 1.0 Nm was 8 N. The actuation stroke of all concepts was less than the solenoid's 2 mm stroke.

For the FA concepts, the magnitude of the actuation force had little effect on the locking torque; the self-locking concepts required no actuation force, but the non-self-locking pawls required over 70 N to lock 1 Nm of joint torque.

Joint torques Both concepts are capable of withstanding joint torques of 1 Nm, though the gear locks require an actuation force of more than 8 N; the self-locking FA concepts were found to withstand torques of up to 2 Nm without damage.

3.1.7 Conclusion

In-phalanx joint locking mechanisms are a feasible way of improving the controllability of underactuated fingers. Though neither the small size of the mechanisms nor the high joint torques proved to be a problem in their development, the locks' actuation force was limited by the small space available for actuation. After testing both concepts, only some of the FA concepts were able to meet all requirements.

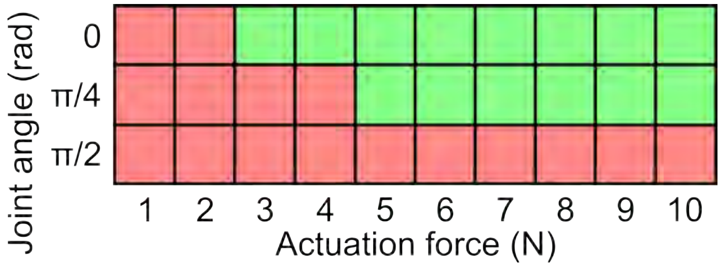

Figure 3.10: The self-locking of FA concept 5 as a function of joint angle and actuation force; green squares represent self-locking, and red squares represent slippage.

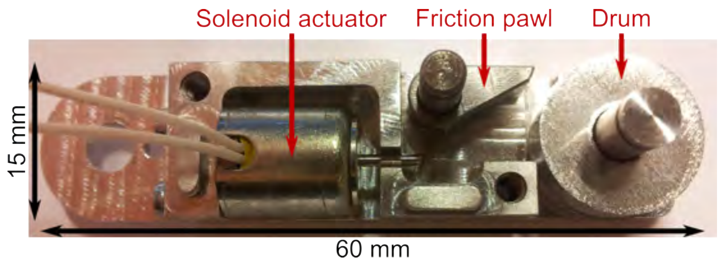

Figure 3.11: Prototype of the FA joint lock concept with solenoid actuation, integrated in a human-sized phalanx.

This is mainly due to their capacity for self-locking, which is entirely absent from the tested gear locking concepts.

The concepts' self-locking capabilities depend mainly on the contact angle of the pawls and the friction coefficient of the materials. Since self-locking was only observed at contact angles below 10 degrees, the friction coefficient appears to lie below expected values. Lower contact angles also resulted in higher contact forces than expected, though the locks experienced no failures with joint torques of up to 2 Nm.

The gear concept can be improved by reducing the tooth angle, as well as investigating other tooth shapes for both locking torque and wear resistance. For the FA concept, joint compliance could be reduced by increasing the mechanism's friction and contact angle.

For future work, four of the FA locks will be implemented in a two-fingered prosthesis prototype, to demonstrate a variety of grasp types with a single main actuator.

The high-level controller will be based on a state machine structure, allowing several grasps and gestures to be intuitively navigated with few control signals. For the low-level controller of the hand several interaction control systems can be evaluated, such as admittance control, impedance control, and intrinsically passive control systems.

3.2 Pneumatic actuation

This section was published as “Evaluation of Pneumatic Cylinder Actuators for Hand Prostheses" [18].

3.2.1 Introduction

Modern externally powered prosthetic hands are almost exclusively actuated by DC motors, which are readily commercially available. Unfortunately, these motors generally have a relatively high mass and size. Also, because prosthesis actuation requires high torques, a transmission is required; the associated gear ratios can reduce the motor's speed to below an acceptable level.

Pneumatic actuators are an alternative to DC motors offering a high power-to-mass ratio and convenient energy storage in the form of disposable gas cartridges [25]. In the field of pneumatic prosthesis actuation, two main approaches have been used to some success: pneumatic cylinders, and pneumatic artificial muscles (PAMs) [26]. Recent research in pneumatics for robotic and prosthetic hands often involves PAMs (e.g. [27, 28, 29, 30]), while cylinder actuators are rarely encountered. However, recent research suggests that properly dimensioned pneumatic cylinders offer advantages in mass, size, and power-to-mass ratio when compared to common PAMs [31]. Therefore, further investigation of pneumatic cylinder actuation for modern hand prostheses is desired.

The goal of this paper is to determine whether the pneumatic cylinder actuator can be a viable option for the actuation of prosthetic hands. To this end, a prosthesis test setup is developed, and both a custom pneumatic cylinder and a commercial DC motor are used to actuate it.

The prosthesis to be used in these experiments is the WILMER central pushrod operated hand [67] (Figure 3.12). The hand has a single degree of freedom (DOF) in the thumb base, for opening and closing. The thumb is connected to a spring, which keeps the hand closed when no force is applied.

A list of hand prosthesis requirements has been derived from user needs during activities of daily living [1]. Test metrics for speed, responsiveness and energy storage are based on these requirements, and used to compare the actuators. The result of these tests serve to demonstrate the effectiveness of pneumatic

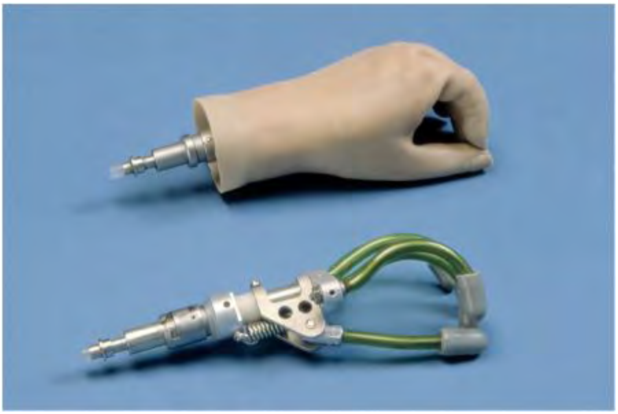

Figure 3.12: The WILMER central pushrod operated hand [67], with and without cosmetic sleeve.

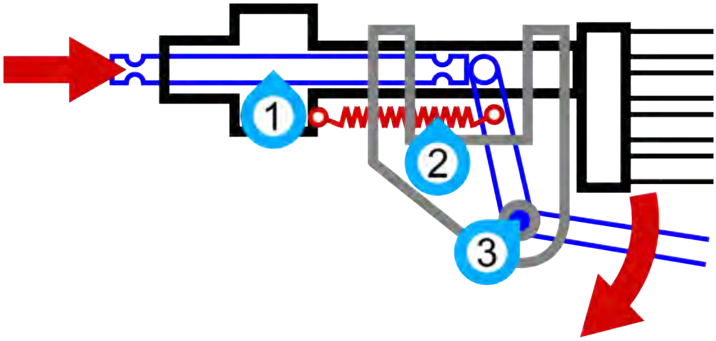

Figure 3.13: A sketch of the WILMER hand's internal mechanics, pointing out key components: (1) the pushrod, (2) the spring, and (3) the lever arm. The red arrows indicate the input force and the movement of the mechanism during hand opening.

cylinder actuation in modern hand prostheses, and can be used to further improve their design.

In Section 3.2.2, the test metrics are described. Section 3.2.3 shows the design of the test setup and the specifications of the actuators and accessories. The test results are listed in Section 3.2.4, and are discussed in Section 3.2.5. The paper is concluded in Section 3.2.6, and directions for future work are provided.

3.2.2 Requirements / test metrics

Based on implementation of the actuators in a hand prosthesis, a list of requirements can be derived. These requirements and the related test metrics are described below.

Speed

The speed of the hand is essential for its acceptance by the user. On average, electrically powered hands currently have closing times between 0.5 s and 1 s [1]. Though the DC motor actuator has a high speed by itself, its relatively low torque requires a significant gear reduction. Also, the pneumatic actuator may need some time to build up sufficient pressure to exert the necessary force. This metric will be evaluated by measuring the time required to open the hand from full flexion to full extension and back. The return time is important even though the hand is forced closed by its internal spring, as the DC motor will need to actively close the hand due to its non-backdrivable transmission.

Responsiveness

High responsiveness of the actuator means a minimal delay between a command being sent and the start of actual movement. A quick response is important for intuitive control. It will be evaluated by measuring the time from sending the initial activation signal, to the time the change in position of the hand first exceeds the average sensor noise level.

Capacity

The standard energy storage system for DC motors in current myoelectric prostheses is a rechargeable Lithium-Ion (Li-Ion) battery pack, while the pneumatic actuator used here runs on compressed CO_2 cartridges. The prosthesis should be continuously usable during the day. The actuators' respective capacities will be determined by measuring the number of grasp cycles that can be performed with a full battery pack or gas cartridge.

Other metrics

Some metrics, while important to the comparison of the actuation systems, can simply be evaluated by inspection or basic measurements. These are the following: the size and mass of the actuator and any accessories (such as transmission or energy storage), the loudness of the actuator, and any changes in performance while grasping an object.

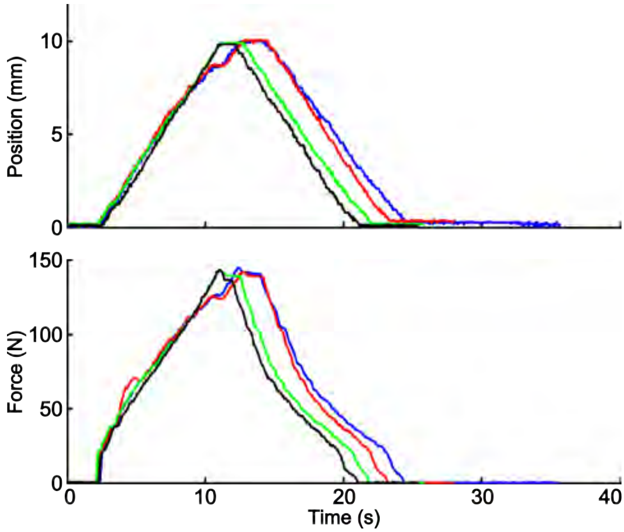

Figure 3.14: Results of the preliminary experiment to determine the required force and stroke for actuation of the test setup.

3.2.3 Test setup

The test setup consists of three main components: the hand prosthesis and its mounting; the DC motor actuation system; and the pneumatic actuation system.

Hand prosthesis

The mechanics of the WILMER hand can be seen in Figure 3.13. The hand uses a ‘voluntary open’ mechanism, which consists of a spring holding the hand closed, and a lever arm connecting the thumb to a pushrod. When the pushrod is pushed, the hand opens, and when the pushrod is released, the spring closes the hand automatically. The hand design exerts a constant force on the actuator while keeping the hand open, which requires the actuation systems to be non-backdrivable.

Two sensors will be attached to the hand during testing, to determine the forces and displacements needed to evaluate the actuators. The actuation force will be measured via a 1-DOF compression force transducer (HBM C9B [68]), fitted between the actuator and the pushrod. The hand position is determined using a linear Hall effect sensor (Allegro A1301 [69]), which measures the distance to a small magnet attached to the force sensor block.

The force and stroke required to actuate the hand were measured in a preliminary experiment. For this experiment, the test setup was connected to a manual

Table 3.5: Maximum and average force and stroke values measured in the preliminary experiment.

Measurement	1	2	3	4
Maximum force (N)	144.65	141.77	142.33	143.21
Average force (N)	77.53	78.01	72.95	70.61
Maximum stroke (mm)	9.80	9.99	9.76	9.75
Average stroke (mm)	5.63	5.70	5.25	5.04

spindle, and the hand was moved from fully closed to fully opened and back. The applied force and spindle position were measured; the results can be found in Figure 3.14 and Table 3.5. For a proper comparison, both actuators should be capable of these forces and strokes.

DC motor actuator

The DC motor actuator needs to be representative of the current state of the art in modern hand prosthesis prototypes [23, 24, 70]. These systems feature small brushless DC motors, which are capable of torques around 1-10 mNm, and use planetary gearheads to increase this torque to the level required to actuate the hand. For this test, a Maxon EC-max 22 motor [71] has been chosen. Its specifications can be found in Table 3.6, along with the specifications of other motors used in several modern prosthesis prototypes. While the EC-max 22's mass and weight are above average, its performance is comparable to that of the other motors.

Because the prosthesis is kept closed by a spring, the transmission needs to be non-backdrivable in order to prevent excessive stall torques on the actuator while holding the hand open. A spindle drive has been selected for this purpose. The required input torque (τ_{in}) depends on the output force (F_{out}), the spindle pitch (p) and transmission efficiency (η) as follows:

$$\tau_{in} = \frac{F_{out} \cdot p}{2\pi \cdot \eta}$$

For this spindle drive, $p = 0.002$ and $\eta = 0.67$. This leads to a τ_{in} of approximately 71.3 mNm. Given that the nominal torque of the motor is approximately 11 mNm, at least a 1:7 gear ratio is required. A 1:14 gear ratio was chosen.

The DC motor is powered by a commercially available prosthesis battery, the Otto Bock EnergyPack 757B20 [72]. This battery has a capacity of 900 mAh at 7.2V, which represents 23.3 kJ of energy. The work to be done by the actuator to open the hand is an average of 72.5 N acting through a distance of 10 mm,

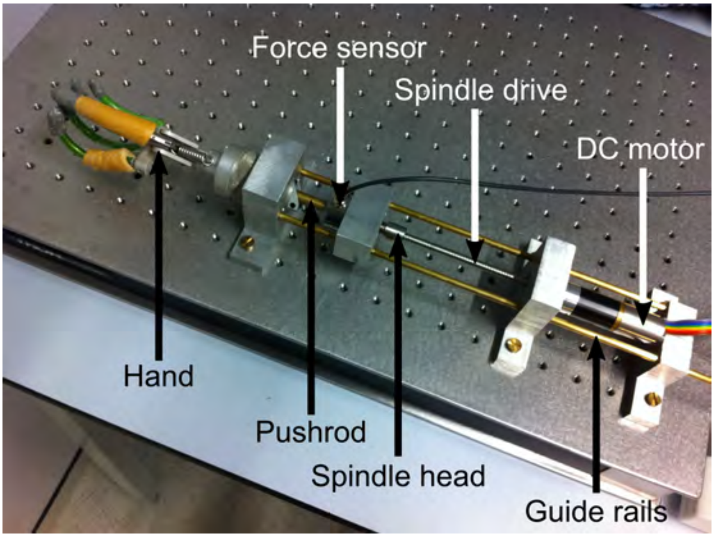

Figure 3.15: A picture of the DC motor test setup, indicating relevant systems.

Table 3.6: DC motor specifications for several modern hand prostheses. (A): Maxon EC 13, (B): Maxon EC-max 22, (C): Faulhaber 2224 U 006 SR, (D): Faulhaber 1727 U 006 C.

Motor	A [23]	B [71]	C [70]	D [24]
Output power (W)	6	12	4.55	2.37
No-load speed (rpm)	28300	10800	8200	7800
Speed constant (rpm/V)	4950	1870	1380	1460
Torque constant (mNm/A)	1.93	5.12	6.92	6.53
Maximum efficiency (%)	63	67	82	70
Mass (g)	15	67	46	28
Radius (mm)	6.5	11	11	8.5
Length (mm)	21.4	32	24.2	27

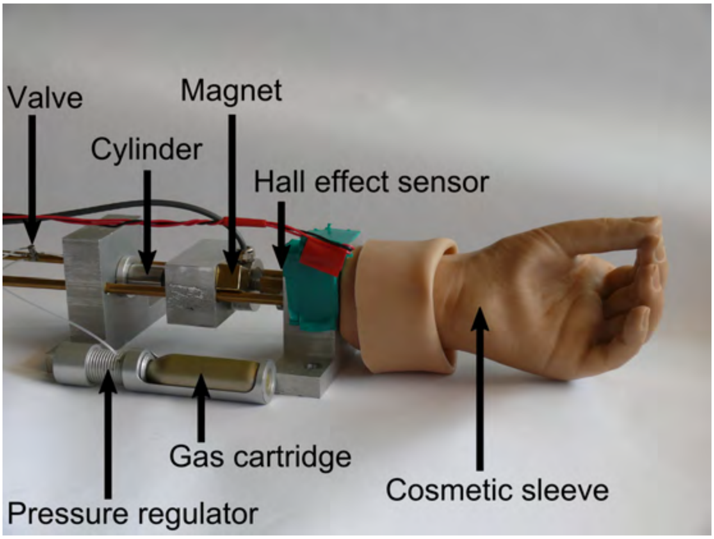

Figure 3.16: A picture of the pneumatic actuator test setup, indicating relevant systems.

or 0.725 J. Given that hand closure needs to be actuated as well, and that both the battery and motor have a rated efficiency of around 66%, this would allow for approximately 3500 hand opening/closing cycles. The design of the DC motor test setup can be seen in Figure 3.15.

Pneumatic actuator

The pneumatic actuator assembly consists of the pneumatic cylinder, connective tubing, a valve, and a CO_2 cartridge with pressure regulator. The test setup including the hand prosthesis can be seen in Figure 3.16, and a pneumatic circuit of the system is shown in Figure 3.17.

The custom-built cylinder (shown in Figure 3.18) has been designed to provide an actuation force comparable to that of the DC motor, while minimizing its size and mass. It is 20.2 mm in length, has a radius of 6.5 mm and a mass of 3.04 g. The cylinder is directly connected to the hand prosthesis, without any transmission. The maximum stroke of the pneumatic actuator is 10 mm. The cylinder is made of steel, and has a very thin wall (0.2 mm). The cylinder is operated at a pressure of 1.2 MPa, which has been shown to use the minimum amount of gas per operating cycle [73]. With this pressure, the piston's surface should be at least 121 mm^2 (a radius of 6.2 mm) to provide sufficient force. An O-ring, placed in a groove in the piston, seals the gap between the piston and the cylinder. By choosing a low groove depth, the O-ring will be compressed between the piston

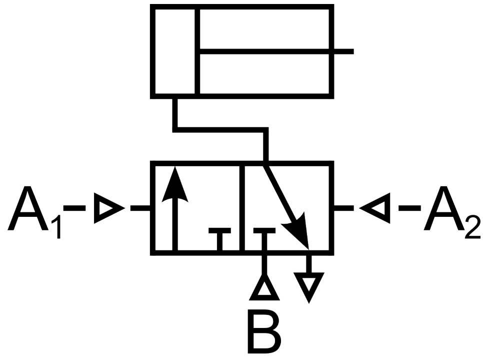

Figure 3.17: Pneumatic circuit of the actuator system used in the experiments. Inputs marked with A_1 and A_2 are connected to an external air supply; the input marked with B is connected to the CO_2 cartridge and pressure regulator.

and cylinder wall. This provides a tighter seal, but also increases friction. However, because the cylinder is single acting, the O-ring is always pushed in one direction. This allows the O-ring to be uncompressed or 'floating', which minimizes friction. The piston shaft is made of polychlorotrifluoroethylene (PCTFE), to reduce friction along the cylinder wall and keep the piston mass low.

The actuator is powered by commercially available CO_2 cartridges, which contain approximately 7.7 grams of CO_2. At 20 degrees Celsius and a pressure of 1.2 MPa, CO_2 has a density of approximately 23.4 kg/m^3. When fully extended, the cylinder's volume is 1250 mm^3, which at this density requires 29.2 mg of CO_2 to fill. Assuming no leaking or temperature variations, a 7.7 g cartridge will therefore contain enough CO_2 for approximately 263 grasping cycles.

The CO_2 cartridges are housed in a custom pressure regulator [25]. To control the flow of CO_2 to and from the cylinder a miniature two-way valve is implemented, which for these experiments is actuated by an external air supply. For implementation in an actual hand prosthesis, a solenoid valve will need to be used. To open the hand, the cylinder is pressurized; when the air is vented from the cylinder, the hand prosthesis' spring delivers the force to return the piston to its initial position.

Experiments

For both actuator types, the following test protocol is used:

1. *Initial testing.* First, the hand performs 10 complete open/close cycles. This test is used to evaluate the actuators' speed and responsiveness; both actuators are controlled between the two end positions of the hand by a simple on-off system.

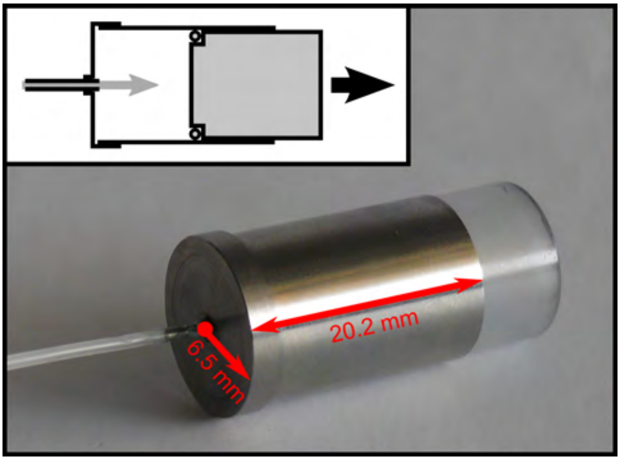

Figure 3.18: The thin-walled pneumatic cylinder actuator, specifically designed for prosthesis applications. A cross-section of the cylinder is shown in the top left corner.

2. *Capacity test.* The associated energy capacity is determined differently for each actuator. For the DC motor, current drain is monitored during initial testing; the average current drain is combined with the battery capacity to determine the maximum operating time. For the pneumatic cylinder, a full gas cartridge is connected and the hand is programmed to perform continuous open/close cycles. The time until the hand stops moving is measured.

3. *Inspection metrics.* Finally, any metrics that can be evaluated by inspection (Section 3.2.2) are measured.

Both test setups are controlled and measured using LabVIEW [74].

3.2.4 Results

In this section, the tests carried out on both actuators are described, and their results are shown.

DC motor testing

The DC motor testing setup is shown in Figure 3.15. The setup is connected to a National Instruments ELVIS II data acquisition device (DAQ) [75], which is in turn connected to a PC running a LabVIEW [74] script for control.

Initial testing The test results for 10 full open/close cycles can be seen in Figures 3.19 and 3.20; average and maximum speed and force values can be found in Table 3.7.

Capacity test The Otto Bock EnergyPack 757B20 [72] has a capacity of 900 mAh. During the initial open/close testing, the motor current was 0.675 A on average during opening, and 0.376 A on average during closing. Under this load a fully charged battery lasts for around 108 minutes, or about 2000 open/close cycles.

Inspection metrics The size and mass values for modern DC motor actuators can be found in Table 3.6. The size of the Otto Bock EnergyPack is 70$\times$32$\times$18 mm, and its mass is 65 g. The sound level of the motor was measured at a distance of 1 meter from the setup. To represent the loudness of the actuator in terms of human sound perception, the measured values have been adjusted by a weighting filter. In this case, A-weighting has been used [76]; the results can be seen in Figure 3.21.

After initial open/close testing, 10 more open/close cycles were performed, this time with an object to be grasped by the hand. While the object removes the load on the actuator when held, the actuator's overall performance is unaffected. It should also be noted that although the spindle drive provides sufficient force to fully open the hand, some backdriving was observed when attempting to maintain a fully open hand position.

Pneumatic cylinder testing

The pneumatic actuator test setup is shown in Figure 3.16. The same DAQ and software are used as with the DC motor tests.

Initial testing The results of open/close cycle testing for the pneumatic actuator can be seen in Figures 3.19 and 3.20; average and maximum speed and force values can be found in Table 3.7.

Capacity test In this experiment, a full gas cartridge was connected, and the hand was programmed to continuously open and close until it was depleted. The cartridge was emptied after completing 300 open/close cycles, which lasted 19 minutes.

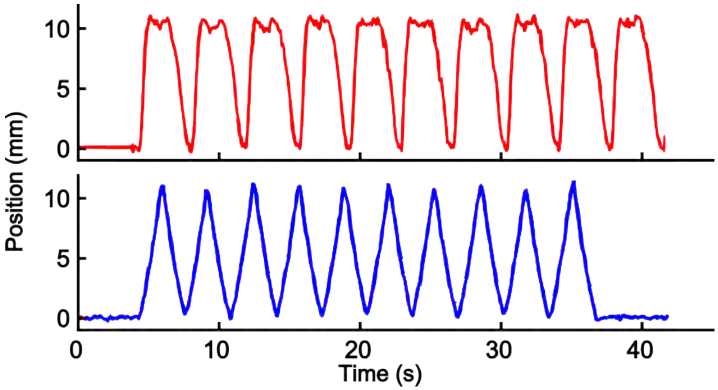

Figure 3.19: The pushrod position during 10 open/close cycles of the pneumatic cylinder (red) and the DC motor (blue).

Table 3.7: Comparison of initial test results for the DC motor and pneumatic cylinder.

Actuator	DC motor	Pneumatic cylinder
Average open/close time (s)	3.03	3.65
Maximum speed (mm/s)	8.57	14.48
Average force (N)	45.1	64.0
Maximum force (N)	125.0	122.2
Capacity (Cycles)	2000	300

Inspection metrics The pneumatic cylinder (Figure 3.18) is 20.2 mm in length, with a radius of 6.5 mm; its overall mass is 3.04 g. The gas cartridges weigh approximately 28.8 g apiece when full, and 21.1 g when empty. They are 66 mm long, with a radius of 8.9 mm. The mass of the pressure regulator is 26.9 g.

As opposed to the DC motor, the speed of the pneumatic actuator is fixed, so only one sound level could be measured; at 1 meter distance, the maximum loudness varied between 40-45 dB. Because the pneumatic actuator relies on the prosthesis' spring for a closing force, grasping an object does not have a significant effect on the force/position characteristics.

3.2.5 Discussion

For each of the metrics listed in Section 3.2.2, the test results are used to compare the performance of the two actuators.

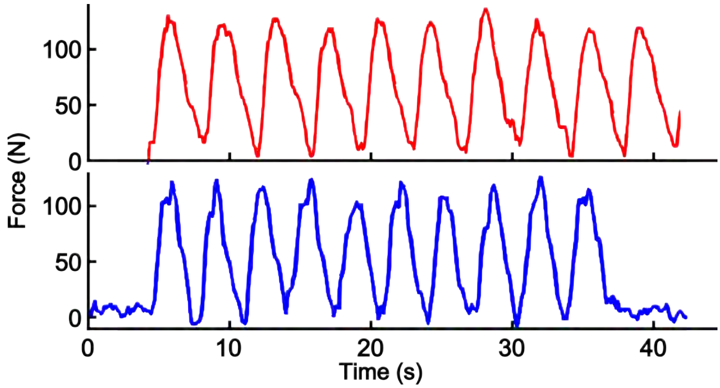

Figure 3.20: The actuator force during 10 open/close cycles of the pneumatic cylinder (red) and the DC motor (blue).

Speed

The differences in the speed of both actuators can be best evaluated by looking at the characteristics of the hand positions over time. The DC motor operates reliably and constantly at its maximum speed of 8.57 mm/s, both when opening and closing the hand. The pneumatic actuator's top speed is almost twice that of the DC motor, but it suffers from its unidirectional action; while the opening of the hand happens within 0.6 seconds, waiting for the CO_2 to vent from the cylinder and the spring to close the hand takes up to 3 seconds. This can partly be attributed to the two-way valve used in the experiment, which was designed previously for a toddler size prosthetic hand mechanism [73], and is not optimized for its current application.

Responsiveness

After the pneumatic actuator's two-way valve is opened, it takes approximately 0.3 seconds for the pressure in the cylinder to overcome the force of the closing spring, and start to open the hand. In contrast, the DC motor reacts almost immediately to an activation signal. This is a significant advantage, as low activation delays are considered important to prosthesis users [1].

Capacity

The capacity of the Li-Ion-based Otto Bock Energypack was sufficient for 2000 open/close cycles, which is roughly half the number calculated in Section 3.2.3. This discrepancy was likely caused by friction losses in the transmission, which were not taken into account. For the pneumatic system a single CO_2 cartridge has been observed to last for 300 grasping cycles, which slightly exceeds the preliminary calculations in Section 3.2.3.

In [77], the number of active uses of a myoelectric prosthesis was found to be around 41 per hour. With this frequency of operation, the DC motor would be usable for an entire day, while the pneumatic cylinder would have to be replaced at least once.

The most noticeable difference between these two for normal operation is that the Li-Ion battery is rechargeable, while the pneumatic cylinders are disposable. It is easy to carry a few spare gas canisters around and quick and simple to replace them, while recharging the battery can take several hours. It should be noted that large numbers of these canisters would be required for continuous use of the prosthesis.

Other metrics

While for this experiment a relatively large and heavy DC motor was chosen (see Table 3.6), other commonly used DC motors are still larger and heavier than the pneumatic cylinder, especially considering the added transmission larger energy storage.

The continuous noise the DC motor generates is much louder than that of the pneumatic actuator, which only produces a hissing sound when venting the cylinder. The sound of escaping CO_2 would also be easier to dampen out or displace when implemented in an actual prosthesis. Grasping an object did not have any effect on either actuator's performance; because the prosthesis contains a voluntary open mechanism, grasping an object does not lead to additional load on the actuators.

3.2.6 Conclusion

For hand prosthesis applications, a thin-walled pneumatic cylinder actuator can compare favorably in performance to commonly used DC motors. The pneumatic cylinder offers equal forces and higher closing speeds, with a mass over 10 times less than the average DC motor. Drawbacks of the current design are a slower return speed and unidirectionality of actuation. To remedy this, the cylinder can be redesigned to enable double action, and the valve design can be optimized for increased gas flow.

The gas cartridges used for pneumatic energy storage are smaller and lighter than their electrical equivalent as well, and though their energy capacity is an

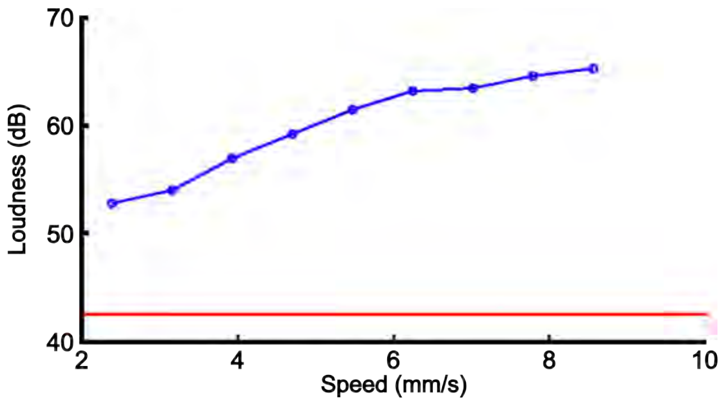

Figure 3.21: The A-weighted volume of the DC motor corresponding to various spindle speeds is shown in blue. The volume (in dB) of the pneumatic cylinder is shown in red.

order of magnitude less than that of commonly used prosthesis batteries, the prosthesis should last up to 8 hours on a single cartridge.

In general, the low mass, small size, and fast action of a pneumatic cylinder makes it an attractive option for actuation of modern hand prostheses. With an improved cylinder design and the addition of miniature solenoid valves, a pneumatic system can be created which outperforms current electric devices, enabling lighter and smaller hand prostheses.

3.3 Sensors

3.3.1 Force

Force sensors for a hand prosthesis should be located where contact with the environment or objects is most likely. For precision grasps such as the lateral and tripod grasps, this contact area is located on the tips of the fingers, but for the cylindrical grasp it can cover the entire palmar surface of the hand. However, placing sensors mainly in the fingertips uses the available space there optimally and still provides relevant information during all three grasps.

BioTac The BioTac system is designed to imitate the human fingertip's sensory capabilities and mechanical properties. Its rubber skin is covered with ridges to increase contact friction, and filled with a liquid which transmits external forces and vibrations from the skin to a sensorized core. This core contains 19 electrodes that measure the magnitude and location of pressure, a single high-frequency pressure sensor to detect vibrations, and a temperature sensor. The advantages of the BioTac system are its high sensor density and human-like fingertip texture, but the relatively high size of the complete system and passive distal joint may hinder integration into an anthropomorphic hand prosthesis.

Takktile The Takktile sensor system is an adaptation of an off-the-shelf atmospheric pressure sensing IC, covering these sensors in urethane rubber to measure forces on the surface of the rubber. An array of these sensors can be indexed via I^2C multiplexer ICs, which can provide a contact location capability similar to the BioTac. The rubber covering of the sensors can be molded into any shape, allowing them to function as complete fingertip replacements. The rubber also improves the grasp quality of the fingers. Although the quality of the Takktile sensors is lower than that of the BioTac, the Takktile sensors have significant flexibility in their application.

3.3.2 Position

Determining the pose of the hand requires the angles of its joints to be known. Joint angles can determined by means of integrated Hall sensor/permanent magnet pairs; the Hall sensor measures the strength of the magnetic field, from which the distance to the magnet can be derived. An advantage of these is that contact between the two components is not necessary and they can be placed relatively freely. However, both ferromagnetic materials and external magnetic fields can disturb the field strength reading.

Flexure sensors measure the change in resistance caused by bending of the sensor. If flexure sensors are wrapped around each joint, the bending of the sensor correlates to a change in joint angle. This solution is less sensitive to external factors, especially if the sensor is made part of a bridge circuit. With both of these systems, regular calibration is required. Using an angular encoder circumvents this requirement, but such systems would need to be attached to the side of the joint, where little room is available.

3.3.3 Actuators

Most DC motors can be fitted with an integrated hall sensor system to determine the position of the motor shaft. Current through the motor can be measured by means of a shunt resistor, the voltage over which is an indicator of the current.

For a pneumatic actuator, the exerted force can be measured by a strain gauge or load cell, depending on whether the actuation relies on tension or compression. The position of the actuator lies along a linear path, and can therefore be determined by a hall sensor as well.

Chapter 4

Two-fingered prototype development

For the development of a control system and further evaluation of the mechanisms developed in Chapter 3, a physical prototype should be constructed. The mechanical design of the prototype will focus on obtaining minimal actuation and restoring DOF control with integrated joint locks. The requirements of the prototype can be summarized as follows:

- The prototype should have human-like fingers capable of grasping an object.
- A single actuator should be connected to all joints.
- Locking mechanisms should be present on all joints.
- Force and joint angle information should be available to the control system.

A two-fingered prototype design with 2-DOF fingers has been chosen, allowing objects to be held with both precision and power grasps. The prototype also contains the first iteration of a two-tiered control system based on EMG sensing and compliant interaction. This chapter has been published as “Development of Underactuated Prosthetic Fingers With Joint Locking and Electromyographic Control" [19].

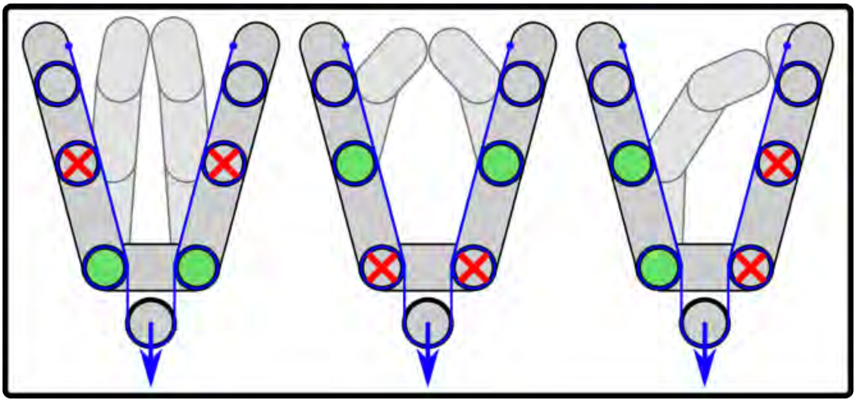

Figure 4.1: Various finger trajectories that can be attained in a two-fingered, underactuated hand by means of joint locking. The paths of the actuator tendons are shown as blue lines. Red crosses indicate locked joints, and green circles indicate unlocked joints.

4.1 Introduction

Modern hand prostheses are becoming more and more anthropomorphic in their design [51, 52, 53]. The most daunting aspect of this trend is the increase in degrees of freedom (DOFs) that have to be actuated and controlled. DC motors are the most common type of prosthesis actuator, and only a few of these large and heavy actuators can be placed inside the palm of the hand.

This can be remedied by actuating multiple degrees of freedom with a single actuator, a technique known as underactuation. This technique has been implemented in other prosthesis projects with varying results. A linkage, such as that implemented in the Southampton hand [23], couples the finger joints' motion using rigid bars. This allows the more distal joints of the finger to flex when the proximal joints' movement is obstructed. To couple multiple finger linkages, a whippletree mechanism can be implemented, which distributes the actuator force appropriately. The movement pattern of the fingers can be influenced by changing the structure of the linkage.

Underactuation can also be achieved via a series of freely rotating pulleys on each joint, which are connected by way of a single communal tendon [22]. Since this system can only apply forces along the flexion direction due to the nature of the tendon, a second tendon or extension springs are required to allow full motion of the finger. The finger's flexion motion depends on the friction and external forces on the joints, but can also be influenced by the relative radii of the pulleys.

An alternative to the underactuation of multiple joints is the inclusion of passive or coupled joints [24]. The distal interphalangeal joints are often implemented as such, because the angle between the distal and medial phalanges is also strongly coupled in the human hand. Similarly, the movement of the little and ring fingers can be coupled while still resembling the human hand's freedom of motion.

Another advantage of some of these systems is that the finger will flex in such a way as to accommodate the shape of a grasped object. However, the main drawback of these underactuated systems is the loss of control over the fingers' motion; in free space, such underactuated fingers will follow a set trajectory determined by their mechanical structure. In modern commercial prostheses with underactuated fingers [51, 52, 53] this trajectory is designed to be usable for both power and precision grasping, but is less then ideal for either.

The ability to selectively disable the motion of certain joints allows a hand to match the fingers' trajectory to the grasp type selected by the user, as seen in Figure 4.1. Also, the motion of certain fingers can be completely disabled, which allows all fingers to be connected to a single central actuator. There has been some research on mechanisms that passively disengage joints [55, 56], as well as active electrostatic joint locking on robotic grippers [78]. In Peerdeman et al. [16], the use of miniature mechanical joint locks is explored for use in hand prostheses. The limitations imposed by an anthropomorphic hand prosthesis lead to a lock actuation system integrated into the phalanges of the fingers, as well as a lock design which eliminates the need for continuous actuation.

We have implemented these joint locks, based on a friction amplification principle (see Figure 4.2), in human-sized fingers. The locks are actuated by solenoids integrated into the body of each phalanx. Though these solenoids provide only a minimal stroke and force, these are sufficient due to the self-locking properties of the friction lock.

When making a prosthesis with a large number of available DOFs, it is important to consider their controllability by the user as well. Detection of myoelectric (ME) signals is the most common method of control for modern externally actuated hand prostheses [1]. It is a non-invasive method of obtaining signals directly correlated to muscle activity, though current classification methods only allow a few usable control signals to be distinguished. This control bottleneck strongly limits the variety of prosthesis motions that can be achieved. To compensate for this, a control system can be constructed around a discrete selection of grasp types, which can be selected and activated manually; the execution of these grasps will be done automatically.

In this article, the mechanical design of a new two-fingered prosthesis prototype is described, using tendon-pulley underactuation and joint locking. An ME

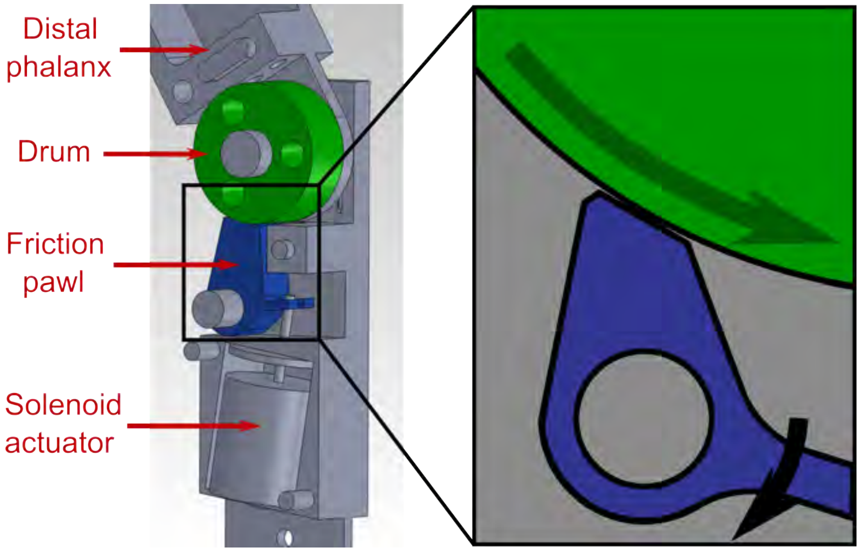

Figure 4.2: **Friction amplification joint locking concept:** If the friction pawl is brought into contact with the drum by the solenoid actuator, friction between pawl and drum will pull the two together, locking the joint.

control system is implemented as well, using electromyographic (EMG) signals to control various grasp types and motions of the prototype. In Section 2, the structure of the prototype is described, from the design of the phalanges to the joint locking and actuation systems. Section 3 describes the implementation of the control system, consisting of an EMG classifier, high-level grasp planner, and low-level finger controller. In Section 4, the experimental setup and test protocol are described. The results are shown in Section 5. A discussion of the results is found in Section 6, as well as the conclusion and directions for future work.

4.2 Mechanical design

The design of the prosthesis prototype is based on achieving a large variety of finger motions with minimal actuation. The prototype consists of two fingers with two flexion/extension DOFs each, which are connected by a single tendon to the main actuator; a diagram of the prototype is shown in Figure 4.3. The under-actuated nature of this tendon-pulley system precludes individual control of the fingers' DOFs. This is compensated for by including joint locking mechanisms to block the flexion motion of specific joints, while leaving the others free to move. By locking different combinations of joints, the fingers can be made to perform a variety of flexion trajectories relevant to grasps in activities of daily living [1].

4.2.1 Finger structure

The external dimensions of the finger need to be close to those of the human finger, for reasons of usability and cosmetic appearance. This puts tight constraints on the size of the joint locking mechanism and its actuators. Therefore, a finger joint diameter of 15 mm is chosen. The phalanx dimensions can be found in Table 4.1, and for reference, phalanx dimensions for a male index finger are shown in Table 4.2. The internal structure of one of the fingers' medial and proximal phalanges is shown in Figure 4.4. Each actuated joint contains a freely rotating pulley, a drum for the joint locking mechanism, and a rotational spring to provide an extension force. The phalanges are constructed out of aluminum, whereas the joint shafts and lock components are made of (hardened) steel.

4.2.2 Joint locking

In Peerdeman et al. [16] two joint locking concepts were evaluated; a gear-based system and a friction-based system. The gear-based system has an inherent indexing resolution and was found to require a higher actuation force. Therefore, the friction-based mechanism has been chosen for the prototype. The principle of friction locking is illustrated in Figure 4.2. This mechanism consists of two main components: a drum fixed to the distal phalanx of a joint, and a friction pawl connected to the proximal phalanx. The friction pawl can be rotated around its pivot by the lock actuator. When the friction pawl is brought into contact with the drum, the rotation of the drum will pull the pawl closer to it, increasing the friction force between both until the joint's motion is completely blocked. This self-locking property means actuation is only needed to bring the lock parts into contact, which reduces the actuator requirements. Once the actuation force is removed from the joint, an extension spring will separate the drum and pawl, releasing the lock.

Table 4.1: Dimensions of the prototype's phalanges.

Phalanx	Length (mm)	Width (mm)	Height (mm)
Distal	28	15	15
Medial	33	18	17
Proximal	50	18	15
Metacarpal	42.5	18	15

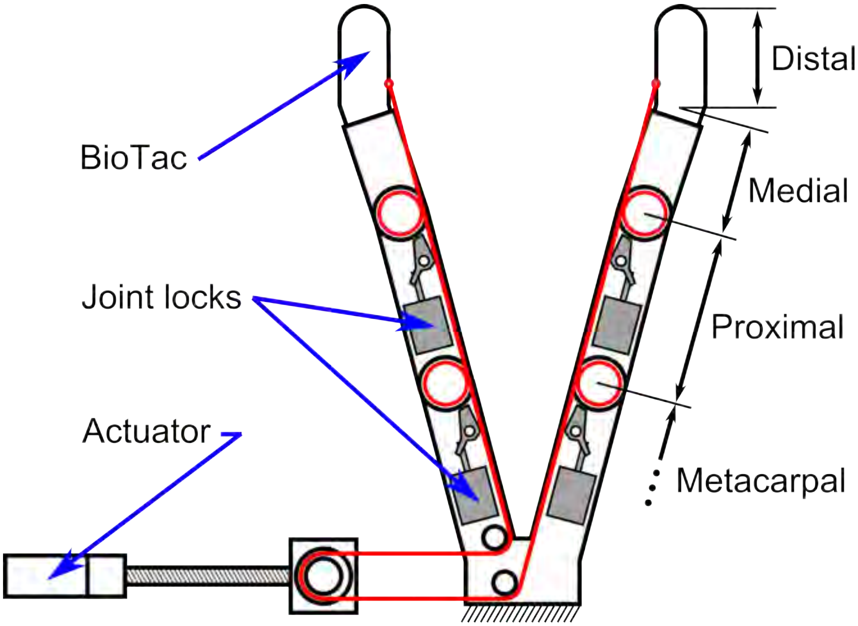

Figure 4.3: The two-fingered prototype, showing internal mechanisms and tendon routings. The phalanges are indicated on the right, while their dimensions are listed in Table 4.1.

Based on initial test results, a new set of friction pawls has been designed for implementation in a phalanx-sized enclosure. The contact surface of these pawls follows a logarithmic spiral around its rotation axis [16], as shown in Figure 4.5. The effect of this surface is shown in Figure 4.5 as well: the effects of changes in the distance between drum and pawl (due to play and tolerances in the components, for example) on the contact angle are minimized.

4.2.3 Actuation

The two fingers of the prototype are actuated by a single DC motor. The motor is a Maxon EC-max 22 (Maxon Motor AG, Sachseln, Switzerland) connected to

Table 4.2: Average dimensions of male index phalanges, with a hand length of 195 mm and breadth of 88.5 mm [57].

Phalanx	Length (mm)	Width (mm)	Height (mm)
Distal	18.9	16.4	13.7
Medial	27.9	18.2	16.3
Proximal	47.8	18.5	18.7

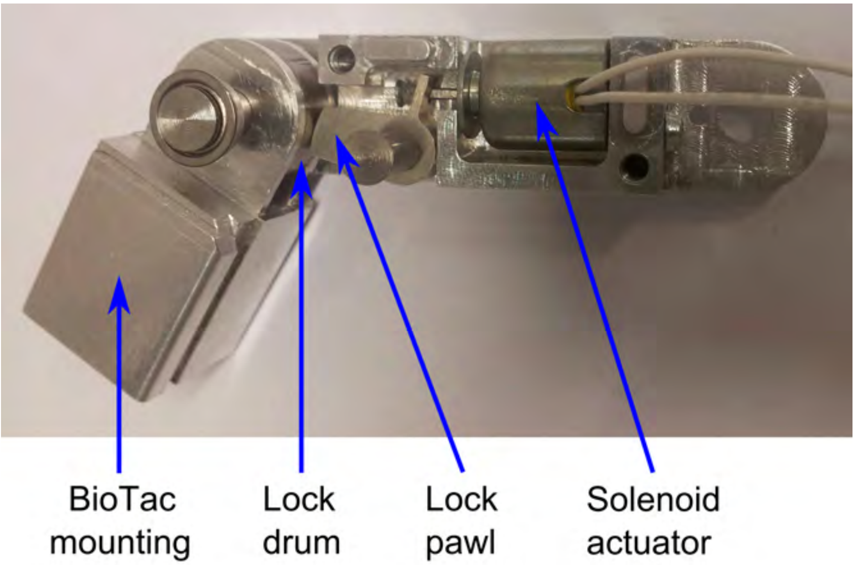

Figure 4.4: Internal structure of one of the fingers' medial and proximal phalanges, showing the friction lock components.

a spindle drive for translational motion. This motor moves a pulley block, which actuates the single flexion tendon routed around all the joint pulleys, as seen in Figure 4.3. The joint locks can then be used in order to actuate only a single finger or enable different grasp types. The locks themselves are each actuated by an in-phalanx pull-type solenoid with extension spring.

4.2.4 Sensors

Effective control of the fingers requires that force and position information be made available to the control system. To this end, each joint contains a Hall-effect based angle sensor, which can be used to determine the pose of the finger. The medial phalanx of each finger is an adapter for a BioTac tactile sensor system (SynTouch LLC, Los Angeles, CA, USA) [79]. The BioTac sensor replaces the distal phalanx of each finger, as shown in Figure 4.6. The device features two sensing modalities relevant to prosthesis control: a series of 19 electrodes that collectively determine the magnitude and location of external pressures on the fingertip, and a main pressure sensor that detects high-frequency variations in the applied pressure. With this information, it is possible to automatically control the fingers' interaction with the environment. However, the user should also be able to control the automated motion of the fingers. Therefore, a two-level control

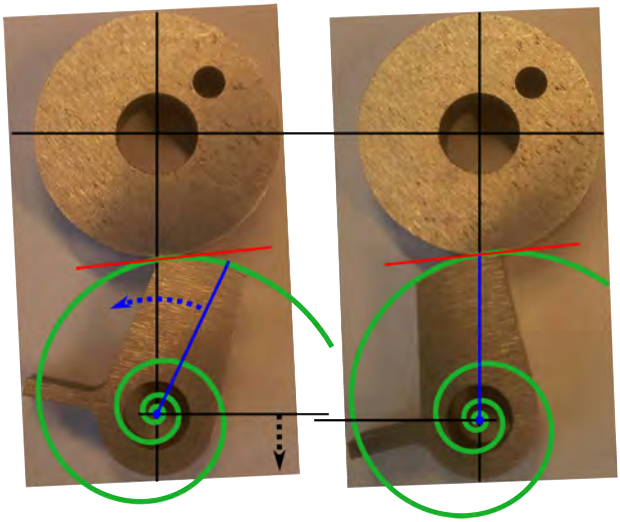

Figure 4.5: **Demonstration of the effect of the logarithmic spiral surface:** Changes in the distance between the rotation axes of the drum and the pawl (black arrow) are compensated by rotation of the pawl (blue arrow), without affecting the contact angle (red line). The green line illustrates the spiral curve.

system has been implemented, which is discussed in the next section.

4.3 Control

The prototype's control system is based on a previously developed controller, which was used on the University of Bologna (UB) Hand IV in Peerdeman et al. [17]. The prototype's range of motions is divided into distinct grasp types, which can be used to grasp a variety of objects, as seen in Figure 4.7. The following grasp types are derived from a general set of activities of daily living [1]:

- Cylinder grasp: For this power grasp the thumb is opposed to the other fingers, and the object to be grasped is surrounded by the hand.
- Lateral grasp: In this grasp, the fingers are fully flexed, and the unopposed thumb is used to hold flat objects such as keys or cards.
- Tripod grasp: This precision grasp uses the index and middle fingers opposed to the thumb. The fingers' distal and medial joints remain extended, while the proximal joints are flexed.

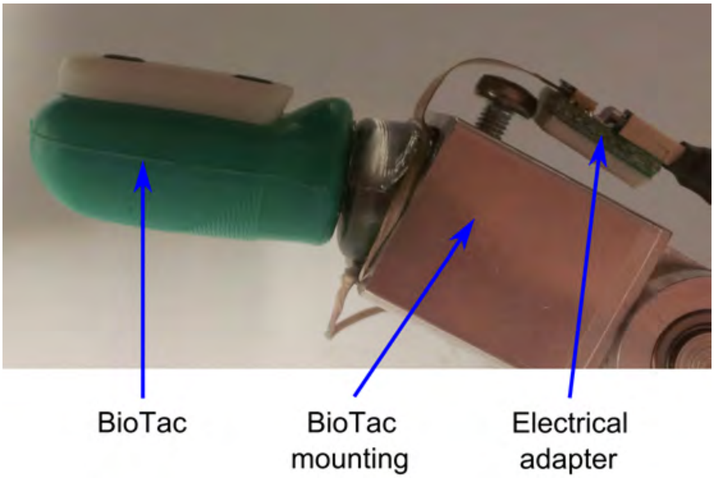

Figure 4.6: Close-up of the distal and medial phalanges of the prototype finger, showing the BioTac sensor, its mounting, and its electrical adapter.

These grasp types cannot be effectively reproduced on the two-fingered prototype. However, each of these grasp types requires different joint locking configurations and finger trajectories, which can be demonstrated:

- Cylinder grasp: No joints are locked; the fingers show normal underactuated behavior. This allows the grasping ability of the finger to be evaluated.
- Lateral grasp: In this grasp, it is important to exclude certain fingers from the grasp motion at different times. One finger will be completely locked, while the other finger remains free to move. This configuration shows that multiple fingers can be individually actuated by a single motor.
- Tripod grasp: This grasp requires the actuation of only the proximal joints; the distal joints will be locked. This demonstrates the ability to increase the controllability of underactuated fingers by temporarily reducing their DOFs.

For the remainder of the paper, the grasp types will be used to refer to these locking configurations. EMG signals from the user are used to select one of these grasp types, and to determine when to open and close the selected grasp. Once a grasp has been selected, the high-level controller plans the grasp, actuating the joint locks based on the motion of each of the fingers. Then, the low-level controller uses the DC motor to control the fingers to the desired end positions with the appropriate forces.

4.3.1 EMG classification

EMG classification is used to couple the activation of different muscle groups in the forearm to the input signals of the high-level control system. Boere et al. [80] used multi-channel EMG to classify up to eight different muscle contraction types by means of an electrode array placed on the forearm. Based on this system, an EMG classifier has been developed using pre-recorded test data. In order to control the prototype, six different signals need to be identified:

- *Cylinder*: This signal selects a grasp without any joint locking.
- *Lateral*: With this signal, all joints of one finger are locked.
- *Tripod*: This signal locks the proximal joints of each finger.
- *Close*: To flex the unlocked joints of each finger.
- *Open*: To extend all finger joints.
- *Stop*: To abort the grasp and return the hand to its fully extended position.

Each of these signals corresponds to a certain muscle contraction type. A test set is constructed from a series of known pre-recorded signals. This test set is used to train a linear discriminant analysis classifier [80]. This classifier can then be used to identify the signal type of a new contraction signal.

4.3.2 High-level control

Considering the limits of EMG classification, the high-level control system should be operable with only a few input signals. This can be accomplished by combining user-controlled and automated actions to perform a grasp. The grasp type is actively selected by the user, but execution of the grasp is performed automatically once a closing signal is received; this keeps grasp control intuitive to the user. The possible actions of the prototype are organized in a state machine, which can be seen in Figure 4.8. The states are described as follows:

- **Preshaping**: Once a grasp type signal (*Cylinder*, *Lateral* or *Tripod*) is received, the system moves to this state immediately. The joint locks are automatically moved into the right positions for the desired grasp. Once the locks are in position, the system moves to the **Ready** state.
- **Ready**: In this state, the hand remains in the preshaping position. Once a *Close* signal is received, the system moves to the **Closing** state.

- **Closing**: The grasp is automatically closed. If the user wishes to stop the grasp, an *Open* signal will move the system to the **Opening** state to extend the fingers. Once each finger involved in the grasp reports sufficient external force to establish contact, the system moves on to the **Hold** state.

- **Hold**: The fingers will automatically exert a constant force on the held object. If the user gives an *Open* signal, the system moves to the **Opening** state and the object is released.

- **Opening**: This state ends the grasp by automatically extending the involved fingers. The system moves to the **Ready** state once the fingers are fully extended.

4.3.3 Low-level control

The low-level controller is tasked with moving the fingers to their desired positions, while applying the proper forces to any external obstructions. Initially, a force controller was implemented, which moves the fingers at a fixed velocity while no external forces are present. Once contact is established, the fingertip force is controlled to a set value.

However, impedance control is a more appropriate way of approaching interaction with the environment [81, 17], and therefore such a controller has been implemented on the prototype instead. The controller derives the force to be applied to the fingers ($\mathbf{F}$) from the difference between their desired state ($\mathbf{x}_d, \dot{\mathbf{x}}_d$) and measured state ($\mathbf{x}, \dot{\mathbf{x}}$) as follows:

$$\mathbf{F} = \mathbf{D}(\dot{\mathbf{x}}_d - \dot{\mathbf{x}}) + \mathbf{K}(\mathbf{x}_d - \mathbf{x}) \tag{4.1}$$

If EMG amplitude information is available, the user can control the applied force directly by changing the value of the controller's stiffness ($\mathbf{K}$) or damping ($\mathbf{D}$) constants.

4.4 Experiments

This section describes the experimental setup, as well as the experiments used to evaluate the prototype's mechanical design and control system.

Figure 4.7: Three objects used in the grasping experiments. From left to right: mug, box, and USB flash drive.

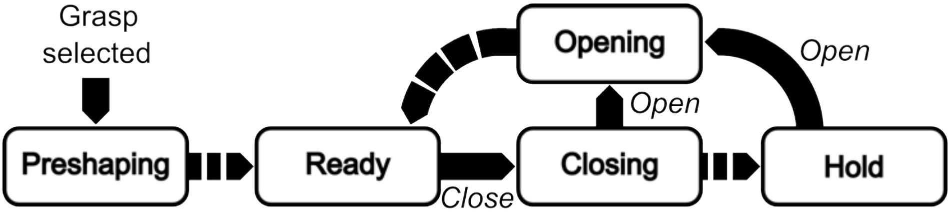

Figure 4.8: **Grasp control state machine:** Dashed arrows are automatic state changes, while the *Open* and *Close* signals originate from the electromyographic classifier.

4.4.1 Experimental setup

The experimental setup consists of the two-finger prototype, its actuation systems (DC motor and solenoids), and its sensing systems (Hall sensors, BioTacs). These are connected to a National Instruments ELVIS DAQ device (National Instruments Corporation, Austin, TX, USA), which is controlled via Matlab (The MathWorks, Inc., Natick, MA, USA). An image of the two-finger prototype indicating relevant subsystems can be seen in Figure 4.9.

4.4.2 Test protocol

Control system

The performance of the EMG classifier and the high-level state machine controller are evaluated by supplying pre-recorded EMG signals to achieve a sequence of grasping motions. These sequences are geared towards basic activities of daily living [1]. The EMG classifier's accuracy and response time are significant parameters, and are tested by repeatedly classifying a random sequence of pre-recorded EMG signals. In earlier research on similar classification by Boere et al. [80], the accuracy was found to exceed 90%. The high-level state machine is evaluated by inspection, and the execution time of the entire control system is measured as well.

Joint locking

The properties of the joint locking system are evaluated by locking different combinations of joints, and observing the resulting finger trajectories without obstructions. Repeated execution of these motions is used to investigate the effectiveness of the locks, as well as the consistency of the trajectories. Important considerations are the compliance of locked joints, which can be caused by play in the locking mechanism [16], and the locks' behavior at high joint torques.

Grasping

The pose of the prototype's fingers and the forces exerted on them are evaluated during grasping. The joint locks and DC motor are controlled to accomplish different grasp types. Although the grasp types used here are a simplification of those used with an anthropomorphic hand prosthesis, the basic variations that are tested here can be combined to allow a single main actuator to perform cylinder, tripod, and lateral grasps with five fingers as well.

An object is placed in between the fingers, and the joint angles and fingertip forces are measured using the Hall sensors and BioTacs, respectively. A specific object is chosen to illustrate the applications of each of the three grasp types: a mug for the cylinder grasp, a small box for the tripod grasp, and a USB flash drive for the lateral grasp.
These objects are shown in Figure 4.7.

4.5 Results

This section summarizes the results of the experiments mentioned in Section 4.4, evaluating the control system, joint locking mechanism, and grasp performance of the prototype.

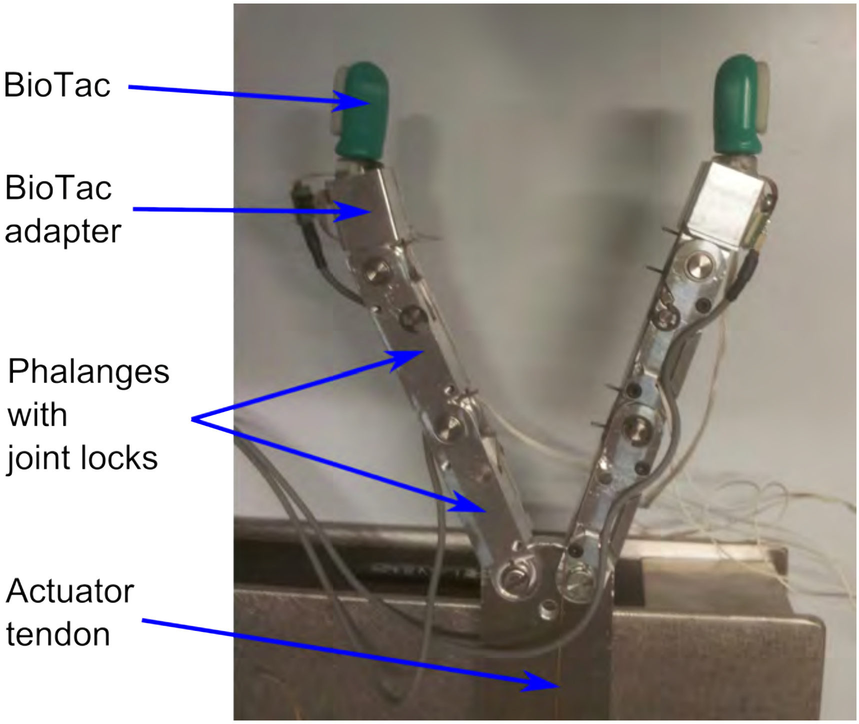

Figure 4.9: Two-fingered prototype experimental setup: Actuation is provided externally, by a DC motor and spindle drive connected to the actuator tendon.

4.5.1 Control system

Electromyographic classification

In these experiments, the accuracy and processing time of the EMG classifier are evaluated. A test set is created from a 90 s training recording divided into 50 ms windows, with the associated classes known in advance. This test set is used to train the classifier; afterward, another window can be loaded, and the appropriate class is determined.

The performance of EMG classification is tested by entering a set of 25 random EMG windows into a trained linear discriminant analysis classifier 100 times. The results of one of these tests can be seen in Figure 4.10. The average accuracy of the classifier was found to be 92.53%, with the average classification time for a single set being 1.6 ms. This computation time is negligible compared to the window size required for classification. The only significant time delay in the high-level control state machine was found between moving the state machine to the **Closing** or **Opening** states and the start of motor activation, which takes

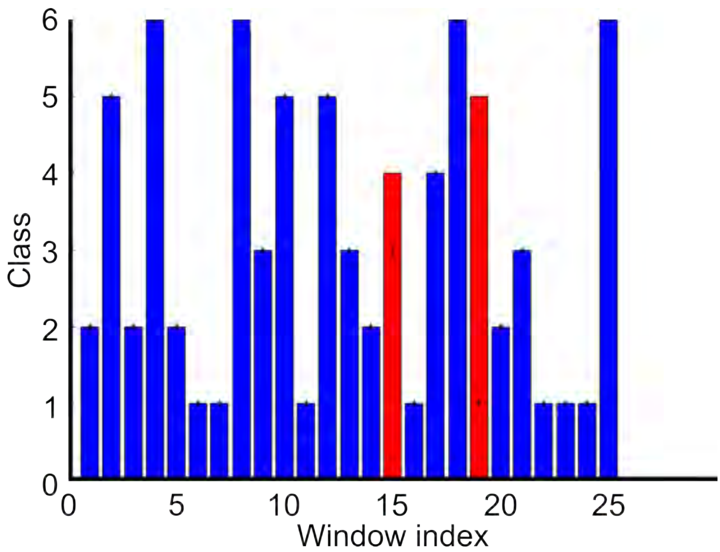

Figure 4.10: **Control system experiment:** A test of the linear discriminant analysis classifier with a set of 25 random electromyographic signal windows [80]. Blue bars denote correct classifications; red bars denote errors.

approximately 96 ms.

4.5.2 Joint locking

To evaluate the functionality of the joint locks, the cylinder, tripod, and lateral grasps are performed without an object to grasp. The fingers are controlled to stop as soon as contact between the fingers is detected. The results of these tests can be seen in Figure 4.11. In the cylinder and lateral grasps, the joint angles of the freely moving fingers tend to stay equal. In the case of the tripod grasp, the joint locking ensures the proximal joint moves further than the locked distal joint. In both the lateral and the tripod grasp movement of the locked joints is still noticeable, though limited to 10 and 15 degrees, respectively. In general, even without object interaction, the functional differences between the three grasp types can be observed. Therefore, the joint locks can be considered an effective method of improving the range of motion of underactuated fingers.

4.5.3 Grasping

In these experiments, the grasping performance of the prototype is evaluated. The three grasp types are performed on various objects seen in Figure 4.7.

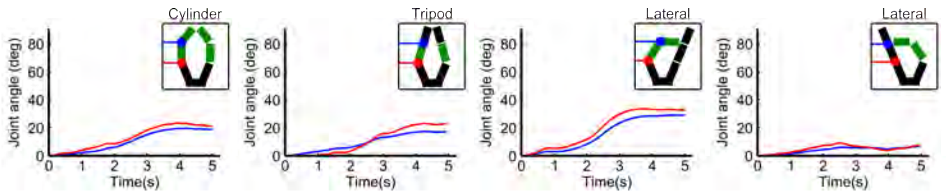

Figure 4.11: **Joint locking experiment:** The cylinder, tripod, and lateral grasps performed without grasping an object. The graphs indicate the fingers' joint angles: the blue line represents the distal finger joint, and the red line represents the proximal finger joint. For the lateral grasp, the locked finger's joint angles are also shown in the far right graph. The pictographs indicate the grasp type: green phalanges are in motion, and black phalanges are fixed.

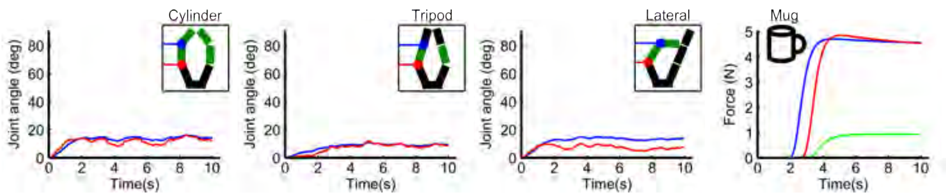

Figure 4.12: **Grasping experiment 1:** The cylinder, tripod, and lateral grasps performed on the mug object, showing joint angles and fingertip forces. The lateral grasp's locked finger is omitted, as its joint angles are the same as in Figure 4.11. In the joint angle graphs, the blue line represents the distal finger joint, and the red line represents the proximal finger joint. For the fingertip forces, the blue line represents the cylinder grasp, the red line represents the tripod grasp, and the green line represents the lateral grasp. The pictographs indicate the grasp type: green phalanges are in motion, and black phalanges are fixed.

Grasping experiment 1 (Grasping the mug object)

The results of this experiment can be seen in Figure 4.12. Because of the mug's size, the joints do not move more than 15 degrees. In the cylinder grasp both joints move roughly equally in the unlocked situation, and a stable grasp is established within approximately 1 s after contact. For the tripod grasp the distal joints are locked, though some joint motion can still be observed. This is due to the joint compliance mentioned in Section 4.4.2. However, in this case the locking of the distal joints has little effect on the performance of this grasp. The left finger is locked entirely for the lateral grasp. The unlocked finger pushes the mug towards the base of the locked finger, and the resulting grasp is unfit for picking up the mug.

Grasping experiment 2 (Grasping the box object)

The results of this experiment can be seen in Figure 4.13. In the cylinder grasp both joints initially move together, as with grasping the mug, but as soon as contact is established the proximal joints are extended in favor of continued distal joint flexion. This is a consequence of the fingers' underactuation and will destabilize the grasp, as only the tips of the fingers stay in contact with the object. With the tripod grasp, the locked joints prevent the proximal joints from being extended, which results in a stable grasp requiring less force. The proximal joint rotation is also higher than in the cylinder grasp, and does not reverse after contact. However, the residual compliance of the joint locks still allows the distal joints to flex up to approximately 20 degrees. During the lateral grasp the active finger shows similar behavior to the cylinder grasp, but the grasp requires less force because of increased fingertip contact with the object. The locked finger still has some compliance, but does not contribute to the grasp.

The difference between the cylinder and tripod grasp types is shown in more detail in Figure 4.14. First, a cylinder grasp is performed on the box object. Because none of the joints are locked, the finger's underactuation causes it to continue flexing after contacting the object, which leads to an unstable grasp. Afterward, the distal joint of each finger is locked to achieve a tripod grasp; this results in a firm hold on the object.

Grasping experiment 3 (Grasping the USB drive object)

The results of this experiment can be seen in Figure 4.15. With the cylinder grasp, the smaller size of the object increases the problems experienced during grasping of the box, which results in repeatedly dropping the USB drive. The cylinder grasp is therefore unfit for this object. For the tripod and lateral grasps, the only difference is additional joint flexion due to the object's smaller size; the grasp stability and fingertip forces are unaffected.

4.6 Discussion

In this section, the results are used to evaluate the general grasp performance of the prototype, as well as its individual subsystems.

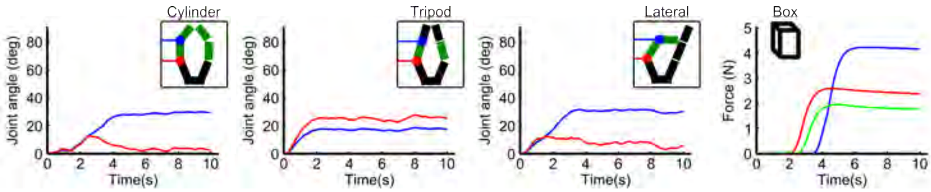

Figure 4.13: **Grasping experiment 2:** The cylinder, tripod, and lateral grasps performed on the box object, showing joint angles and fingertip forces. The lateral grasp's locked finger is omitted, as its joint angles are the same as in Figure 4.11. In the joint angle graphs, the blue line represents the distal finger joint, and the red line represents the proximal finger joint. For the fingertip forces, the blue line represents the cylinder grasp, the red line represents the tripod grasp, and the green line represents the lateral grasp. The pictographs indicate the grasp type: green phalanges are in motion, and black phalanges are fixed.

4.6.1 Experiments

Control system

The EMG classifier showed an accuracy of over 90%, though it could still lead to occasional missed or misinterpreted commands. This can be addressed by evaluating several 50 ms signal windows for a single command, increasing the reliability of the classifier. The time required to evaluate a signal window was shown to be negligible relative to the length of the windows themselves. The high-level controller was functional in allowing the user to engage and release the chosen grasp, though qualitative evaluation of the system would require additional test subjects. The time delay between switching to the **Closing** or **Opening** state and actual motor activation can reduce the intuitiveness of the system and should be minimized. The low-level controller was able to reliably stabilize the applied grasping force based on the BioTac's sensor data, irrespective of the orientation of the fingertips with regard to the object.

Joint locking

The results show the effectiveness of the joint locks in establishing different grasp types. Also, they prevent motion of the fingers after establishing contact due to the fingers' underactuation. The different objects used in grasp testing also illustrate the use of different grasp types for activities of daily living. The joint locks did show between 10 to 15 degrees of compliance before joint motion stopped, though this did not prevent any of the grasp types from being performed.

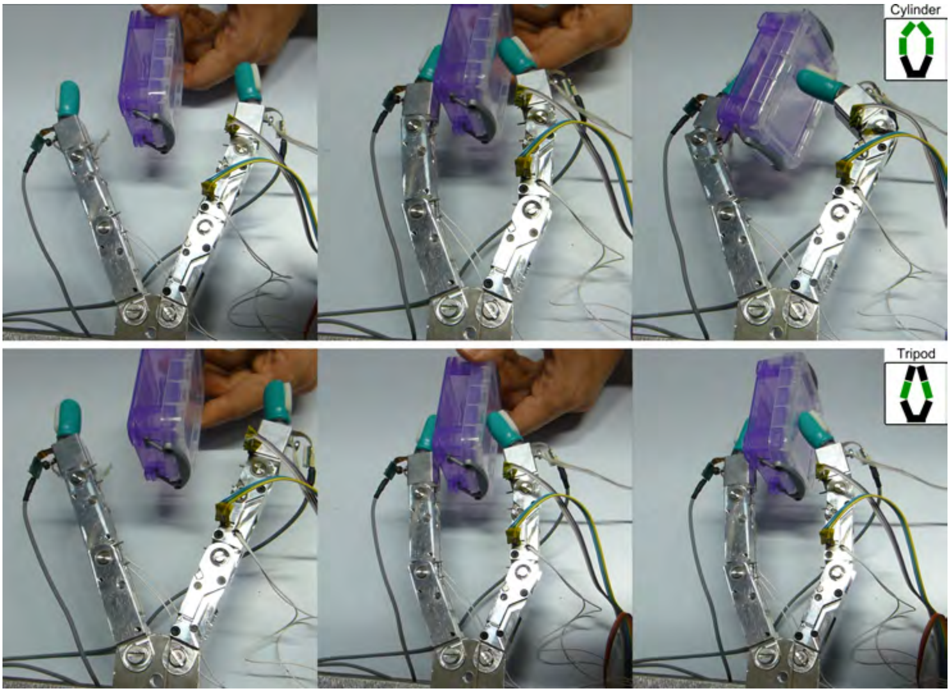

Figure 4.14: Video frames of the box object being grasped with a cylindrical grasp (top) and a tripod grasp (bottom). For each grasp, the image frames are spaced 1 second apart. The pictographs indicate the grasp type: green phalanges are in motion, and black phalanges are fixed.

Grasping

Stable grasps were established for 7 out of 9 combinations of grasp types and objects. A notable exception to this is the cylinder grasping of the box object, because the fingers' underactuation prevented the fingertips from establishing proper contact with the box. The forces exerted on the objects varied between 5 N for the mug, and 2 N for the USB drive. In general, applying the proper grasp type to either of the objects demonstrated the effectiveness of offering a variety of grasps, as lower forces and stable grasping could be achieved. The average time required to complete a grasp was approximately 1.5 seconds, depending on the size of the object and grasp type used.

4.6.2 Conclusion

The combination of EMG classification, high-level grasp planning, and low-level finger control provides an accurate and simple way of controlling a prosthesis'

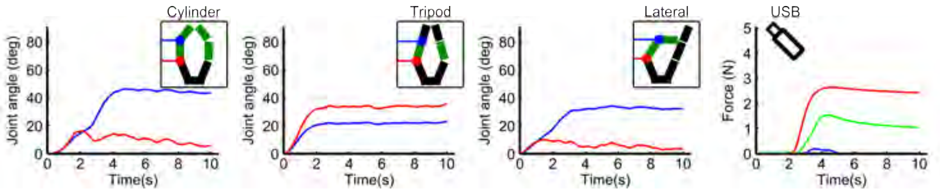

Figure 4.15: **Grasping experiment 3:** The cylinder, tripod, and lateral grasps performed on the USB drive object, showing joint angles and fingertip forces. The lateral grasp's locked finger is omitted, as its joint angles are the same as in Figure 4.11. In the joint angle graphs, the blue line represents the distal finger joint, and the red line represents the proximal finger joint. For the fingertip forces, the blue line represents the cylinder grasp, the red line represents the tripod grasp, and the green line represents the lateral grasp. The pictographs indicate the grasp type: green phalanges are in motion, and black phalanges are fixed.

automated grasping motions. With a combination of cylinder, tripod, and lateral grasps, a variety of objects can be picked up and most activities of daily living can be performed. In the two-fingered prosthesis prototype, these grasp types are executed with a single main actuator, due to the inclusion of joint locking mechanisms. Implementation of these control systems and mechanisms would decrease the size and weight of a prosthesis by reducing the number of actuators, while still allowing for multiple different flexion trajectories for each finger.

4.6.3 Future work

In order to expand this prototype to a five-fingered, anthropomorphic hand prosthesis, the actuation system will require the most attention. Though the joint locks reduce the number of actuators needed, a system is needed to distribute the actuator force across all fingers. The development of a thumb opposition system will also be necessary, which may require separate actuation from the main grasping system. A new main actuator should also be investigated, as increasing the speed of grasping is a priority.

Patient interaction with the system should be investigated for a proper evaluation of the control system's intuitiveness. This would also allow for real-time EMG data to be evaluated. The current implementation of the low-level controller would be unfit for coordinated grasp control with five fingers; an intrinsically passive controller could be adapted to improve this [17]. The joint locking mechanism can still be improved. Specifically, the compliance in the locked joints should be addressed, by ensuring play in the joints and lock mechanisms is minimized. If the joint locks' solenoid actuators can be reduced in size or replaced by a smaller system, this would free up space for larger friction pawls and also reduce the relative effect of play. The control systems and mechanisms demonstrated in this paper have the potential to provide a modern myoelectrically-controlled hand prosthesis with sufficient degrees of freedom to be considered dynamically anthropomorphic, without complicating its control for the user or weighing down the prosthesis with high numbers of actuators.

Chapter 5

Mechanical design of the UT Hand I

Several lessons were learned during the design, manufacture and evaluation of the two-fingered prototype. The joint locks are fully functional, but suffer from significant compliance in locked joints. Improving the friction between the pawl and drum would not only alleviate this problem, but also allow for smaller lock components and solenoid actuation. The DC motor actuating the prototype is unsuitable for use in a human-sized palm, as not only the spindle drive, but even the motor/gearbox combination alone is too large for inclusion in a human-sized palm.

A number of new design choices need to be made in order to progress from a two-fingered experimental prototype to an anthropomorphic five-fingered design: Transferring the actuation and transmission from an external setup to an integrated palm design is challenging, especially considering the number of DOFs connected to the underactuation system is doubled. In order to accurately mimic the fingers of the human hand, the distal finger joints should be made active, and their rotation should be coupled to that of the intermediate joints. The requisite mechanisms should be as small as possible, as space in the fingers is limited. The design of the thumb will also differ strongly from that of the fingers, as the combination of its opposition and flexion DOFs can be difficult to realize.

The resulting five-fingered prosthesis prototype has been named the "UT Hand I"; this chapter covers its mechanical design and evaluation. It has been accepted for publication as “The UT Hand I: A Lock-Based Underactuated Hand Prosthesis" [20].

5.1 Introduction

In recent years, several advanced myoelectric hand prostheses have become commercially available [52, 53, 51]. These hands offer a significantly higher number of degrees of freedom (DOFs) than traditional prostheses. However, despite their increased functionality, a large percentage of myoelectric prostheses still go unused by their owners [5, 1].

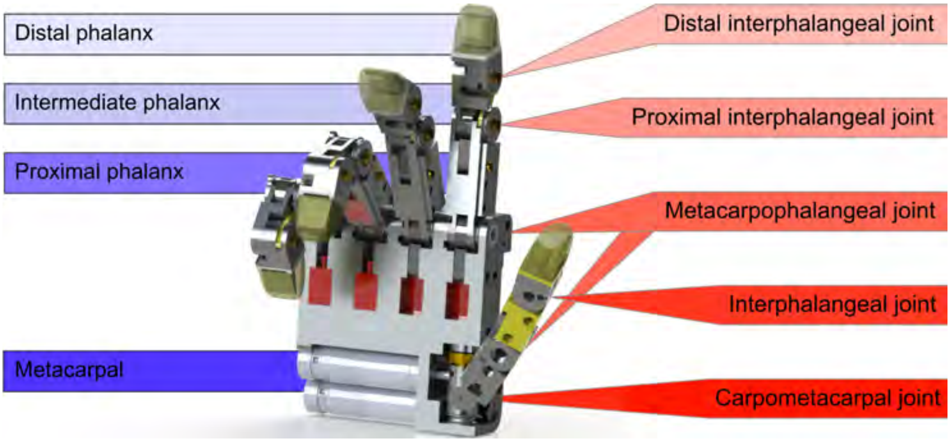

Figure 5.1: A rendering of the UT Hand I prosthesis prototype, indicating phalanx and joint names.

To circumvent this problem, a list of requirements has been set up based on input by users, clinicians and engineers [1]. For the mechanical design of a hand prosthesis, these requirements can be divided into two categories:

- Anthropomorphic: the prosthesis should resemble the human hand as much as possible, in both appearance and functionality. This not only affects the size and weight of the hand, but also the fingers' dynamic behavior and thumb opposition.

- Grasping: activities of daily living for single-sided amputations almost invariably involve grasping and holding of objects with the prosthesis, while the able hand performs manipulation tasks. To this end, the prosthesis should be able to perform a variety of grasp types relevant to these activities (see Figure 5.2):

  - Lateral grasp, which keeps all fingers flexed and uses the thumb to grasp flat objects

Figure 5.2: Three grasp types commonly used in activities of daily living, from left to right: cylindrical, lateral, and tripod [1].

- Cylindrical grasp, which uses all fingers and an opposed thumb to firmly grasp larger objects
- Tripod grasp, which uses the index and middle fingers and the thumb to grasp smaller objects while keeping the ring and little fingers flexed
- An index finger point gesture should also be supported

Minimizing actuation is a crucial part of prosthesis design; a low number of actuators requires less volume and reduces weight. Underactuation has already been used in the development of several prototype hand prostheses [82, 33, 24, 38, 56, 83, 84, 85], where it is achieved by means of many different strategies, such as:

- Mechanisms for rigid joint coupling [82, 33, 24, 38, 56]
- Tendon-pulley drive [83]
- A Geneva drive to alternately actuate different DOFs [24, 56]
- Compliantly linking the actuation of multiple fingers [83, 33, 38, 56]
- Passive, compliant joints [24, 84]

However, every one of these mechanisms reduces the effective number of controllable DOFs. A system of joint locks has been developed to re-establish a measure of control over the motion of underactuated fingers [16].

In this paper, a new design for an underactuated hand prosthesis is presented: The UT Hand I. The prototype implements a robotic finger concept based on ideas put forth in Wassink et al. [86]. A combination of a tendon-pulley system and four-bar linkages is used to actuate the four fingers' 12 DOFs with a single DC motor. The joint locking systems have been improved for the UT Hand I; 8 locks

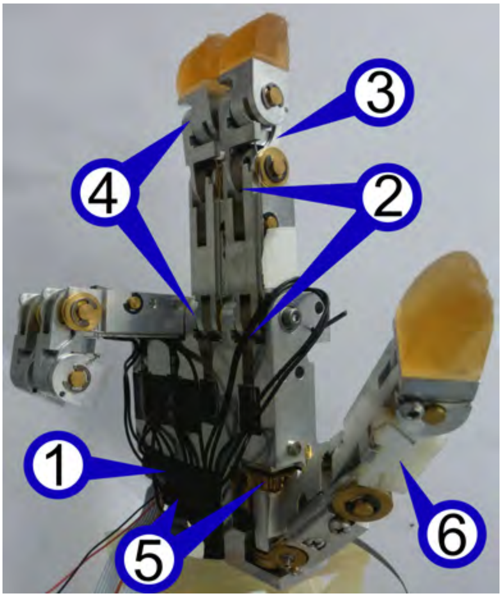

Figure 5.3: The UT Hand I prosthesis prototype; 1 - 6 indicate relevant subsystems.

are installed in the palm and proximal phalanges to control the hand's grasping motions. The system also includes a 3-DOF thumb with two actuators.

The joint locking technology is the core of the underactuation strategy of this prototype. It allows a reduction in the number of continuous actuators, while maintaining the possibility of controlling different DOFs individually and adding only a small amount of weight and volume. This gives the UT Hand I an advantage with respect to many existing hand prostheses, the advertised DOFs of which often include both active and passive ones.

The design of the prototype is described in detail in Section 5.2. Section 5.3 covers the kinematic analysis of the system. In Section 5.4, the results of the preliminary prototype tests are shown and discussed. Section 5.5.1 concludes the paper.

5.2 Prototype concept and design

In Figure 5.3, the UT Hand I is shown. The hand features the following mechanisms:

1. The hand's underactuation is obtained by implementing a single DC motor to flex all joints of the four fingers.

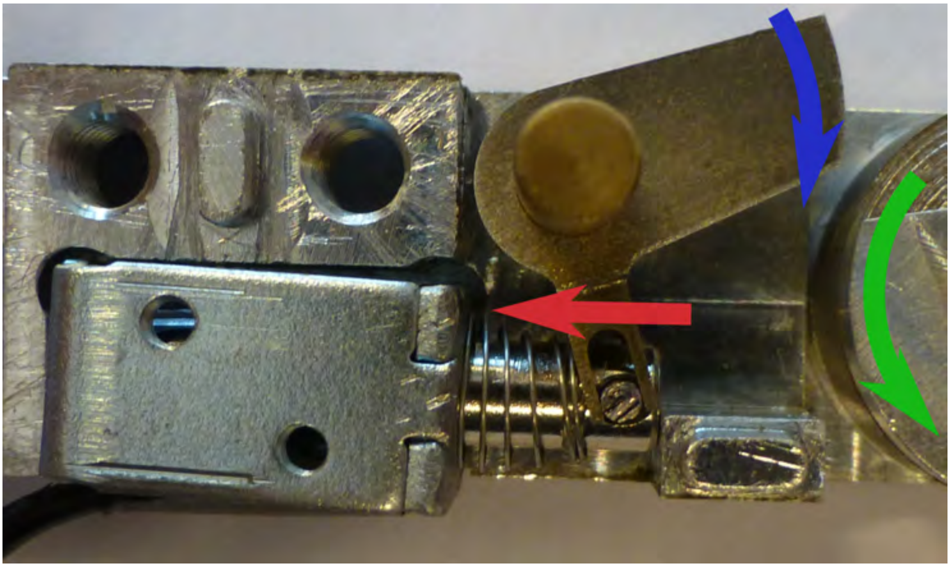

Figure 5.4: The joint locking mechanism. The arrows indicate the operating direction of the solenoid (red) and pawl (blue), and the locking direction of the drum (green).

2. Each of the four fingers is equipped with two friction-based joint locks, actuated by small solenoids. Different grasp types are obtained by locking certain finger joints, allowing selective actuation of the unlocked joints [16].

3. In each finger, the rotation of the DIP joint is coupled to that of the PIP joint by a four-bar mechanism.

4. Extension springs are implemented to extend the fingers and maintain tension in the tendon transmission.

5. To actuate the thumb, two DC motors are used: one for flexion, and a smaller one for opposition.

6. The thumb's IP joint rotation is coupled to that of its MCP joint by a tendon coupling.

5.2.1 Joint locking

In Peerdeman et al., a mechanism was designed to individually lock the joints of an underactuated finger [16]. By using a friction-based self-locking principle, the mechanism shown in Figure 5.4 can continuously block the rotation of an actuated joint with only a single low force solenoid actuator. These mechanisms

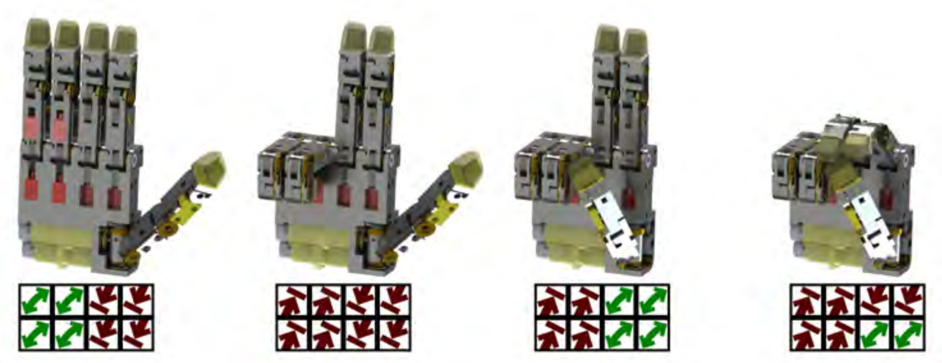

Figure 5.5: The different hand configurations required for tripod grasping. The symbols show the state of all joint locks; green arrows represent unlocked joints, and red arrows indicate a locked direction. From left to right: 1: Index and middle fingers are locked in the flexion direction; little and ring fingers are fully flexed. 2: Little and ring fingers are locked in the extension direction. 3: Index and middle fingers are unlocked while thumb is brought into opposition. 4: Fingers and thumb are flexed, while locking the distal finger joints to ensure a stable grasp.

have been implemented and tested in a two-fingered setup [19]; based on the results of those tests, several improvements have been made. Most notably, the lock's drum is coated with a layer of 10 μm silicon carbide particles embedded in nickel, which serves to increase the friction of the drum. This increase in friction allows for a higher contact angle between pawl and drum while keeping the self-locking property of the system intact. A higher contact angle in turn reduces the contact forces in the locking system and the compliance of the locked joints. The increased friction and contact angle of the new design also allow for a smaller solenoid actuator, reducing the general dimensions of the mechanism. In this prototype, the updated joint locks are used to control four fingers with a single actuator. Four of the locking mechanisms are integrated into the palm, and one is integrated into the proximal phalanx of each finger.

The current implementation of the joint lock is unidirectional, and therefore the desired locking direction needs to be considered for each joint. The tripod grasp requires separate extension of the index and middle fingers with regard to the ring and little fingers, which need to remain flexed while the grasp is being executed. A description of the tripod grasp and associated joint locking is shown in Figure 5.5. To this end, the index and middle fingers have locks in the flexion direction, and the ring and little fingers can be locked in the extension direction. This configuration does not interfere with the cylinder and lateral grasps, and also allows the hand to perform an index finger point.

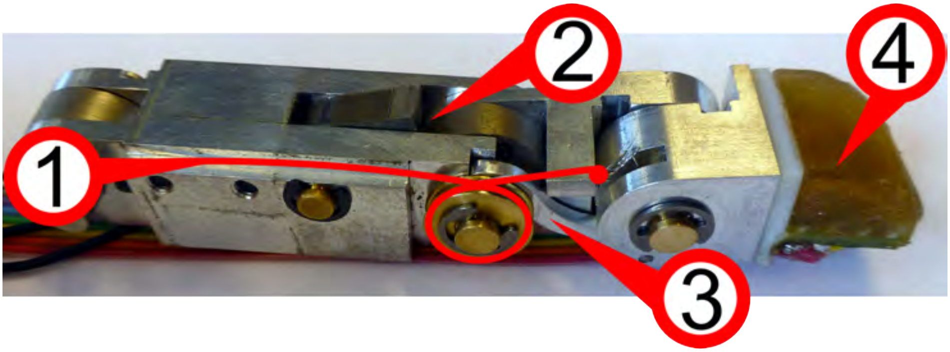

Figure 5.6: The index finger and its subsystems: 1: tendon-pulley actuation, 2: joint locking mechanism, 3: four-bar coupling, and 4: tactile sensor array.

5.2.2 Finger design

A picture of the index finger is shown in Figure 5.6, highlighting its various subsystems. The structure of the other fingers is identical, except for the orientation of the joint locking mechanism. The fingers are connected to a steel actuation tendon at the intermediate phalanx, which actuates their flexion. Extension is done by a pair of torsion springs placed in the proximal and distal joints. The DIP and PIP joints are coupled by a four-bar linkage. A tactile sensor array is placed inside the fingertip, and flexure sensors are placed on each joint to measure its rotation angle.

Four-bar coupling

In the fingers of the human hand, the rotation angle of the DIP joint with respect to the PIP joint is characterized by a transmission ratio of approximately 2:3 [13]. Considering this ratio, a coupling between the two joints would reduce the number of DOFs without affecting the dynamic appearance and function of the hand. Coupling the motion of multiple finger joints can be achieved in several ways, such as mechanical linkages [87, 23] or tendon-pulley systems [24, 83]. For the fingers of this prototype, a four-bar linkage has been chosen, as it requires little space and provides a bidirectional coupling. The structure of the linkage is shown in Figure 5.7.

To determine the relative orientation of the distal phalanx, an analytical approach is used. Compared to the use of closure equations simplified by Freudenstein's equation [88], this approach serves to evaluate the mechanism's variable coupling ratio across the joint's entire range of motion. The approach is illustrated in the inset of Figure 5.7; definitions of the variables used in this approach can

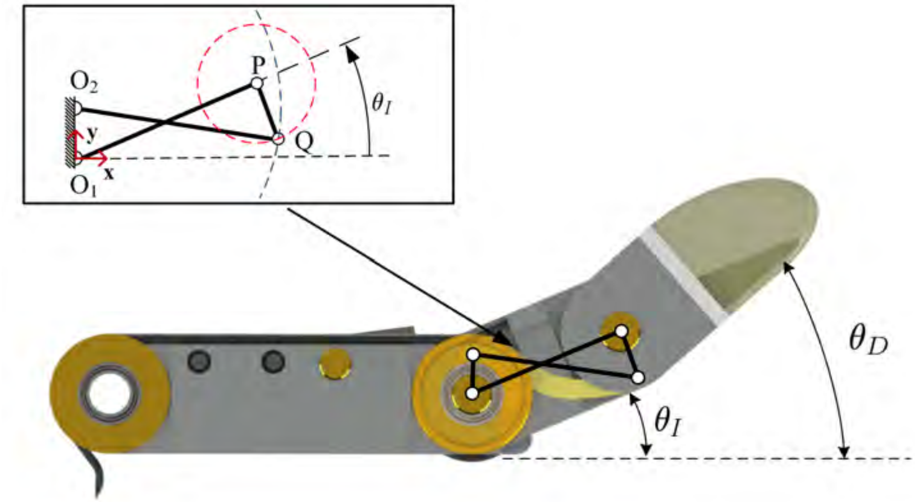

Figure 5.7: The four-bar mechanism of the finger. P, Q, O_1 and O_2 indicate the positions of the mechanism's joints. The rotation angles of the intermediate (θ_I) and distal phalanges (θ_D) are indicated with respect to the proximal phalanx.

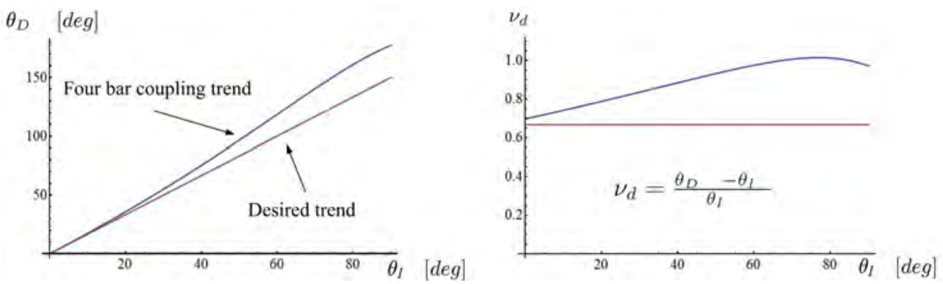

Figure 5.8: The desired and actual angles of the intermediate (θ_I) and distal phalanges (θ_D) due to the four-bar mechanism.

be found in Table 7.1 in the appendix. With the coordinates of P being defined as $\{b_{PO_1}\cos(\theta_I)\,,\, b_{PO_1}\sin(\theta_I)\}^T$, the coordinates of Q can be derived from the following equations:

$$\begin{gathered}\big(x_Q - x_P(\theta_I)\big)^2 + \big(y_Q - y_P(\theta_I)\big)^2 = b_{PQ}^2 \\ (x_Q - x_{O_2})^2 + (y_Q - y_{O_2})^2 = b_{QO_2}^2\end{gathered} \tag{5.1}$$

The analytical function $\theta_D(\theta_I)$ describing the distal phalanx's motion can then be obtained by means of Equation 5.1 and the following:

$$\frac{\partial\theta_D}{\partial\theta_I} = \frac{\partial \arctan\left(\frac{y_Q - y_P}{x_Q - x_P}\right)}{\partial\theta_I} \tag{5.2}$$

Due to the presence of the shaft, bearings and locking mechanism at the intermediate joint, the choice of position for the linkage joints is very restricted. The best solution for our purposes generates a slope described in Figure 5.8. The distal phalanx rotation differs from the desired behavior at high angles, but this will only occur when the finger is nearly fully flexed, which will not affect the grasping action.

Sensors

Proper control of the hand prosthesis requires information on the pose of each finger and any contact forces applied to the fingers. This information is provided by a set of angle sensors placed on each joint, and a tactile sensor array which can be integrated into the fingertip. The tactile sensors are based on the Takk-Tile system [89]. The sensor consists of an array of MEMS barometers covered in a molded urethane rubber fingertip, which also serves to improve the hand's grasping performance. To determine the angle of each joint, a flexure sensor is wrapped around the outside of the joint. This provides the necessary information without requiring significant space in the finger.

5.2.3 Thumb design

The structure of the thumb is shown in Figure 5.9. Compared to the fingers, the most notable difference is its opposition motion. In this prototype, opposition is accomplished by placing the thumb at a 45° angle to both the other fingers and the plane of the palm. This causes the thumb itself to move along a cone centered on the shaft, approximating the opposition motion of the human hand with a single DOF.

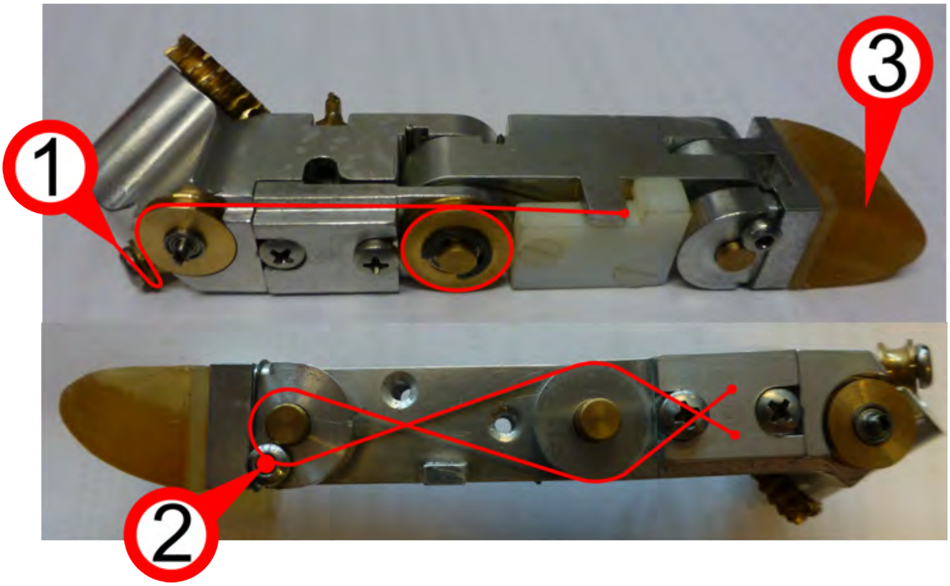

Figure 5.9: The thumb and its subsystems: 1: tendon-pulley actuation, 2: tendon coupling, and 3: urethane rubber tip.

Actuation

Flexion of the thumb is actuated by a single tendon connected to the thumb's proximal phalanx. This tendon has to be routed along several pulleys in order to align with the thumb's flexion plane. It should also be noted that opposition of the thumb will result in flexion of the thumb or slacking of the flexion tendon. Therefore, opposition of the thumb should be coordinated with movement of the flexion motor; this is addressed in Section 5.3.2. The opposition motor is only used during preshaping, and is not required to exert the higher forces involved in grasping; however, external forces due to grasping or contact with the environment require some measure of non-backdrivability in the opposition joint. Therefore, a worm wheel transmission has been placed between the thumb shaft and the opposition motor.

Tendon coupling

The ratio between the thumb's distal and proximal phalanges' flexion angles is different from that of the fingers. Based on the relative motion of the human thumb's joints [90], an approximate ratio of 2:1 between the prosthesis' IP and MCP thumb joints has been chosen. The combination of this transmission ratio and the spatial

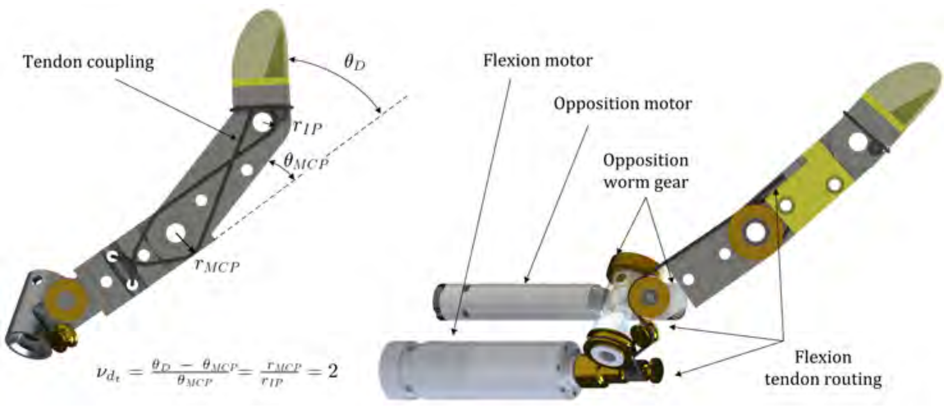

Figure 5.10: A diagram of the thumb's tendon coupling, and the elements of its actuation system. For the tendon coupling, relevant angles and radii are indicated.

limits of the thumb would lead to a four-bar mechanism that reaches a singular position. Though the mechanism's behavior would be close to the desired one, a high transmission ratio is present at low flexion of the distal phalanx. Therefore, a tendon coupling has been implemented. Although such a mechanism requires additional space, this does not pose a problem as the thumb is wider than the fingers and its phalanges do not contain joint locks.

The design of the tendon coupling is shown in Figure 5.10. It consists of a crossed connection of two nylon tendons, which are routed around two circular cams. The crossed cables provide a bidirectional coupling of the distal phalanx angle. The transmission ratio of the coupling is defined by the ratio $\frac{r_{MCP}}{r_{IP}}$, and can therefore be set exactly to the desired 2:1.

Sensors

The sensors of the thumb are identical to those of the fingers. However, the thumb can also be equipped with a socket for a BioTac sensorized fingertip [79]. This will eliminate the thumb's distal DOF, but allow for a more accurate measurement of external forces on the tip.

5.2.4 Palm design

As with the rest of the prototype, the design of the palm is restricted to a size similar to the human hand. The dimensions of the palm have been chosen to be 90×82×26 mm, in accordance with an average male hand [57]. The palm can be divided into several sections, housing the finger joints, thumb joint, joint locks,

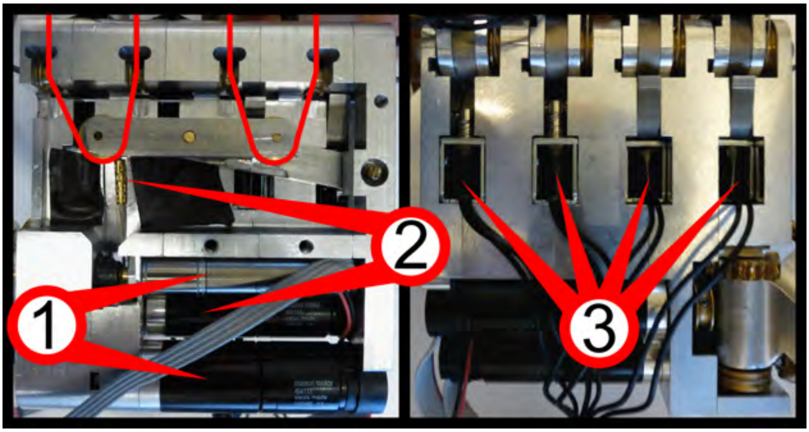

Figure 5.11: The palm and its subsystems: 1: thumb actuation motors, 2: finger actuation motor and tendon-pulley linkage, and 3: joint locking mechanisms.

linkage system, and actuators. These sections are shown in Figure 5.12. The palm has been manufactured in 5 parts, which are connected and aligned by two shafts running through the palm.

Actuation system

Due to the variety in the length of the remaining limb after a transradial amputation, most recent hand prostheses implement an actuation system that is included in the palm of the hand [82, 83, 33, 24, 38, 56, 84, 85, 91, 92]. These prostheses also almost exclusively feature DC motor actuation, although actuation by means of pressurized CO_2 cartridges [92, 18], monopropellant gases [36], or shape memory alloy actuators [93] have also been investigated. In this prototype, for reasons of reliability and controllability, DC motors have been chosen over more experimental actuation methods.

The palm contains three DC motors (Maxon Motor AG, Switzerland), used to actuate the four fingers' flexion and thumb's flexion as well as the opposition of the thumb. The two flexion motors are 16mm brushless DC motors (Maxon RE16), with a 157:1 planetary gearhead, whereas for opposition a 10mm brushless DC motor (Maxon DCX10) with a 16:1 reduction is used. The flexion motors have been chosen with regard to maximum torque and maximum velocity requirements. A 5-10 N load for each of the four fingers is considered, and 15-20 N for the thumb; for flexion velocity, complete flexion of all the fingers in 1 second was considered acceptable.

All motors are located in the lower part of the palm, in order to concentrate

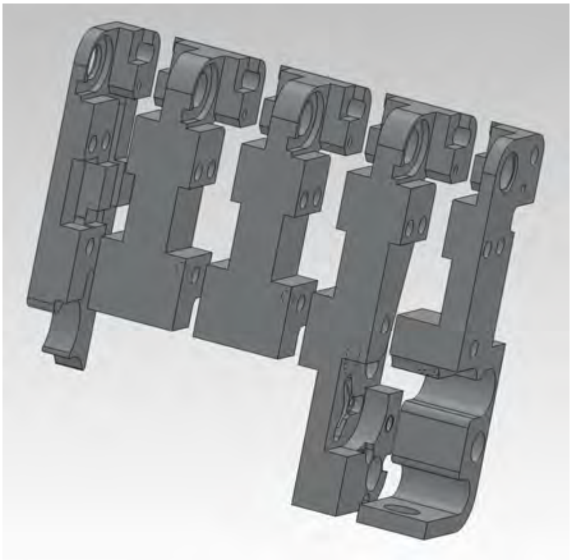

Figure 5.12: The palm structure, divided into its constituent parts.

the hand's mass as close as possible to the hypothetical wrist. Their position optimizes the available volume; it also allows room for motion of the transmission elements (pulley tree, tendon reels and worm gear).

Transmission

The relative position of the fingers can vary based on the selected grasp type and the object being grasped. Therefore, the mechanism that distributes the actuator force across the four fingers needs to be adaptable. The four fingers are connected by tendons in pairs of two, each of which is actuated by a single pulley. The two pulleys are connected to a linkage, which can be seen in Figure 5.11; a diagram of the actuation system is shown in Figure 5.13. The linkage is actuated by a single tendon connected to the far end of the main beam. This configuration allows the pulleys to assume any relative position by rotating the beams, and distributes the actuator force evenly across the fingers. The combination of the linkage system and tendon transmission ensures the adaptability of the grasp: the linkage allows relative motion of the two pairs of fingers, and the tendons permit the two fingers of each pair to move independently. The extension springs in the DIP and MCP finger joints maintain the tendons' tension.

As already mentioned, two motors govern the thumb's motion. Thumb flexion is controlled in a similar way to finger flexion, with a single tendon on a reel con-

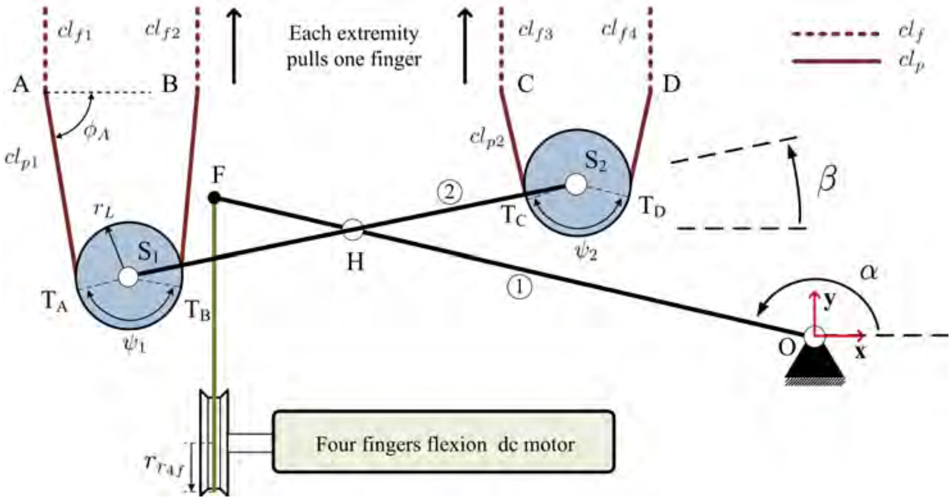

Figure 5.13: A diagram of the finger actuation pulley tree linkage, indicating points, angles and lengths used in the kinematics calculations. See Tables 7.1 and 7.3 in the appendix for a description of the symbols used in this figure.

nected to the motor. Thumb opposition is actuated via a worm gear transmission to ensure non-backdrivability. The positioning of the thumb shaft with respect to its actuators is shown in Figure 5.10.

5.3 Modelling and kinematics

A kinematic analysis of the prototype is essential for the future development of its control system. The actuation systems of the fingers and the thumb will be analyzed to determine the velocities and forces that can be applied.

5.3.1 Fingers

Determining the motion of the four fingers with regard to the motion of their actuator can be complicated, given the nature of the tendon transmission and the adaptability of the underactuated mechanism. A diagram illustrating the situation is shown in Figure 5.14. It should be noted that the actual finger joint velocities are also influenced by external forces, both of which will need to be detected by the prosthesis' sensor suite. However, the kinematics of the system are relevant to determining the desired motor velocity for different lock configurations and hand poses.

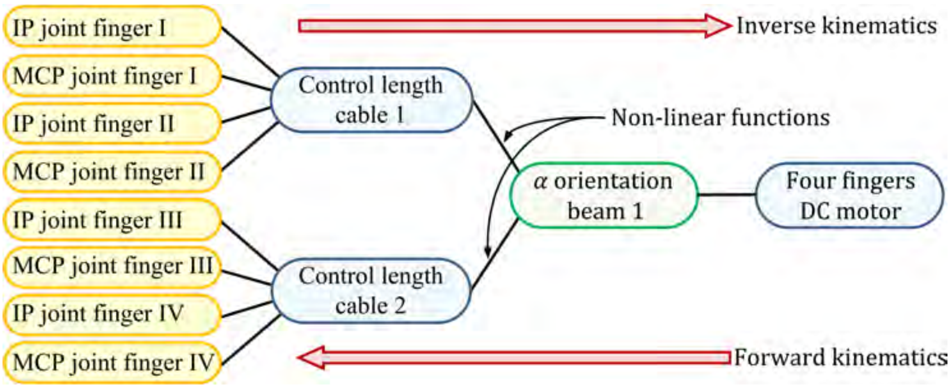

Figure 5.14: A diagram of the forward and inverse kinematics of the system.

To evaluate the mechanism, the total length of each of the two tendons (l_1 for the index and middle finger tendon, and l_2 for the ring and little finger tendon) can be divided into three 'control lengths': the lengths of the tendon paths in the fingers ($cl_{f1}$to cl_{f4}, from the index finger to the little finger), and the tendon paths in the palm ($cl_{p1}$and cl_{p2}). A row of 4 small pulleys (A-D in Figure 5.13) separates the tendon paths in the palm from those in the fingers. As tendon stretching is considered to be negligible, the combination of a palm control length and its two associated finger control lengths will be constant.

During movement of the fingers, the tendon path around the fingers is determined only by the joint angles. The tendon path in the palm is more complex, due to the floating pulleys (S_1 and S_2) in the pulley tree mechanism seen in Figure 5.13. The linkage supporting the floating pulleys has 2 rotational DOFs, α and β. Thus, the location of each floating pulley is a function of the angles of both links of the linkage:

$$\begin{aligned} S_1 &= b_{OH}\begin{bmatrix}\cos\alpha\\ \sin\alpha\end{bmatrix} - b_{HS_1}\begin{bmatrix}\cos\beta\\ \sin\beta\end{bmatrix} \\ S_2 &= b_{OH}\begin{bmatrix}\cos\alpha\\ \sin\alpha\end{bmatrix} + b_{HS_2}\begin{bmatrix}\cos\beta\\ \sin\beta\end{bmatrix} \end{aligned} \tag{5.3}$$

The variation in the tangent points of each tendon with the smaller upper pulleys is considered negligible as well. The tangent points of the tendon with the floating pulleys (T_A, ..., T_D) vary with the pulleys' position. This is expressed in the following equations for l_{AT_A} and T_A, in which r_L is the radius of the two pulleys:

$$l_{AT_A} = \sqrt{\|A - S_1\|^2 - r_L^2} \tag{5.4}$$

$$\phi_A = \arctan(\frac{|y_A - y_{S_1}|}{|x_A - x_{S_1}|}) + \arctan(\frac{r_L}{l_{AT_A}}) \tag{5.5}$$

$$T_A = A + \begin{bmatrix} l_{AT_A}\cos(\phi_A) \\ -l_{AT_A}\sin(\phi_A) \end{bmatrix} \tag{5.6}$$

The other tangent points T_B, T_C and T_D (and corresponding lengths l_{BT_B},l_{CT_C},l_{DT_D}) can also be obtained in this way. The palm control lengths can then be determined by adding the lengths of tendon between the tangent points on pulleys A, ..., D and the tangent points on the floating pulleys to the tendon contact arcs along the floating pulleys. The contact arc angles can be calculated as follows:

$$\psi_1 = 2\ \arcsin\left(\frac{\|T_A - T_B\|}{2\,r_L}\right), \qquad \psi_2 = 2\ \arcsin\left(\frac{\|T_C - T_D\|}{2\,r_L}\right) \tag{5.7}$$

This leads to the following equations for the palm control lengths:

$$cl_{p1} = \psi_1 r_L + l_{AT_A} + l_{BT_B}, \qquad cl_{p2} = \psi_2 r_L + l_{CT_C} + l_{DT_D} \tag{5.8}$$

The pulley positions, and therefore the palm control lengths, vary non-linearly with regard to the linkage angles; Figure 5.15 shows the relation between linkage angles and palm control lengths. The variations in the linkage angles were purposefully made as close as possible to a linear relation; the only significant exception occurs at minimal values for both α and β, which cannot occur simultaneously given the geometry of the palm linkage. This allows for the following approximation (see Table 7.2 in the appendix for exact values of the constants):

$$\widetilde{cl_{p1}}\,(\alpha, \beta) = a_1\alpha + a_2\beta + a_3 \tag{5.9}$$

$$\widetilde{cl_{p2}}\,(\alpha, \beta) = b_1\alpha + b_2\beta + b_3 \tag{5.10}$$

Figure 5.15 also shows the error of the closest linear approximation as in Equations 5.9 and 5.10. The maximum error in palm tendon length between this approximation and reality is less than 1 mm. Since the variation in palm tendon length can be up to 44 or 50 mm (depending on the pulley) this is considered acceptable; closed-loop control can be used to minimize this discrepancy even

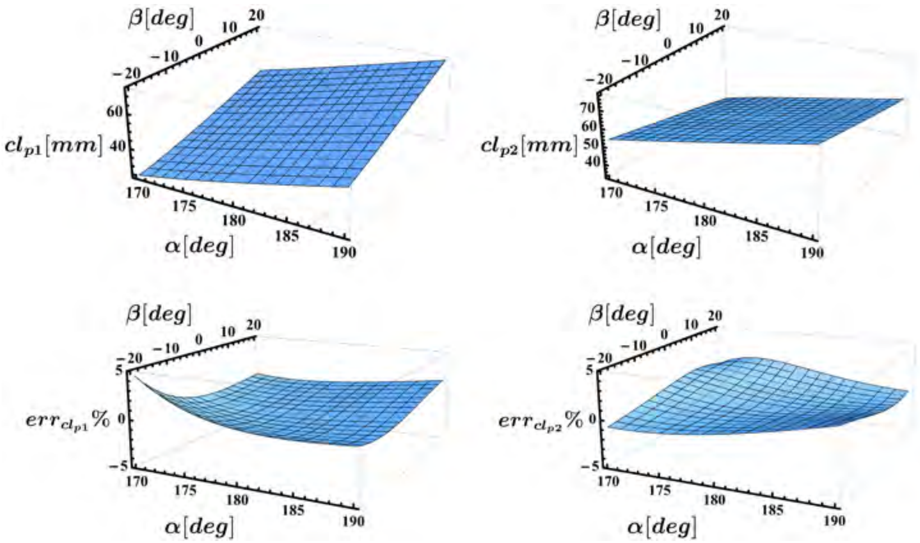

Figure 5.15: Evaluation of the linkage mechanism. The top two graphs show the relationships between palm control lengths cl_{p1} and cl_{p2} and linkage angles α and β. The bottom two graphs show the error percentage between the relationship above and a linear approximation.

further.

Inverse kinematics

To determine the required motor velocity to attain a desired set of finger joint velocities, the inverse kinematics of the system should be calculated. With r_J being the radius of each joint pulley, a desired change in the finger joint angles can be converted to changes in finger control lengths, and subsequently to palm control lengths as in Equation 5.11. $\triangle\theta_{PIP_i}$ and $\triangle\theta_{MCP_1}$ represent the changes in the PIP and MCP joint angles of each finger.

$$\begin{aligned}\triangle cl_{p1} &= -(\triangle cl_{f1} + \triangle cl_{f2}) = r_J\left(\triangle\theta_{PIP_1} + \triangle\theta_{MCP_1} + \triangle\theta_{PIP_2} + \triangle\theta_{MCP_2}\right)\\ \triangle cl_{p2} &= -(\triangle cl_{f3} + \triangle cl_{f4}) = r_J\left(\triangle\theta_{PIP_3} + \triangle\theta_{MCP_3} + \triangle\theta_{PIP_4} + \triangle\theta_{MCP_4}\right)\end{aligned} \tag{5.11}$$

Using the results of Equations 5.9 and 5.10, the following linear approximation of the linkage angle α can be made, based on the palm control lengths $cl_{p1}\text{and}$ cl_{p2} and constants c_1, c_2, and c_3:

$$\widetilde{\alpha}\left(cl_{p1},\, cl_{p2}\right) = c_1 cl_{p1} + c_2 cl_{p2} + c_3 \tag{5.12}$$

This also has the benefit of removing the unknown angle β from the equation, owing to the symmetric placement of the pulleys with respect to the pivot point of the main bar. $\widetilde{\alpha}$ is then converted to the necessary motor output shaft rotation angle, $\varphi_{m_{4f}}$:

$$\varphi_{m_{4f}} = \frac{l_{OF}}{r_{r_{4f}}}\,\widetilde{\alpha} \tag{5.13}$$

Deriving the relations of Equations 5.11 - 5.13 provides the following partial Jacobian matrices:

$$\mathbf{J}_{cl}^{\theta} = \left[\frac{\partial cl_{p_i}}{\partial \theta_j}\right] = r_J \begin{bmatrix} 1 & 1 & 1 & 1 & 0 & 0 & 0 & 0 \\ 0 & 0 & 0 & 0 & 1 & 1 & 1 & 1 \end{bmatrix} \tag{5.14}$$

$$\mathbf{J}_{\alpha}^{cl} = \begin{bmatrix} c_1 & c_2 \end{bmatrix} \tag{5.15}$$

As well as the following ratio between motor velocity and change in linkage angle α:

$$\nu_{m_{4f}}^{\alpha} = \frac{b_{OF}}{r_{r_{4f}}} \tag{5.16}$$

Multiplication of these relations allows us to obtain the required velocity of the motor, given the desired finger joint velocities:

$$\omega_{4f} = \overbrace{\nu_m^{\alpha}\,\mathbf{J}_{\alpha}^{L}\,\mathbf{J}_{L}^{\theta}}^{\mathbf{J}_{m_{4f}}^{\theta_f}}\,\dot{\boldsymbol{\theta}}_f \tag{5.17}$$

$$\mathbf{J}_{m_{4f}}^{\theta_f} = \frac{b_{OF}}{r_{r_{4f}}}\,r_J \begin{bmatrix} c_1 & c_1 & c_1 & c_1 & c_2 & c_2 & c_2 & c_2 \end{bmatrix} \tag{5.18}$$

Assuming that the internal stiffness and friction of each finger joint is approximately equal to the others, all unlocked joints will flex at the same velocity. This velocity depends on the number of unlocked finger joints (from 0 to 4), represented by f_1 for the index and middle fingers and f_2 for the ring and little fingers. In this prototype, the ring and little fingers can only be locked in the extension direction, so f_2 is fixed at 4. The motor velocity ω_{4f} required to flex all unlocked joints at a desired velocity $\hat{\dot{\theta}}_f$ can then be derived as follows:

$$\omega_{4f} = \frac{b_{OF}}{r_{r_{4f}}}\,r_J\,(c_1 f_1 + c_2 f_2)\,\hat{\dot{\theta}}_f \tag{5.19}$$

Forward kinematics

Calculation of the forward kinematics involves determining the velocity of the fingers' joints, given a certain motor velocity and status of the joint locks. As shown in Figure 5.13, a decrease in length of the motor tendon will lead to an increase in the palm control lengths. The flexion of each finger joint is in turn caused by the corresponding decrease in the finger control lengths. As mentioned earlier, it is assumed that the internal frictions and stiffnesses for each joint are approximately equal, leading to an even distribution of force and velocity. Therefore, the total control length variation can be expressed as a single value l_u, which represents the control length variation for each unlocked joint. The change in l_u can then be expressed as a function of $\widetilde{\alpha}$, f_1 and f_2:

$$\widetilde{\alpha}\left(l_u\right) = c_1 f_1 l_u + c_2 f_2 l_u + c_3 \Rightarrow \frac{\partial \widetilde{l_u}}{\partial \alpha} = \frac{1}{c_1 f_1 + c_2 f_2} \tag{5.20}$$

It is then possible to express the forward Jacobian based on Equations 5.11 and 5.13, with $\mathbf{d}$ representing the status of all 8 joint locks (d_i is 0 for a locked joint, and 1 for an unlocked joint):

$$\widetilde{\dot{\boldsymbol{\theta}}_f} = \overbrace{\mathbf{d}\,\frac{r_{r_{4f}}}{r_J\, b_{OF}(c_1 f_1 + c_2 f_2)}}^{\mathbf{J}_{\theta_f}^{m_{4f}}}\,\omega_{m_{4f}} \tag{5.21}$$

The Jacobian matrices derived in this section illustrate the possible shortcomings of minimally actuated finger flexion. Mainly, direct control over each individual DOF is not possible, and the use of joint locking mechanisms causes a non-linear relationship between the finger joint velocities and the joint lock status variables d_i, due to their discrete nature.

Grasp force

The force exerted by one of the fingers on an object depends on the tendon tension (F_t), finger dimensions (l_P, l_I, and l_D), pulley radius (r_J), joint angles (θ_{MCP}, θ_{PIP}, and θ_{DIP}), and the stiffness (k) of the extension springs in the MCP and DIP joints. The torques on each finger joint can be derived from these and the coupling between the DIP and PIP joints ($\theta_{DIP} = \frac{2}{3}\theta_{PIP}$) as follows:

$$\tau_{MCP} = F_t \cdot r_J - k \cdot \theta_{MCP}, \qquad \tau_{PIP} = F_t \cdot r_J - \frac{2}{3} \cdot k \cdot \theta_{DIP} \tag{5.22}$$

Based on Equation 5.22 and the pose of the finger, the fingertip force ($\mathbf{F}_{MCP}$) resulting from the MCP joint torque ($\boldsymbol{\tau}_{MCP} = [0, 0, \tau_{MCP}]^T$) can be calculated:

$$\|\mathbf{F}_{MCP}\| = \frac{\|\boldsymbol{\tau}_{MCP}\|}{\|\mathbf{l}_{MCP}\|} \tag{5.23}$$

$$\mathbf{l}_{MCP} = \begin{bmatrix} l_P \cos(\theta_{MCP}) + l_I \cos(\theta_{MCP} + \theta_{PIP}) + l_D \cos(\theta_{MCP} + \theta_{PIP} + \theta_{DIP}) \\ l_P \sin(\theta_{MCP}) + l_I \sin(\theta_{MCP} + \theta_{PIP}) + l_D \sin(\theta_{MCP} + \theta_{PIP} + \theta_{DIP}) \\ 0 \end{bmatrix} \tag{5.24}$$

$\mathbf{F}_{MCP}$ can be determined using Equations 5.23 and 5.24; the direction of $\mathbf{F}_{MCP}$ is perpendicular to both $\boldsymbol{\tau}_{MCP}$ and $\mathbf{l}_{MCP}$. The fingertip force resulting from the PIP joint torque can be calculated in a similar way. Assuming the motor torque to be equally divided across the four finger tendons, the average force exerted by one of the fingers during a cylinder grasp will be approximately 3.6 N.

5.3.2 Thumb

The kinematics of the thumb are related to its flexion and opposition movements, which have a single (effective) DOF each; as mentioned earlier, the rotation of the IP joint is compliantly coupled to that of the MCP joint. It should be noted that flexion and opposition are not completely decoupled: the flexion tendon travels around a freely rotating pulley on the thumb opposition shaft, the path of which is shortened or lengthened during opposition. Due to this, the inverse Jacobian matrix that relates flexion and opposition velocities to those of the motors is not diagonal, as expressed in Equation 5.25:

$$\begin{bmatrix} \omega_{f_t} \\ \omega_{o_t} \end{bmatrix} = \overbrace{\begin{bmatrix} \frac{r_{J_t}}{r_{r_t}} & \frac{r_{S_t}}{r_{r_t}} \\ 0 & \nu_w \end{bmatrix}}^{\mathbf{J}_{m_t}^{\theta_t}} \begin{bmatrix} \dot{\theta}_{MCP_t} \\ \dot{\theta}_{OPP_t} \end{bmatrix} \tag{5.25}$$

Additionally, it follows from this relation that the flexion motor could actuate both flexion and opposition degrees of freedom; this is prevented by the non-backdrivable worm wheel transmission between the opposition motor and the thumb. The forward kinematics of the thumb can be obtained by inverting Equation 5.25.

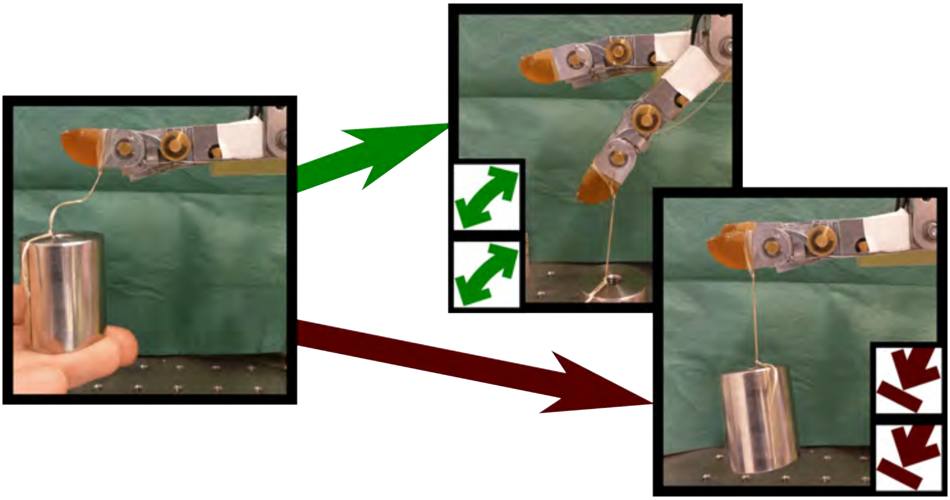

Figure 5.16: A demonstration of the functionality of the joint locking mechanisms.

Grasp force

The thumb tip force can be calculated by using the tendon tension and thumb pose, as demonstrated in Equations 5.22, 5.23 and 5.24. These calculations lead to an average thumb tip force of approximately 12 N.

5.4 Preliminary test results

To demonstrate the functionality of the underactuation mechanisms and the joint locking system, preliminary testing consists of the demonstration of three grasp types (see Figure 5.2), as well as the general functionality of the joint locks.

5.4.1 Joint locking

To test the joint locking mechanisms in a demonstrable way, a 250 g weight is suspended from the index fingertip, as shown in Figure 5.16. When the joint locks are not engaged, the finger simply flexes as the weight is released; however, the joint locks keep the finger straight when activated, even if the solenoid actuators are disabled after locking the joint.

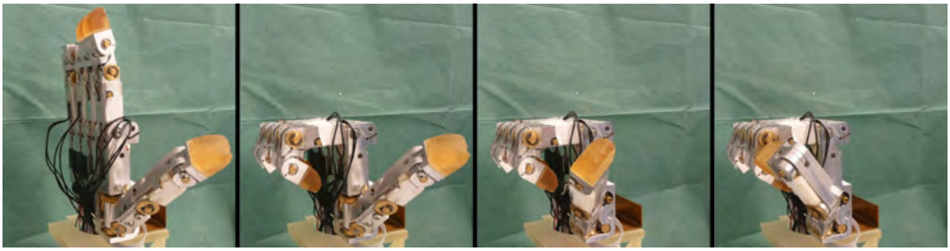

Figure 5.17: A selection of frames illustrating a lateral grasp performed by the prototype.

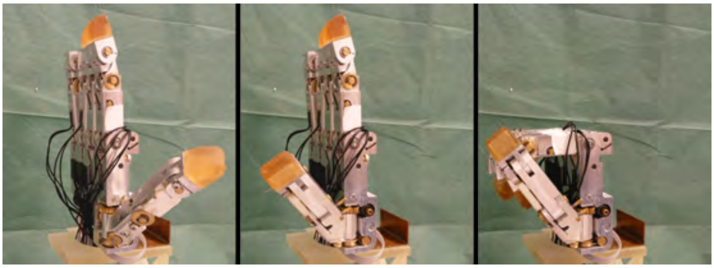

Figure 5.18: A selection of frames illustrating a cylindrical grasp performed by the prototype.

5.4.2 Grasping

The various stages of each grasp are shown in Figures 5.17, 5.18, and 5.19. Three videos showing the prototype performing each of these grasps are available in the electronic version of this paper. An index finger point is also executed; its result can be seen in Figure 5.20.

Lateral grasp

Preshaping of this grasp consists of full flexion of the fingers; no joint locking is required. Once the fingers are flexed, the slightly opposed thumb can be flexed to grasp small objects between it and the side of the index finger.

Cylindrical grasp

Preshaping of this grasp consists of opposition of the thumb; no joint locking is required. The differences visible in the motion of the fingers are due to friction/stiffness inequalities; once the joints near full flexion or contact is established this effect disappears. The thumb is flexed a short time after the start of finger flexion.

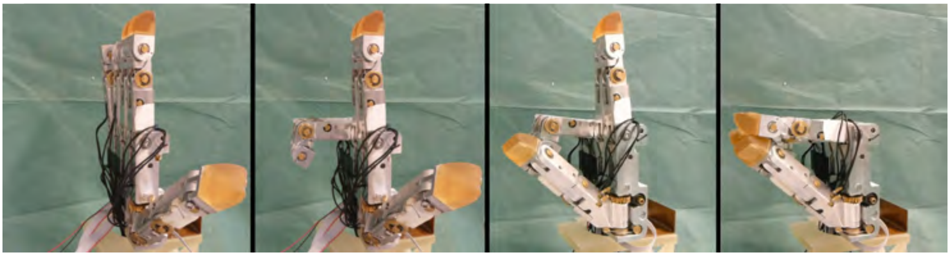

Figure 5.19: A selection of frames illustrating a tripod grasp performed by the prototype.

Figure 5.20: The prototype performing an index finger point, by locking both joints of the index finger and flexing the fingers and thumb.

Tripod grasp

Preshaping of this grasp involves first flexing the fingers while locking the index and middle fingers' flexion. Once the ring and little fingers are fully flexed, they are locked from extending, while the index and middle fingers are unlocked. Lastly, the thumb is opposed. Flexing the fingers and thumb simultaneously, while locking the distal and intermediate joints of the index and middle fingers, will complete the grasp.

5.5 Discussion

The joint locking mechanisms are successful in enabling the hand's different grasping motions with minimal actuation. With the previous implementation of the joint locks in a two-fingered prototype [19], a significant degree of compliance was observed in the locked joints. The new locks' improved friction and contact angle has eliminated this compliance, and the smaller mechanism size allows all 8 MCP and PIP joints of the finger to be fitted with a lock.

The tendon-pulley underactuation linkage serves to evenly distribute the actuator force across the four fingers. The presence of small deviations in friction and stiffness on each joint can lead to an uneven flexion/extension of the fingers. The tripod and lateral grasps are executed in approximately one second, as per the requirements. However, during the cylinder grasp, the fingers take up to three or four seconds to fully flex. This is due to total stiffness of the fingers' extension springs being higher than expected. A set of more compliant springs, with some additional pretension, should be evaluated as an alternative. The fingertip force exerted during the cylindrical and tripod grasps was measured to be around 5 N; for the lateral grasp, 12 N was measured. While the thumb force matched the result of the force calculations, the fingertip force was somewhat higher than expected. Though these results are on the low end of the requirements, they are sufficient for the hand to establish a stable grasp.

The couplings between the distal and proximal joints of the fingers and thumb reduce the hand's DOFs to a manageable number while maintaining an anthropomorphic dynamic appearance. The compliance of the thumb tendon coupling also allows for a more flexible grasp; replacing the rigid bar in the fingers' four-bar coupling with a compliant alternative can offer such flexibility to the fingers as well. The thumb opposition worm wheel provides a non-backdrivable transmission, though the current implementation has noticeable play between the teeth. However, the existing coupling between thumb flexion and opposition helps the thumb to remain fixed while grasping.

5.5.1 Conclusion

This paper shows the development of the UT Hand I, a new anthropomorphic hand prosthesis prototype designed to execute several grasps relevant to activities of daily living. The hand's primary innovation is the minimal actuation system of its four fingers, the DOFs of which can be individually locked by means of miniature joint locking mechanisms. This system provides a way for modern hand prostheses to support a human-like number of controllable DOFs, while adhering to the stringent weight and size requirements imposed on anthropomorphic hands.

In order to develop a control system for the hand, its kinematics are analyzed. The transmission of actuator velocity to that of the finger joints is calculated based on the number of locked joints and current position of the fingers and pulley linkage. The required actuator velocity to attain a desired set of joint velocities is also determined, and a calculation of the fingertip forces is done.

The functionality of the hand is evaluated by executing three different grasp types and an index finger point gesture. In these preliminary tests, the effectiveness of the joint locking mechanisms, joint couplings and thumb opposition is demonstrated. The combination of joint locks and underactuation proves effective in controlling the four fingers' 8 DOFs with a single actuator. Though it does not allow full simultaneous control over all DOFs, the implementation of joint locks leads to an effective variety of grasping motions and gestures, while maintaining the adaptive properties of underactuated fingers.

5.5.2 Future work

In future work, the control system of the UT Hand I will be developed. Using electromyographic input signals as well as the position and force sensors of the hand, the system will consist of high-level user control and low-level automatic control. The high-level controller will be based on a state machine structure, allowing several grasps and gestures to be intuitively navigated with few control signals. For the low-level controller of the hand several interaction control systems can be evaluated, such as admittance control, impedance control, and intrinsically passive control systems.

Chapter 6

Myoelectric prosthesis control

The general structure of the Myopro myoelectric control system is as follows: Using a selection of EMG input signals, the user determines one of the available grasp types. The hand then preshapes the fingers and thumb, and waits for the user to move the hand into position and signal the closing of the grasp. When this signal is received, the hand closes its fingers around an object automatically, compliantly grasping it with a user-controlled level of force. Another signal can open the hand again and return it to a neutral position.

Like the mechanical design, the development of a complete control system for myoelectric hand prostheses has taken several iterations. Before a physical prototype was available, several variations of low-level interaction control were tested on a biomechanical model, based on the structure of the human hand. These controllers increase the ability of the fingers to compliantly interact with their environment. These interaction controllers were later applied to control a fully actuated, 20-DOF robotic hand testbed: the UB Hand IV [35]. With the development of the two-fingered prototype, the high-level state machine determining the hand's general behavior was included as well.

This chapter is a collection of papers and paper segments discussing the various iterations of the control system, culminating in the version implemented to control the UT Hand I as part of the Myopro prosthesis system.

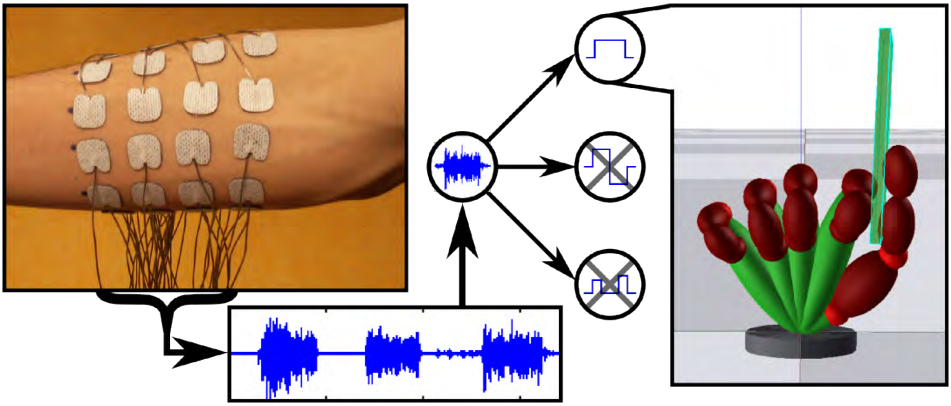

Figure 6.1: **Diagram representing signal processing from electromyographic sensing to control:** Myoelectric signals are acquired and classified, leading to control signals for grasp selection and execution. These signals are then sent to the model, where they control the motions of a virtual representation of a prosthetic hand.

6.1 Biomechanical model

This section was published as “A Modeling Framework for Control of Myoelectric Hand Prostheses" [15].

6.1.1 Introduction

The loss of an upper limb is a life-altering event. It involves not only the loss of the appendage itself, but also the disruption of the intricate systems that plan and execute its motions. Through advanced prostheses, modern technology is able to replicate a small part of the human hand's functionality; however, in performing normal daily activities the patient's ability to control a prosthesis' limited functions is as essential as the functions themselves. To this end, most current prostheses combine a sensing system to ascertain the user's intended motion with a control system to execute that motion with the correct speed and force. The development of such a control system requires knowledge of the exact structure of the prosthesis, as well as information about the environment obtained through sensors. A modeled representation of the prosthesis can be used to support control system development while a physical prototype is not available. Further, any changes to the mechanical design can be accommodated in the model and the necessary sensor information can be directly extracted from the state of the model.

Models of the human hand have been developed by several other groups. A large number of these aim to provide insight into the way the human hand performs the grasping of objects, for use in industrial and/or medical research [94, 95, 58]. Others are used for the generation of realistic computer graphics [96, 97]. These models are often focused on natural human hands, instead of the mechanical approximations found in prosthetic hands. A good example of a kinematic model used for prosthesis design can be found in Dragulescu and Ungureanu [98]. However, though the kinematic model had twenty-three degrees of freedom (DOFs), the completed model was reduced to fifteen DOFs and lacks physical contact modeling.

In this paper, a model based on the human hand's biomechanical structure is demonstrated. This model serves as a testbed for the development of control systems based on electromyographic (EMG) input, which is the current standard in the non-invasive control of electrically powered prostheses. Myoelectric signals are the electrical expression of the neuromuscular activation generated by skeletal muscles [44]; they are rich in information regarding the user's intent and can therefore serve as an effective control input. The information derived from these signals is transferred to the control system (Figure 6.1), which determines and executes the specific motions of which the intended movement consists. The parameters of this model are based on analysis of human hand dimensions [94, 57] and inertial properties [12]. The underactuated joints of the fingers and thumb are connected through a system of bond graphs, which model the distribution of motor torque across the joints. A contact model based on [99] is implemented, using an ellipsoidal approximation of the phalanges.

The sensing and control systems that provide input to the model are detailed in Section 6.1.2. Section 6.1.3 contains details on the model's high-level structure, and the parameters and equations that make up the model. In Section 6.1.4, the results of several simulated grasps are discussed. We conclude with Section 6.1.5 and provide directions for future work.

6.1.2 EMG input and control system

The block diagram describing the interactions between the different parts of the control system and model can be seen in Figure 6.2. The input of the control system is generated by an EMG sensing system. EMG sensing uses surface electrodes to detect the myoelectric potential generated when a muscle contracts. However, the potential arriving at the electrodes is very small in comparison to other detected signals, e.g. cardiac-related noise, environment noise and motion artifacts. Therefore, amplification and a filtering method must be applied to reduce these noise signals [45, 100]. In most current EMG systems, the signal data is then segmented into small intervals of which features (i.e. characteristic

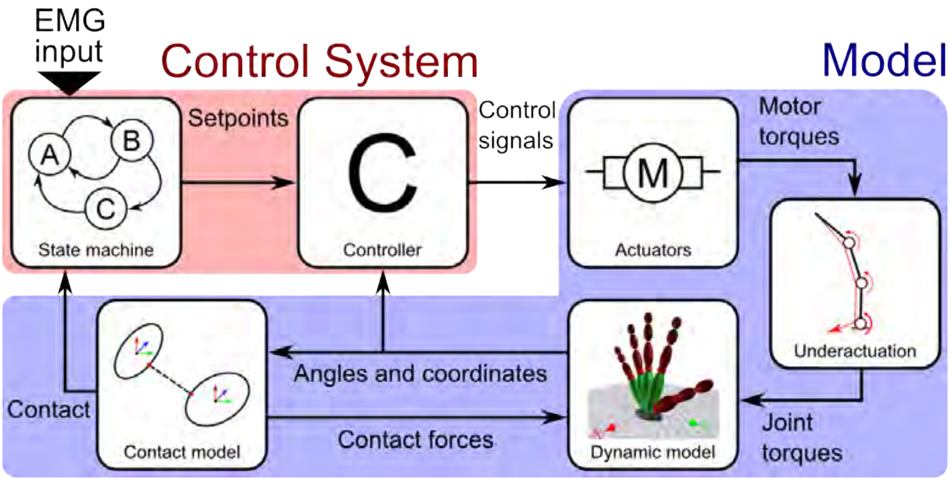

Figure 6.2: Block diagram illustrating the flow of information through the control system and model.

parameters related to user intent) are extracted. Several parameters in the time, frequency, and time-frequency domains can be used as features, such as the root mean square, mean absolute value, mean frequency, and wavelet transform coefficients.

Detection of a certain number of intended actions requires the same number of unique muscle activity patterns. Each pattern is described by a specific set of features that are entered into a classifier, which determines the movement intended by the user [100, 47, 48]. Examples of frequently used classifiers in literature are linear discriminant analysis [49] and artificial neural networks [50]. In this study, the results of the classification process are gathered into a sensing vector, serving as the EMG input in Figure 6.2. This vector is made up of the intended grasp type [101], direction and force of opening and closing of the hand, and the direction and speed of wrist movement.

A grasp type determines two things: the starting pose of the hand, and the relative timing between flexion of the individual fingers and thumb. When a certain grasp type is detected by EMG sensing, the control system will automatically move the relevant joints to their starting angles. This process is called preshaping. Once the grasp is preshaped, hand opening/closing and wrist movement signals control the execution of the grasp. The interaction between high-level EMG user input and low-level prosthesis control signals can be described by a set of state machines. Through the control signals contained in the sensing vector, the user can change the state of the control system, which determines the automated low-level behavior of the prosthesis. The state machine describing the hand opening/closing behavior is shown in Figure 6.3. Implementation of wrist control is straightforward, and will be done in a future version of the model. Based on the state of the control system and feedback from the model, desired torque values are sent to the model to control the joint angles and applied forces.

6.1.3 Model structure

After receiving the desired actuator torques from the control system, the individual joint torques are determined by an underactuation model. It represents the tendon-and-pulley mechanisms that are present in many modern hand prostheses [33, 103, 36]. Here, the underactuation results in a both natural and effective grasping motion; when one of the phalanges of a finger encounters an object, the other phalanges automatically continue wrapping around it. The model of the finger underactuation is designed using bond graphs [104]. Bond graphs are an inherently energy conserving and domain independent way of modeling dynamic systems. Additionally, the equations describing the behavior of the system can be algorithmically derived from the graph itself. As an example, the bond graph representing the underactuated index finger is shown in Figure 6.4; similar graphs are implemented on the other fingers and thumb. This system distributes actuator torque across the joints based on their relative stiffnesses and friction. The stiffnesses of the joints are based on [105, 106], and the friction parameters were determined by experimentation. When all joint torques have been calculated, they are entered into the dynamic model, which functions as the mechanical structure of the hand.

The dimensions, joint locations, and other parameters of the dynamic model are based on those of the human hand, the bone and joint structure of which can be seen in Figure 6.5. The fingers' interphalangeal (IP) joints are functionally equivalent to one-DOF flexion/extension joints. The metacarpophalangeal (MCP) joints at the base of the fingers have an additional abduction/adduction DOF. The thumb contains five DOFs: one (flexion/extension) in its IP joint, and two in both its MCP and carpometacarpal (CMC) joints [107]. In reality, the latter two joints have a complicated surface geometry, resulting in joint axes that are neither completely perpendicular nor coincident. In this model these are approximated by two-DOF flexion/extension and abduction/adduction joints. The individual joint ranges of motion are implemented as described in [13, 108].

In [57], the average dimensions of the human hand were examined in detail. A linear relation between hand segment sizes and hand breadth/length was determined, the results of which can be found in Table 6.1. These dimensions can be

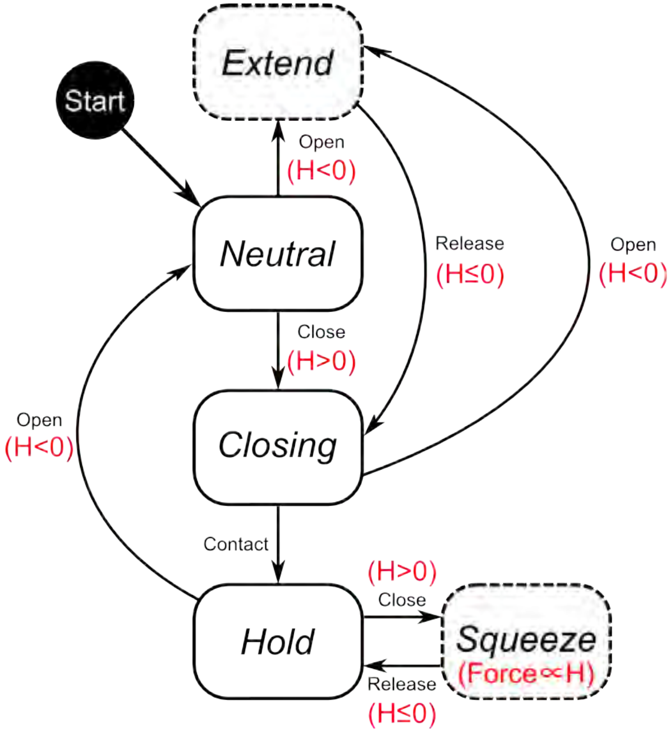

Figure 6.3: **Hand opening/closing state machine:** Similar to the Southampton Adaptive Manipulation Scheme [102], this system allows the user to switch between basic grasping states using a single control signal (hand opening/closing, or H). Starting from the *Neutral* state where preshaping takes place, the grasp can be closed using a single close (H>0) signal. The *Closing* of the grasp continues automatically at fixed speed until interrupted by an open signal (H<0) or contact is detected by the model. In the *Hold* state, the prosthesis will automatically apply sufficient force to counteract slipping of the held object. The *Extend* state enables grasping of larger objects, and the *Squeeze* state gives the user direct control over the force applied to a held object. This system is arranged to allow opening and closing of a grasp with a minimal number of commands for ease of use. States with a dashed border are only active as long as the signal to enter them is maintained.

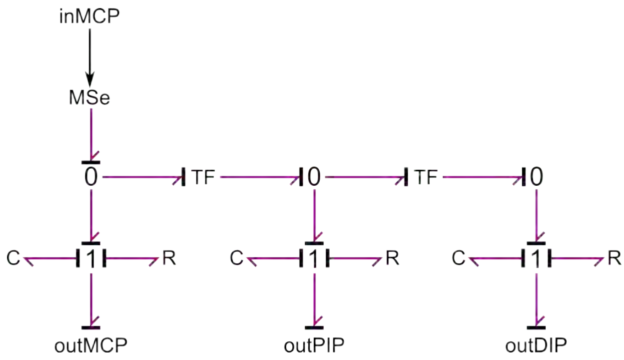

Figure 6.4: **Bond graph of the underactuated index finger:** The actuator is represented by an MSe element, providing torque which is distributed across the joints through junction (0, 1) and transformer (TF) elements. The capacitive (C) and resistive (R) elements represent the individual joints' stiffness and friction, respectively.

Table 6.1: Average radii of model phalanx ellipsoids (a, b, c), relative to total hand breadth (a, b) and hand length (c) [94, 57].

	Thumb	Index	Middle	Ring	Little
Carpal	(0.10,0.10,0.06)	-	-	-	-
Metacarpal	(0.07,0.08,0.13)	(0.10,0.12,0.23)	(0.09,0.13,0.22)	(0.09,0.14,0.21)	(0.08,0.13,0.21)
Proximal	(0.05,0.05,0.10)	(0.05,0.05,0.12)	(0.06,0.05,0.13)	(0.06,0.05,0.12)	(0.05,0.05,0.10)
Intermediate	-	(0.05,0.05,0.07)	(0.05,0.05,0.09)	(0.04,0.05,0.08)	(0.04,0.04,0.06)
Distal	(0.05,0.06,0.08)	(0.04,0.05,0.05)	(0.04,0.05,0.05)	(0.04,0.05,0.05)	(0.04,0.04,0.05)

used to approximate the phalanges by ellipsoid bodies [57]. Although this approximation does have significant deviations near the joints, this causes no problems during normal grasping; the parts of the phalanges that contact an object lie near the middle of the ellipsoids or at the tips of the fingers.

The average inertial parameters of the human hand were described in [12]. In this model, the individual phalanges' inertial parameters are approximated using the inertia tensor equations for a homogeneous ellipsoid with radii a, b, c as in Table 6.1, and mass m (all other components of the inertia tensor $\mathcal{I}$ are 0):

$$\mathcal{I}_{xx} = 0.2m(b^2 + c^2).$$
$$\mathcal{I}_{yy} = 0.2m(a^2 + c^2).$$
$$\mathcal{I}_{zz} = 0.2m(a^2 + b^2).$$

With the implementation of the dynamic model, the system is able to determine the effect of internally applied forces and torques. To complete the model, interaction forces with the environment and the hand itself have to be computed

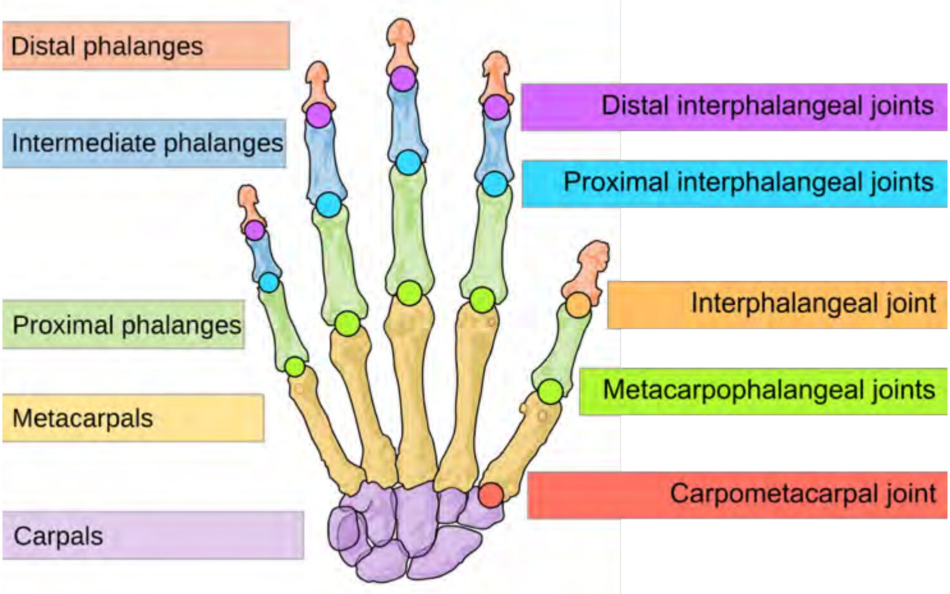

Figure 6.5: **Bone and joint structure of the human hand:** Bone names are listed on the left, while joint names are on the right. Edited image; original by Villarreal, M. R. "Main division on the human hand." <http://commons.wikimedia.org/wiki/File:Scheme_human_hand_bones-en.svg>

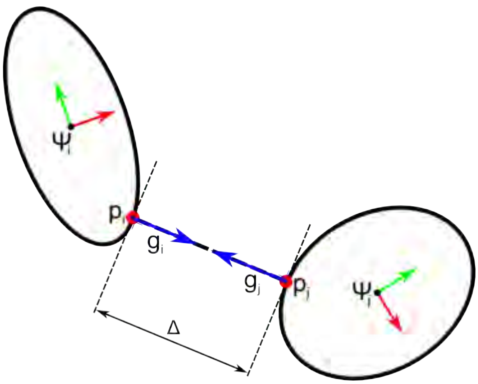

Figure 6.6: Closest point calculation of two ellipses (i, j) with minimal distance Δ. Note that the perpendicular vectors g_* are directly opposed to one another at the contact points p_*.

as well, using a contact model. A contact model needs to determine when and where two bodies intersect one another, and calculate the forces that need to be applied to the contacting bodies.

The points of least distance between an ellipsoid of the dynamic model and a plane (with which various test objects can be constructed) can be determined analytically [109]. Between two of the model's ellipsoids, this solution no longer applies and another method is required. In [99] such a method is described; a two-dimensional example can be seen in Figure 6.6. Take two three-dimensional ellipsoids (i, j) with coordinate frames Ψ_* and points of least distance p_* , where $*$ is i or j. At these points, separated by a distance Δ, the normal vectors g_* of the ellipsoids are directly opposed to one another. Taking P_i^j as the coordinates of point p_i in frame Ψ_j and H_j^i as the homogeneous coordinate transformation between coordinate frames j and i, Δ can be defined as the following inner product $(\langle , \rangle)$ [99]:

$$\Delta = \left\langle g_i, H_j^i P_j^j - P_i^i \right\rangle = \left\langle g_j, H_i^j P_i^i - P_j^j \right\rangle$$

Note that this distance will become negative as the bodies pass through one another, which allows contact to be defined as a zero crossing. The relationship between the coordinates P_i^i and P_j^j can be written as a function of g_j, Δ, and H_j^i as follows:

$$P_i^i - \Delta H_j^i g_j = H_j^i P_j^j$$

By then taking the time derivative of both these equations, with $\tilde{T}_j^{i,i}$ as a skew-symmetric matrix containing the translational and rotational velocities of frame j with respect to frame i expressed in frame i, the time derivative of these coordinates can be calculated by [99]:

$$\left(\dot{g}_i + H_j^i \dot{g}_j H_i^j \left(I + \Delta \dot{g}_i\right)\right) \dot{P}_i^i = \tilde{T}_j^{i,i} g_i + H_j^i \dot{g}_j \left(\dot{\Delta} g_j - \tilde{T}_i^{j,j} P_j^j\right)$$

The equations provided above allow analytical calculation of the movement of the two points of least distance, given the initial conditions which can be found through numerical iteration. When the distance between these points crosses below zero, contact has been established. The resulting forces applied to the colliding bodies are modeled viscoelastically, by combination of linear elastic and damping elements. With all model subsystems in place, the model can be tested, using only EMG input signals to directly control the grasping of a simple object.

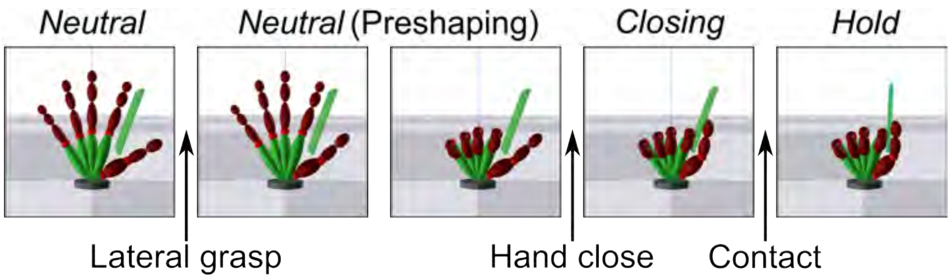

Figure 6.7: Lateral grasp simulation results, indicating the control system's state (above) and received inputs from EMG sensing and the environment (below).

6.1.4 Model applications and results

A pair of basic grasp types are executed to test the model's performance: a lateral grasp and a tripod grasp. For both grasps, the EMG control input consists of a grasp selection signal, followed by a hand close signal. The preshaping of the lateral grasp consists of minimal thumb opposition and full flexion of all fingers; preshaping of the tripod grasp requires the full flexion of the little and ring fingers, abduction of the index and middle fingers, and the thumb to be brought in opposition to the index and middle fingers.

The lateral grasp results are used to illustrate the model's response to the inputs received by EMG sensing, while the tripod grasp will show the functioning of the model's internal structure through a plot of the generated joint angles and forces. The progress of the lateral grasp can be observed in Figure 6.7. First, the control system receives a grasp selection signal for the lateral grasp. This causes it to control the thumb to the proper opposition angle, and to fully flex all fingers by applying a constant motor torque (*Neutral*). The grasp is now fully preshaped, and when a hand close signal is received afterward, the thumb is flexed at constant torque until a contact signal is received from the model (*Closing*). After contact, a continuous force is applied to keep the object in place (*Hold*).

The execution of the tripod grasp can be observed in Figure 6.8 along with several of the thumb's state variables, indicating the model's dynamic behavior. At the initial position, all joint angles are 0. When preshaping begins, the thumb opposition angle is controlled to the right position for the tripod grasp. After receiving the hand close signal, the underactuated structure of the thumb causes its joints to flex in a natural motion as motor torque is applied. When contact is made, the thumb's shape adapts to the object, which can be seen by the change in its joint angles as a consequence of the contact force. After the impact has been resolved, the joint angles stabilize. These figures demonstrate the success-

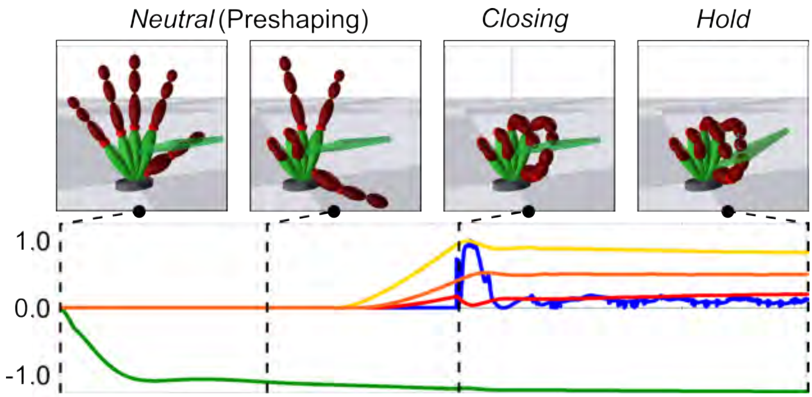

Figure 6.8: Tripod grasp simulation results, showing the thumb's opposition angle (rad) in green, the individual thumb joint flexion angles (rad) in red (IP joint), orange (MCP joint) and yellow (CMC joint), and the normalized total contact force on the thumb in blue.

ful operation of the model and control system.

6.1.5 Conclusions and future work

In this paper, a three-dimensional hand prosthesis model is described, based on the biomechanical structure of the human hand. The model is used as a testbed for a prosthesis control system based on input from EMG sensing. The model's validity is tested by executing two different grasp types on a simple object, demonstrating preshaping of the hand and subsequent flexion of the fingers and thumb. The correct operation of the control system, underactuation, contact model and dynamic model have been demonstrated. This model can provide control systems with any necessary information, including internal and external forces/torques, joint angles and velocities, and contact positions.

For future work on this model, the first point to be addressed is an extension of the dynamic model and control system to accommodate wrist motions. The addition of wrist rotation and flexion/extension would allow the model to exhibit the full functionality of modern hand prostheses.

Additionally, the mechanical design of a hand prosthesis could be tested as well. Many recently developed prosthetic hands employ methods such as linked finger flexion [103], passive joints [24] and reduced thumb opposition DOFs [33]. This is done to reduce the number of required actuators, due to the strict space and weight limitations present in hand prostheses. By establishing performance metrics based on grasping tests performed with this model, the relative effectiveness of models with mechanical simplifications could be evaluated.

Another future purpose of this system could be a combination of the model and its EMG-based control system in a real-time application for patient prosthesis training. For this to be useful, the user should be able to move the hand model in three dimensions as though it were connected to the forearm. An accelerometer mounted on the stump could be connected to the model to accomplish this. With the completion of these additions, this model could be used as a complete prosthesis design application. A prosthesis' control systems and mechanical design could then be tested and developed simultaneously, using input from patient trials to improve ease of use while optimizing functionality at the same time.

6.2 UB Hand tests

This section was published as “Development of Prosthesis Grasp Control Systems on a Robotic Testbed" [17].

6.2.1 Introduction

Unilateral amputees often use their sound hand to perform single-handed tasks. During bi-manual activities, the sound hand is used to manipulate objects while a prosthesis is used for support, which mostly involves the grasping and holding of objects. Current commercially available myoelectric prostheses [52, 53, 51] and recently developed prosthesis prototypes [24, 32, 103] are becoming increasingly anthropomorphic, with a high number of degrees of freedom (DOF). To effectively use this increased functionality while still remaining intuitive to the user, new grasp control systems are required. Such a system needs to provide a small but versatile selection of distinct grasp types (Figure 6.9), which can be operated with simple myoelectric commands for grasp selection, opening and closing. The grasp controller itself will then determine the right finger positions and orientations. Once the target positions have been determined, the fingers also need to be properly controlled to their end position. Since the hand has to interact with an unknown environment while remaining sufficiently safe for human interaction, this control needs to be both compliant and robust [1].

Basic position or force control systems respond badly to interaction with the environment [110]. To remedy this, several variations of interaction control have been developed, which seek to establish a dynamic relationship with the environment. While this improves these systems' ability to handle contact, they often require additional information about the system or its environment. The intrinsically passive controller (IPC) [110] provides an alternative to these types of interaction

(a)

(b)

(c)

Figure 6.9: Illustration of the different grasp types to be analyzed: (a) The lateral grasp; flexing all fingers and using the thumb to grasp flat objects. (b) The cylindrical grasp; surrounding an object with all fingers and the thumb. (c) The tripod grasp; using the index finger, middle finger and thumb to pick up small objects.

control. It consists of virtual springs exerting forces on the fingertips of the hand; these springs are connected to each other by a virtual object, which serves as the focus of the grasp. An advantage of this system is that it only requires fingertip position information.

The combination of IPC with a high-level grasp planner allows a multifunctional prosthesis to perform a variety of compliant grasps, while remaining intuitively controllable with only few myoelectric input signals.

In this paper, the viability of the IPC system for prosthetic grasp control is evaluated in comparison to position, admittance, and impedance control. Initially a bio-mechanical model of the hand [15] is used for testing the interaction controllers; the IPC controller then is implemented on the University of Bologna's (UB) robotic hand, the UB Hand IV. Though not a prosthesis itself, the UB Hand IV is used as a testbed for the control of hand prostheses because of its anthropomorphic design and high number of DOF.

This paper is organized as follows: in Section 2, the design choices and features of the UB Hand IV are described. Section 3 covers the various control systems and their components. In Section 4, the control system parameters are derived, and the experimental protocol is explained. Section 5 describes the experimental results. We conclude in Section 6, and the results and directions for future work are discussed.

6.2.2 UB Hand IV design

Current robotic hands are mainly designed based on conventional mechanics and robotics. Alternatively, the human hand can inspire an innovative robotic hand design. This approach has been adopted within the DEXMART project [111] for

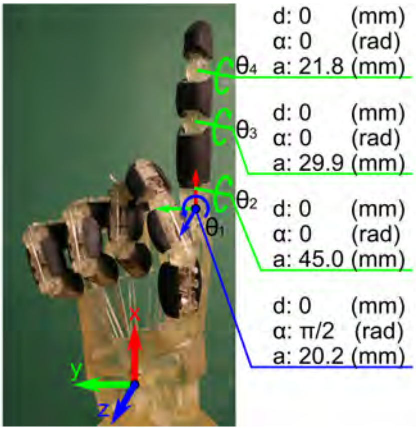

Figure 6.10: A diagram illustrating the UB Hand IV's wrist base frame, index finger base frame, and the Denavit-Hartenberg parameters of the fingers.

the development of the UB Hand IV. In this section, the main features of the hand's anthropomorphic design are discussed.

Parameters

The UB Hand IV possesses a total of 20 independent DOF, divided across 5 identical fingers. Each finger has three flexion/extension DOF, with one adduction/abduction DOF in the proximal joint. The distal flexion joint of each finger is passive; it is coupled to the middle flexion joint by an internal tendon.

The Denavit-Hartenberg parameters of the fingers are shown in Figure 6.10. The joint angles of each finger are mechanically constrained to the following intervals:

$$\theta_1 \in [-\pi/18,\, \pi/18] \text{ and } \theta_{\{2,\,3,\,4\}} \in [0,\, \pi/2] \quad \text{(rad)} \tag{6.1}$$

Endoskeletal structure

The endoskeletal design of the UB Hand's fingers allows sufficient room in the hand for sensors and related electronics. However, the complex shapes of the links are difficult to manufacture conventionally. Therefore, an additive manufacture technology (fused deposition modeling) has been implemented. Currently, integrated pin joints are used to connect the phalanges [112]; the design of these joints can be seen in Figure 6.11.

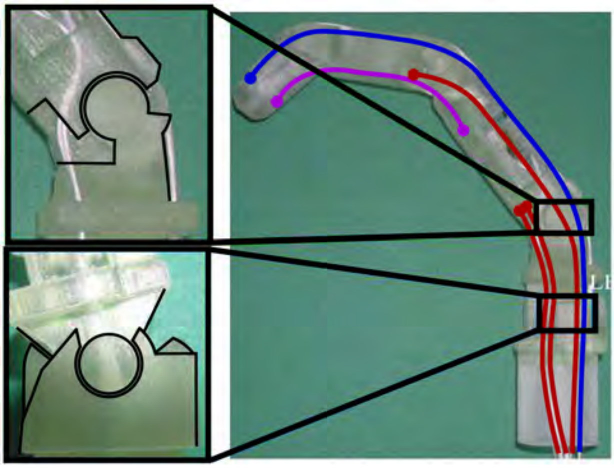

Figure 6.11: A close-up view of the UB Hand IV's integrated pin joints, as well as its internal tendon paths. Flexion tendons are marked in red, the extension tendon is blue, and the passive tendon is marked in purple.

Tendon-based transmission

As current technology does not allow the placement of more than a few actuators in an anthropomorphic robotic hand, it is necessary to place the actuators remotely, and use tendons for force transmission. Various tendon configurations have been proposed in literature [113, 114]. For the UB Hand IV, an '$N+1$' tendon configuration has been adopted, which can be seen in Figure 6.11. In this configuration, each joint DOF is actuated by a separate flexion tendon, with a single communal tendon for extension. It allows control of all joint DOF with a minimal number of actuators, and without any pretension mechanisms.

Routing the tendons from the motors to the joints is often done via pulleys attached to the joints, which is mechanically complicated. In the UB Hand, the tendons are routed through canals within the endoskeletal structure of the phalanges. The use of these tendon canals is a convenient solution due to its simplicity, though it introduces distributed friction along the tendon, which needs to be accounted for [115, 116]. A complete description of the UB Hand IV finger kinematics and tendon network can be found in [35].

Control

The hardware used to control the UB Hand IV can be seen in Figure 6.12. Since the I/O board does not possess a sufficient number of input and output channels, two interfacing boards for the multiplexing/demultiplexing of the signals have

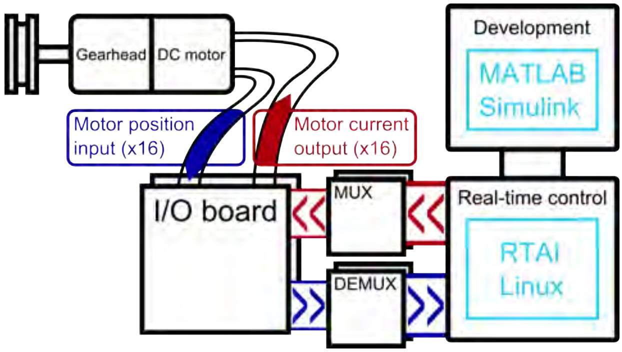

Figure 6.12: A block diagram describing the UB Hand IV control hardware. For actuation, commercial DC motors with integrated speed reducers and absolute encoders are used. The I/O board is a Sensoray 626 PCI analog and digital I/O card. The real-time control PC is a Pentium 4 at 1.8 GHz running the RTAI Linux operating system [**?**].

been built. The controllers are developed in a Matlab/Simulink [117] environment on a separate PC, using the Matlab Real-Time Workshop toolbox. As modern hand prostheses continue to increase in both anthropomorphism and DOF, the UB Hand's design makes it a fitting testbed for the control of future hand prostheses.

6.2.3 Control system structure

To provide an intuitive way of governing the complex motions of all the prosthesis' joints, the control system is organized hierarchically. Based on myoelectric input signals from the user, a high-level grasp planner provides target behaviors for the low-level controller, which governs the individual fingers. Various possible implementations of these systems, and their advantages and disadvantages, are discussed in this section.

High-level control: grasp planning

To allow the user to easily perform a grasp, the grasping process has to be divided into several discrete stages, which can be switched between by means of input signals. In general, two stages can be defined: preshaping and grasp execution. Once a grasp type has been selected, the grasp is preshaped by moving the fingers to the correct starting position for that grasp. Grasp execution involves the automatic closing of the grasp around an object, the degree to which can be controlled by the user.

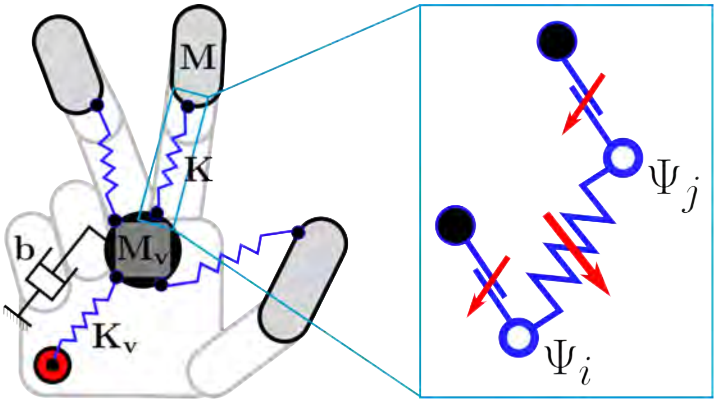

Figure 6.13: The various components of the IPC. Virtual springs (blue) with stiffness $(\mathbf{K})$ connect the virtual object $(\mathbf{M_v})$ to the fingertips $(\mathbf{M})$. The virtual object is connected by another spring $(\mathbf{K_v})$ to the virtual end position (red). A damper $(\mathbf{b})$ is also connected to the virtual object. On the right, a detailed view of a virtual spring is shown, with variable endpoint frames Ψ_i and Ψ_j.

According to the requirements analysis performed in [1], three important grasp types for daily activities are the lateral, tripod, and cylindrical grasps. The end positions of these grasps are shown in Figure 6.9.

The lateral grasp (Figure 6.9(a)) can be used for grasping flat objects securely. Preshaping is performed by fully flexing the index through little fingers, with grasp execution consisting of flexion of the fully unopposed thumb.

The cylindrical grasp (Figure 6.9(b)), for powerfully grasping larger objects, is preshaped by fully opposing the thumb and executed by flexing the thumb shortly after starting to flex all other fingers simultaneously.

The tripod grasp (Figure 6.9(c)) is a precise grasp used to pick up small objects. It is preshaped by opposing the thumb to the index and middle fingers, and fully flexing the little and ring fingers. Grasp execution consists of flexion of the index finger, middle finger and thumb.

To control a grasp with this system, only five input signals need to be distinguished; three for selecting the grasp type, and two for opening and closing the grasp.

Low-level control systems

These control systems calculate the desired wrench to be applied to each fingertip $(\mathbf{W}_{EE})$, which is converted into torques on the individual joints of the finger using the Jacobian $(\mathbf{J}(\theta))$:

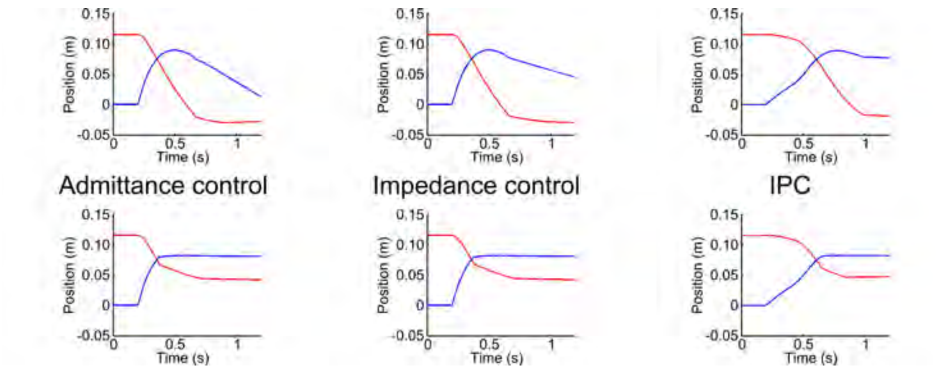

Figure 6.14: Simulation results for cylinder grasp testing on the UB Hand model in free space (above) and with an object (below). The index fingertip x position is shown in red, and its z position in blue (see Figure 6.10 for the finger base frame).

$$\boldsymbol{\tau}_{joints} = \mathbf{J}(\theta)^T \mathbf{W}_{EE} \tag{6.2}$$

The desired joint torques are then converted to actuator torques by the UB Hand IV's torque controller [35].

Proportional control The most basic method of control used here is a Cartesian proportional control system. It applies a fingertip force linearly dependent on the distance from the fingertip position ($\mathbf{x}$) to the target ($\mathbf{x}_d$), defined by the gain value ($\mathbf{K}$):

$$\mathbf{W}_{EE} = \mathbf{K}(\mathbf{x}_d - \mathbf{x}) \tag{6.3}$$

Proportional control is easy to implement, but is not a valid method of handling interaction [81]. Therefore, the use of this type of control system is limited to preshaping the hand or performing free space motion.

Interaction control To make a control system more robust to contact, it can be designed to control the dynamic interaction with the environment. Several possible approaches are available, all of which establish a relation between internal/external forces and positions/velocities of the fingers.

One way of approaching this is admittance control. It involves implementing a basic proportional controller, and changing its reference position based on external forces. The relationship between the measured external forces ($\mathbf{F}_{ext}$) and target/reference positions ($\mathbf{x}_d/\mathbf{x}_r$) is modeled as a mechanical admittance, with inertia ($\mathbf{M}$), damping ($\mathbf{D}$), and stiffness ($\mathbf{K}$):

$$\mathbf{M}\ddot{\mathbf{x}}_r + \mathbf{D}(\dot{\mathbf{x}}_r - \dot{\mathbf{x}}_d) + \mathbf{K}(\mathbf{x}_r - \mathbf{x}_d) = \mathbf{F}_{ext} \tag{6.4}$$

The resulting new reference position ($\mathbf{x}_r$) is then entered into the proportional controller (6.3) instead of the previous target ($\mathbf{x}_d$) to calculate the fingertip wrench to be applied.

In [81], it is argued that the environment of any manipulator can best be described as an admittance, and that for proper dynamic interaction the manipulator should behave like its complement, an impedance. In impedance control, the difference between the fingertip's current state (position, orientation, and their derivatives) and that of the target determine the wrench to be applied. In this case, its implementation is similar to a spring-damper system:

$$\mathbf{W}_{EE} = \mathbf{D}(\dot{\mathbf{x}}_d - \dot{\mathbf{x}}) + \mathbf{K}(\mathbf{x}_d - \mathbf{x}) \tag{6.5}$$

Alternatively, this control can also be located in the joints themselves, establishing a direct relation between the current and desired joint angles/velocities, and the joint torques [118].

It should be noted that the mentioned interaction control systems may require more advanced information on the system, such as external forces and velocities. While improving the dynamic behavior, these added requirements can be restrictive.

Intrinsically Passive Control (IPC) This control method [110] establishes virtual springs between the fingertips and a virtual object, the dynamics of which are modeled in the controller. The virtual object is the center of the grasp, and is connected via another spring to a virtual end position. A diagram representing this controller can be seen in Figure 6.13. The virtual springs, shown in Figure 6.13, exert wrenches ($\mathbf{W}$) on their end points i and j, with coordinate frames Ψ_i and Ψ_j, respectively. These wrenches consist of torque ($\mathbf{m}$) and force ($\mathbf{f}$) components, and are based on the differences in orientation ($\mathbf{R}_j^i$) and position ($\mathbf{p}_i^j$) of the endpoints as follows [110]:

$$\mathbf{W}_i = \begin{bmatrix} \mathbf{m}_i \\ \mathbf{f}_i \end{bmatrix} \tag{6.6}$$

$$\tilde{\mathbf{m}}_i = -2(\mathbf{G}_o\mathbf{R}_i^j)_A - (\mathbf{G}_t\mathbf{R}_j^i\tilde{\mathbf{p}}_i^j\tilde{\mathbf{p}}_i^j\mathbf{R}_i^j)_A - 2(\mathbf{G}_c\tilde{\mathbf{p}}_i^j\mathbf{R}_i^j)_A \tag{6.7}$$

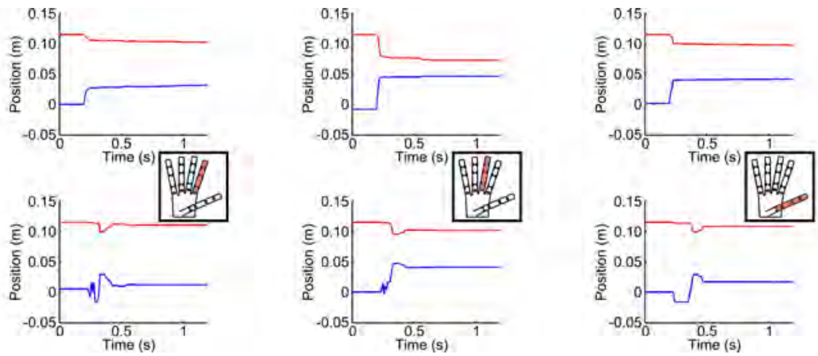

Figure 6.15: Experimental results for free-space tripod grasping with the proportional controller (above) and IPC (below), implemented on the UB Hand IV. The fingertip x position is shown in red, and its z position in blue (see Figure 6.10 for the finger base frame).

$$\tilde{\mathbf{f}}_i = -\mathbf{R}^i_j(\mathbf{G}_t\tilde{\mathbf{p}}^j_i)_A\mathbf{R}^j_i - (\mathbf{G}_t\mathbf{R}^i_j\tilde{\mathbf{p}}^j_i\mathbf{R}^j_i)_A - 2(\mathbf{G}_c\mathbf{R}^j_i)_A \tag{6.8}$$

$\tilde{}$ represents the twist operation, and $()_A$ determines the anti-symmetric part of the matrix. These torques and forces are based on translational ($\mathbf{G}_t$), orientational ($\mathbf{G}_o$) and coupling ($\mathbf{G}_c$) co-stiffnesses, which can be calculated from regular stiffness matrices ($\mathbf{K}_t, \mathbf{K}_o, \mathbf{K}_c$) as follows:

$$\mathbf{G}_* = \frac{1}{2}\mathrm{Tr}(\mathbf{K}_*)(\mathbf{I} - \mathbf{K}_*) \tag{6.9}$$

where $* = t, o, c$ and $\mathbf{I}$ is a 3×3 identity matrix. These stiffnesses can be changed in order to control the applied force. Additionally, the springs' rest length can be controlled by changing their connection points [119].

A damping force is applied to the virtual object, which guarantees the asymptotic stability of the system [110]. As the virtual object's state is fully observable, the implementation of damping can be done without requiring additional sensors. The points on the virtual object where the virtual springs are connected can be chosen in such a way as to surround an object with the fingers, which improves grasp performance. The grasp planner can control the system's dynamic behavior through manipulation of the virtual spring parameters and the location of the virtual end position.

6.2.4 Experiment design

Before implementing and evaluating the different controller types, the appropriate parameters and setpoints should be determined. Afterward, the test protocol for simulation and UB Hand experimentation is described.

Controller parameters

The main parameters governing the interaction controllers' behavior are the damping ($\mathbf{D}$) and stiffness ($\mathbf{K}$) gains, which are chosen with regard to the maximum force that the hand's motors can continuously provide. In the UB Hand's case, this is approximately 50 N. The stiffness value is set accordingly, and the damping value is then tuned experimentally.

Relevant parameters for the IPC (Figure 6.13) include the inertial parameters of the virtual object ($\mathbf{M_v}$), the damping coefficient ($\mathbf{b}$), and the stiffnesses of the virtual springs ($\mathbf{K}$, $\mathbf{K_v}$). The virtual springs' stiffness values can be determined in the same way as with the interaction controllers. To make sure the higher-order system created by the application of damping directly on the virtual object resembles a basic second-order system as closely as possible, two limits are placed on the parameters: the mass of the virtual object should be lower than the mass of the rest of the system, and the spring connecting the virtual object to the virtual end position should be more compliant than those connecting the virtual object to the fingertips [**?**]. Additionally, to achieve critical damping, the damping coefficient ($\mathbf{b}$) should be determined as follows:

$$\mathbf{b} = \mathbf{I} \cdot \sqrt{K_v M} \tag{6.10}$$

where (K_v) is the (scalar) stiffness of the spring connecting the virtual object to the virtual end position and (M) represents the weight of the finger.

Grasp planning

Depending on the grasp type, the interaction control grasp planner assigns preshaping and grasping setpoints for each finger; these can be switched between by the user. To move the fingertips across a naturally curling trajectory, a path planner is implemented, using polar interpolation between the current fingertip position and the desired end point.

The IPC grasp planner determines two main parameters based on the grasp type: the location of the virtual end position (which influences the virtual object's location), and the location of the virtual spring end points, which represent the desired end configuration of the fingertips. Additionally, fingers that are not participating in the grasp are set to full flexion, and are not connected to the virtual object. For preshaping, the virtual springs' rest length is set to a high value, surrounding the virtual object with the fingertips and allowing the user to position

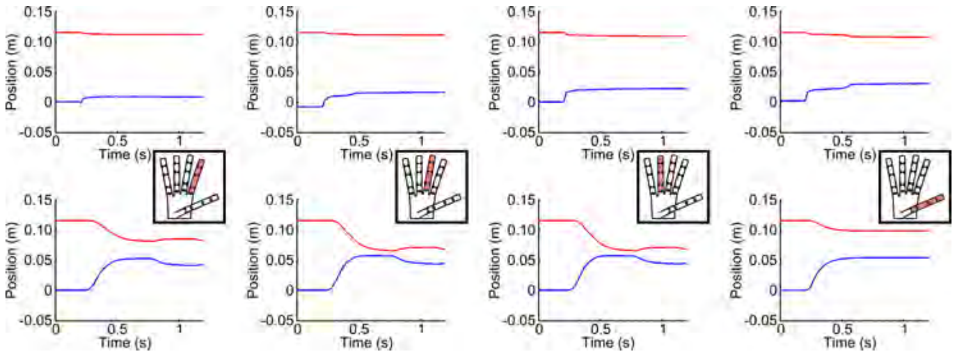

Figure 6.16: Experimental results for cylinder grasping of an object with the proportional controller (above) and IPC (below), implemented on the UB Hand IV. The fingertip x position is shown in red, and its z position in blue (see Figure 6.10 for the finger base frame).

the hand around the target. To close the grasp, the rest lengths are gradually reduced. During grasping, any obstruction of the fingers' movement will result in displacement of the virtual object, and the grasp focus will shift accordingly. This allows the hand to adapt to varying object shapes and motions, increasing the stability of the grasp.

Test protocol

As the current UB Hand hardware does not have sensors capable of determining joint velocity or external forces, the tested impedance and admittance controllers could not be implemented on it. Therefore, initial testing and evaluation of all controllers is done on a dynamic model of the UB Hand [15], implemented in Simulink [117]. In this simulation, the controllers are used to perform grasping motions with and without a simulated obstruction. After initial evaluation, the IPC system is transferred to the UB Hand hardware. It is then used to execute the three grasp types shown in Figure 6.9 with and without an object.

6.2.5 Results

The performance of the controllers was evaluated both in simulation and actual experiments on the UB Hand. The simulations and grasp trials all lasted for 1.2 seconds, with the controller changing from preshaping to closing at $t = 0.2$ s. The results of the simulation tests can be seen in Figure 6.14.

During free-space grasping, the IPC transferred from preshaping to grasping without discontinuity, while the interaction controllers exhibited a sudden start of motion. This did result in a response time delay of 0.1 s for the IPC. After the initial simulation tests, a cylindrical object was added to the model. While all controllers handled contact with the object well, the IPC reached its equilibrium position sooner than the interaction controllers.

Testing on the UB Hand IV was performed using IPC, as well as a proportional controller already present on the system. The results of these tests are shown in Figures 6.15 and 6.16. During free-space grasping the IPC showed some oscillations before arriving at a stable position, whereas the proportional controller moved directly to the target position.

The compliant behavior of the IPC during grasping resulted in a stable grasp; for example, when the thumb's limited abduction angle did not allow it to move to the virtual object's position, this caused the virtual object to shift accordingly, moving the grasp focus and completing the grasp. The proportional controller did not perform as well in this scenario, stopping before the fingers fully surrounded the object and not accommodating the object's motion.

6.2.6 Conclusions and future work

To compensate for the increased number of DOF in modern myoelectric prosthetic hands, advanced hierarchical control systems are necessary. The system developed here contains a global grasp planner, which sends setpoints to low-level finger controllers. This paper features the UB Hand IV, an anthropomorphic robotic hand developed by the University of Bologna using a three-dimensional printing process. It is used as a testbed for the development of prosthetic hand controllers; given the increase in DOF of modern prosthetic hands, control systems tested on the UB Hand IV can be considered suitable for implementation in future hand prostheses. After evaluating several types of interaction control, IPC was selected for testing, as it provides compliant control while working with only joint position information. This makes it useful for the control of prosthetic hands, which often interact with the environment and have tight constraints on available space and weight.

IPC has been implemented and tested on the UB Hand IV, performing three basic grasp types that represent activities of daily living. The results show that the IPC system is able to compliantly grasp a variety of objects and capable of dynamically adapting the focus of the grasp.

In future work, the development of a multifunctional prosthesis prototype with joint-mounted Hall sensors for angular position and force sensors in the fingertips would allow for the evaluation of IPC and interaction control systems in a practical setting. Additionally, real-time myoelectric input signals from test subjects can be used for evaluation of the high-level control system.

6.3 Control of the UT Hand I

This section has been submitted as “EMG-Based Grasp Control of the UT Hand-I" [21].

6.3.1 Introduction

The improvements of modern prototype hand prostheses [23, 33, 56, 36, 103, 24] over commercially available hands [51, 52, 53] often include an increase in degrees of freedom (DOF). However, maintaining a human-like weight and size requires significant underactuation, which leads to a loss of controllability. A method of selecting or blocking certain DOF can be used to perform various motions with a single primary actuator. Such a mechanism has been implemented in a new minimally actuated prototype hand prosthesis: the UT Hand-I [20].

The UT Hand-I (Figure 6.17) has 15 DOF, which are actuated by 3 DC motors through a tendon-pulley system. The underactuated finger joints of the hand are equipped with a series of joint locks. Different finger motions are selected by blocking the movement of certain joints. Furthermore, the motion of selected fingers can also be disabled entirely. The evaluation of the UT Hand-I as a viable alternative to modern hand prostheses requires the development of an intuitive control system. The control system is based on EMG signals from the user selecting automated motions of the hand. These hand motions are mainly focused on grasping, which is a major part of activities of daily living for single-sided amputees [1]. The goal of this study is to develop and evaluate the UT Hand-I's new EMG-based control system.

Related work

Relevant research on the topics of hand prosthesis design and control are reviewed to determine the requirements of the UT Hand-I and its control system.

Prosthesis prototypes A significant factor in the design of modern hand prostheses with regard to their control is underactuation, as the number of required actuators should be kept low while a high number of DOF is desired. It also provides a natural dynamic appearance, as the mechanisms can be designed

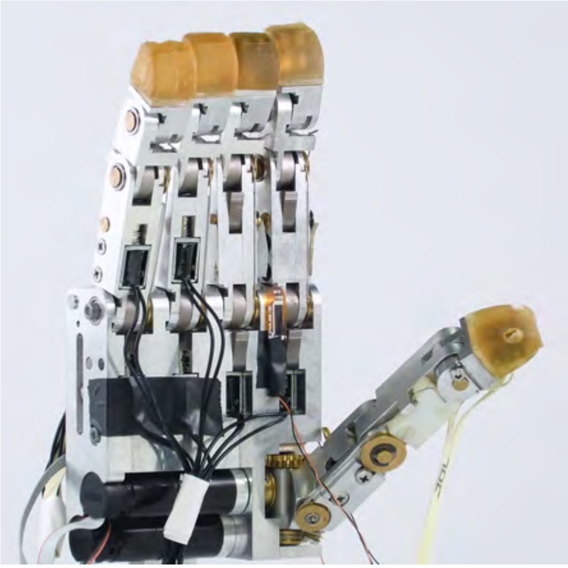

Figure 6.17: The UT Hand-I prosthesis prototype, featuring 15 DOF actuated via a tendon-pulley system and four-bar linkages. Integrated joint locking mechanisms maintain controllability of the underactuated joints.

to have the finger wrap around grasped objects. Some examples of prosthesis prototypes with various methods of underactuation are the following:

- The Southampton hand [102], AR hand III [33], and KNU hand [56] use four-bar mechanisms to rigidly couple the motion of the finger joints.
- The VU hand [36] and Smarthand [103] use a tendon-pulley system to flex the fingers, with extension springs to extend them and maintain tendon tension.
- The MANUS-HAND [24] uses a combination of tendon-pulley actuation for the index and middle fingers, passive compliant ring and little fingers, and an intermittent actuation system for the flexion and opposition of the thumb.

The UT Hand-I also features underactuated grasping. The four fingers are coupled by a tendon-pulley system, which is actuated by a single DC motor. This underactuation would normally preclude direct control over the individual DOF. By using joint locking mechanisms, specific sets of joints can be actuated [16], which allows the UT Hand-I to perform several distinct grasp types used in activities of daily living. These motions can be controlled by the user via an EMG sensing system.

EMG interface The current EMG control systems for most modern commercial hand prostheses [51, 52, 53] provide only one or two control signals. These signals are used to open and close a basic grasping motion with all fingers, which can be adjusted by means of the (active or passive) thumb and wrist.

In recent research, advanced EMG sensing is implemented to provide a larger number of control signals. In Boere et al. [80], up to 8 control signals were isolated with an accuracy of over 96%. This increase in control signals can allow the user to access the improved functionality of modern prosthesis prototypes. However, this will also require increased attention on the part of the user.

The requirements of the control system are driven by the limitations of EMG sensing and the user. The system should allow the user to control all possible grasping motions and gestures. However, this needs to be done with as few control signals as possible and without requiring continuous control input from the user. In recent research on the requirements for state-of-the-art EMG-based prostheses [1] automated grasp execution is favored, while the user controls grasp selection and the magnitude of grasping speed and force. These functions can be provided by means of a two-tiered system, consisting of high-level and low-level controllers.

Hand control The user-controlled selection and execution of grasps is handled by the high-level control system. In Peerdeman et al. [1], various methods of high-level prosthesis control used in modern research prototypes were investigated. A selection of several discrete grasp types is considered beneficial, although most modern prostheses are unable to distinguish grasp types in ways other than the thumb's opposition angle. The UT Hand-I is able to provide separate finger flexion motions for precision and power grasps, and can selectively actuate fingers for various gestures. This selection of grasps and gestures can be accessed by means of a state machine, such as the one implemented in the Southampton hand [41].

The automated motions of the hand are governed by the low-level control system. In Engeberg et al. [120], several low-level controllers are implemented on a 1-DOF prosthetic hand. Similarly, a range of interaction control systems is evaluated on a robotic hand in Peerdeman et al. [17]: admittance control, impedance control [81], and Intrinsically Passive Control [110, 121].

Contributions

This paper presents a novel method of myoelectric prosthesis control, implemented on the UT Hand-I: a multifunctional underactuated prototype hand prosthesis. The increased control functionality of the UT Hand-I is accomplished via the following subsystems:

- A multi-channel EMG sensing system, capable of classifying the muscle activation patterns of up to 8 functional hand motions. Each of these patterns corresponds to a grasp type, neutral, or hand opening signal. The intensity of the EMG activity is derived from its root mean squared (RMS) value, and is used to proportionally control grasping speed and force.
- The EMG control signals are interpreted by a high-level state-machine control system, which gives the user control over the global grasping behavior of the hand.
- Low-level control of the individual fingers and thumb is performed automatically. This provides several advantages: handling quick changes in position or external forces; reduction of stress on the user; and reducing sensitivity to errors and noise in the EMG signal. An intrinsically passive interaction control system is developed and experimentally evaluated.

The structure of this paper is as follows: In Section 2, the structure and kinematics of the UT Hand-I are modelled. Section 3 covers the design of the control system's various components. The control system is evaluated by means of various grasp tests in Section 4, and Section 5 contains the conclusion and suggestions for future work.

6.3.2 Modelling

Development of a low-level control system for the UT Hand-I requires a model of its mechanical structure and kinematics. In this section, these are analyzed in detail.

Prosthesis structure

The UT Hand-I was designed to emulate the human hand's structure and dynamic behavior. All actuators and mechanisms are housed within the palm and phalanges of the hand.

Fingers The hand has four fingers with 3 flexion DOF each. The fingers are actuated by a single DC motor (RE16, Maxon Motor AG, Sachseln, Switzerland) via a tendon-pulley system. The joints of each pair of fingers are connected by a tendon each. Both tendons are routed around actuation pulleys, which are in

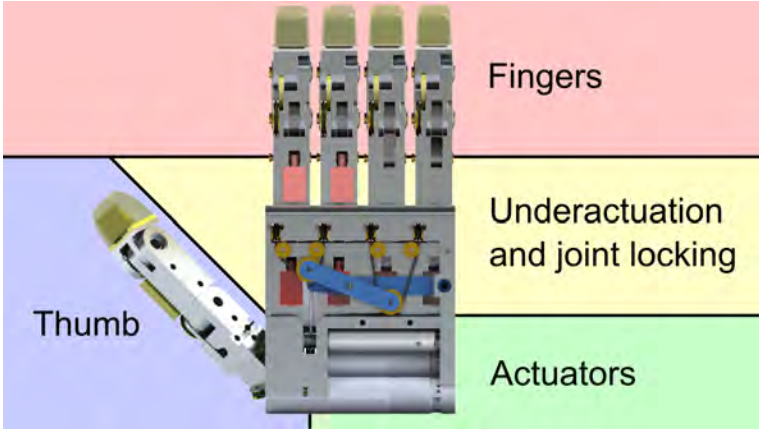

Figure 6.18: A rendering of the UT Hand-I, indicating relevant subsystems.

turn connected to the primary actuator by a rotating linkage. The structure of the underactuation system can be seen in Figure 6.18.

The distal interphalangeal (DIP) joints of each finger are not connected to the tendon-pulley system, but are instead directly coupled to the proximal interphalangeal (PIP) finger joints by four-bar linkages. These linkages ensure a ratio between the distal and proximal joint angles of 2:3, which is similar to that observed in human fingers [13].

Joint locking The underactuation of the fingers' 8 uncoupled DOF is controlled by a series of locking mechanisms on the joints. These joint locks can selectively disable certain DOF, while leaving the others free to move. In this way, various finger motions can be performed. Also, individual fingers can be locked entirely. The joint locks operate on the basis of friction between a drum connected to the joint, and a movable pawl, as shown in Figure 6.20. This mechanism is designed to be self-locking once the pawl and drum are brought into contact, and therefore requires minimal actuation force. Miniature solenoids (F0415L, Transmotec Sweden AB, Täby, Sweden) are sufficient to provide this force, allowing the entire locking mechanism of a joint to be integrated into the phalanx.

Thumb In contrast to the four fingers, the thumb is actuated by 2 DC motors (DCX10 & RE16, Maxon Motor AG, Sachseln, Switzerland) for opposition and flexion of the metacarpophalangeal (MCP) joint. The thumb's interphalangeal (IP) joint is passively linked to its MCP joint by a tendon coupling. The thumb is opposed via a non-backdrivable worm wheel transmission, which prevents the

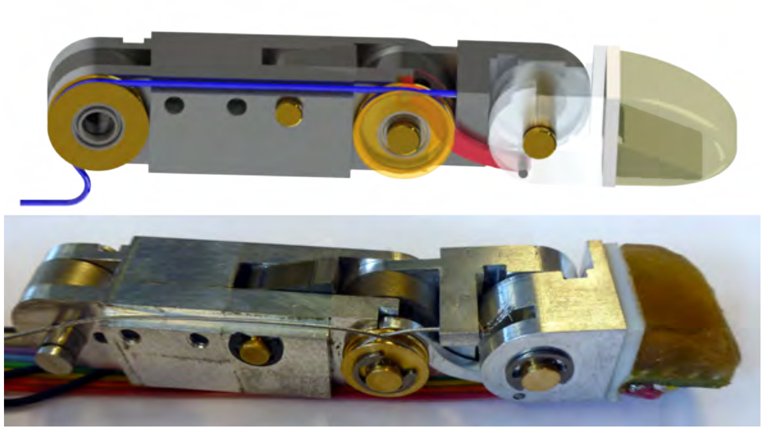

Figure 6.19: The fingers of the UT Hand-I. A rendering of the finger highlights the joint coupling bar (red) and actuation tendon (blue).

smaller opposition motor from having to resist external forces on the thumb. The thumb is placed at a 45 degree angle to the other fingers and the palm. This requires the tendon used for its flexion to be routed around the opposition shaft and several pulleys to align it with the proximal phalanx. The thumb is shown in Figure 6.22.

Sensors A hand prosthesis needs information on external forces and the position of its fingers to provide the user with feedback and assist in interaction with its environment. The UT Hand-I measures its joint angles with 3 cm long Bend Sensors (Flexpoint Sensor Systems, Inc., Draper, UT, USA), which are routed along the outside of the finger's joints. Resistance changes while bending are converted into usable angle data, which can be entered into the kinematic model of the hand (see Section 6.3.2) to determine its pose.

Each fingertip consists of urethane rubber cast over a 3D-printed base, which improves grasping by increasing both compliance and friction. Based on the TakkTile system [89], an array of MPL115A2 barometer ICs (Freescale Semiconductor, Inc., Austin, TX, USA) is embedded in the rubber under vacuum. This allows the sensors to detect contact forces instead of air pressure. Each fingertip array contains four sensors, which are individually addressable.

Prosthesis model

Analysis of the kinematics of the UT Hand-I can be divided into the underactuated fingers and fully actuated thumb.

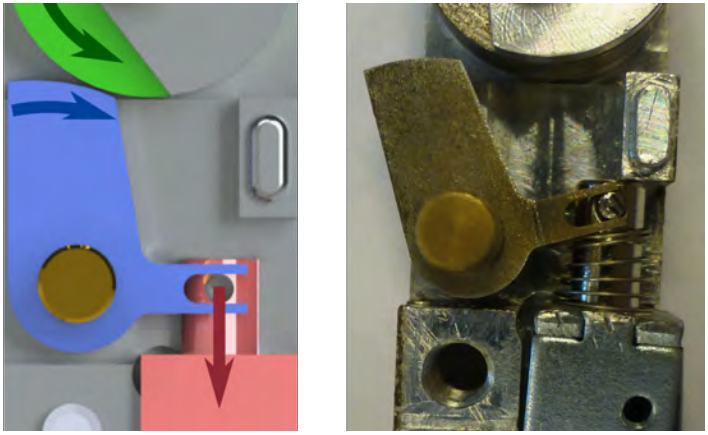

Figure 6.20: The joint locking system in the proximal phalanx of the finger. A rendered version of the joint lock highlights the solenoid (red), pawl (blue), and drum (green), as well as their direction of motion.

Fingers The underactuation system of the UT Hand-I controls the motion of the fingers' 8 effective DOF (of the 12 joints, the 4 DIP joints are rigidly coupled to the PIP joints) with a single DC motor. To control the behavior of this system, kinematic analysis is required; a diagram of the underactuation linkage is shown in Figure 6.23. Because of the small rotation range of the fingers' underactuation linkage, its non-linearities can be approximated by a linear solution with an error of below 5%. If we assume a roughly equal stiffness and friction in all joints, the relation between the motor velocity (ω_{4f}) and average finger joint velocity ($\widehat{\dot{\theta}_f}$) can be obtained by the following equation:

$$\omega_{4f} = \frac{b_{OF}}{r_{4f}}\, r_S\, (f_1 c_1 + f_2 c_2)\, \widehat{\dot{\theta}_f} \tag{6.11}$$

In this equation, b_{OF} represents the length of the first link of the pulley tree, r_S is the radius of the mobile pulleys and r_{4f} is the radius of the tendon reel connected to the finger flexion motor. f_1 and f_2 are the numbers of active joints on each tendon path, and c_1 and c_2 are constants determined by the linear approximation of the tendons' behavior. This simplification of the underactuated kinematics allows a relatively straightforward control of the hand during grasping.

Thumb The thumb's 2 effective DOF are each actuated by separate motors. A coupling is present between the two DOF, as the thumb's flexion tendon is routed around the opposition shaft, changing its path length during opposition. A non-backdrivable worm gear between the opposition motor and thumb shaft

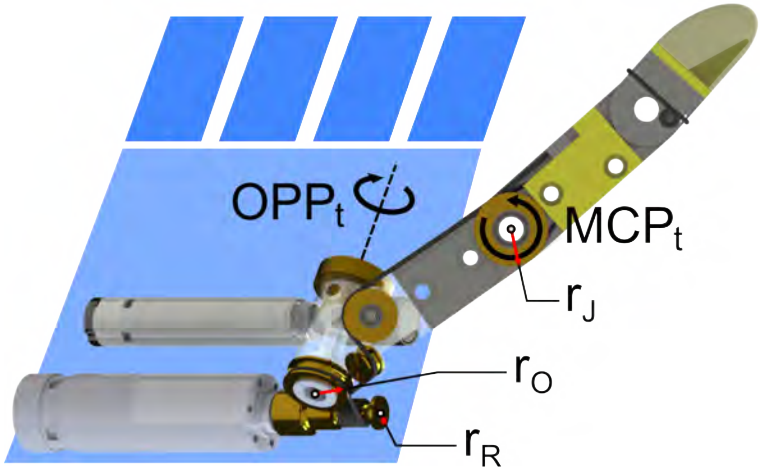

Figure 6.21: A rendering of the thumb actuation system, showing its position relative to the rest of the hand (blue). The thumb's opposition (OPP$_t$) and metacarpophalangeal (MCP$_t$) DOF are indicated, as well as the radii of the MCP joint pulley (r$_J$), opposition pulley (r$_O$), and flexion motor reel (r$_R$).

prevents the more powerful flexion motor from opposing the thumb. However, during opposition the flexion motor should move as well to prevent unwanted flexion. This coupling is described in the kinematics of the thumb as follows:

$$\left\{ \begin{array}{c} \omega_{f_t} \\ \omega_{o_t} \end{array} \right\} = \left[\begin{array}{cc} \frac{r_J}{r_R} & \frac{r_O}{r_R} \\ 0 & \nu_w \end{array} \right] \left\{ \begin{array}{c} \dot{\theta}_{MCP_t} \\ \dot{\theta}_{OPP_t} \end{array} \right\} \tag{6.12}$$

Where ω_{f_t} and ω_{o_t} represent the motor velocities for flexion and opposition, and $\dot{\theta}_{MCP_t}$ and $\dot{\theta}_{OPP_t}$ represent the joint velocities of the DOF shown in Figure 6.21. r_J, r_O and r_R are the radii of the pulleys on the MCP joint, opposition shaft, and thumb flexion motor, respectively. ν_w is the transmission ratio of the worm gear.

6.3.3 Control system design

The two-tiered control system of the UT Hand-I enables a small number of control signals from the user to control several automated grasping motions. The high-level control system is a user-controlled state machine which is used to select a grasping behavior and control its execution. The low-level controller performs the desired grasp and interacts with the environment.

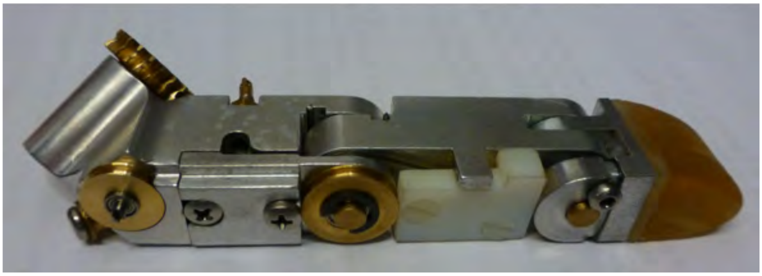

Figure 6.22: The thumb of the UT Hand-I. A rendered version of the thumb shows the path of the thumb's coupling tendon.

High-level control

The high-level control state machine is navigated via the control signals obtained from EMG sensing.

Figure 6.24 shows the high-level controller as a state-machine diagram. The states are defined as follows:

Neutral: This is the basic state of the hand in rest. Any non-neutral grasp type signal (*2-5*) will cause it to move to **Preshaping**.

Preshaping: In this state, the hand moves its fingers and thumb into position for the desired grasp type. Joint locking is also performed here.

Ready: Once preshaping is completed, the hand will remain still, allowing the user to position the hand around an object to be grasped. When the user continues to provide a grasp type signal (*2-4*), the hand moves to the **Closing** state. If an *Open* signal is received, the hand moves to **Preshaping** for the neutral grasp type.

Closing: The hand will start to close automatically. Its grasping behavior depends on the intensity of the EMG signal provided by the user. If an *Open* signal is received, the hand moves to the **Opening** state.

Opening: In this state, the fingers and thumb involved in the grasp are extended. The appropriate grasp type signal (*2-4*) will return the hand to the **Closing** state. If the hand reaches its preshaping position, it moves to the **Ready**

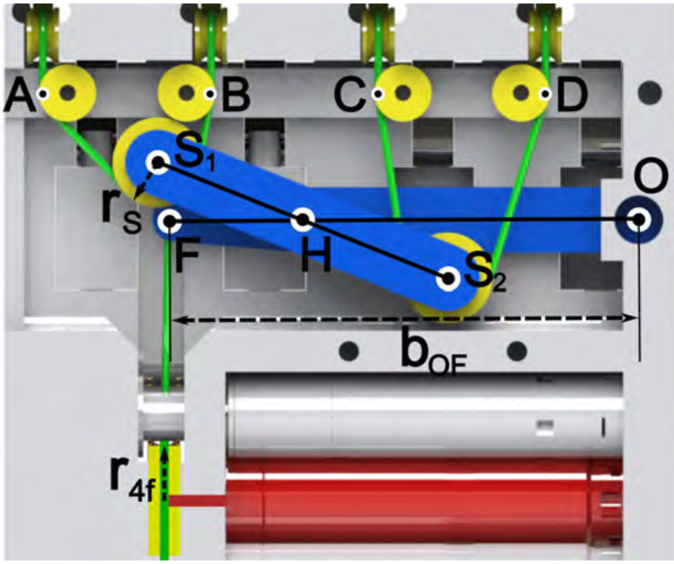

Figure 6.23: A rendering of the palm underactuation system. The flexion motor (red), underactuation linkage (blue), pulleys (yellow), and tendons (green) are highlighted. Linkage lengths (b_{OF}) and pulley radii (r_S, r_{4f}) relevant to the hand's kinematics are indicated.

state.

The design of the high-level control system gives the user a selection of different grasp types and allows for direct control of grasping force and speed. However, the system also offers simplicity of use, as continuing to hold a certain grasp type signal will automatically execute that grasp. Also, giving a continuous *Open* signal will always return the hand to a neutral position.

Low-level control

The low-level controller should move the fingers and thumb to the desired end positions (depending on the grasp type) with the desired force and speed. However, another important task of the controller is to interact with the environment in a compliant way. One method of controlling the position of a finger is proportional control: The force applied to the four fingers by the primary actuator ($\mathbf{F}_f \in \mathbb{R}^{3\times1}$) depends on the distance between the fingertips' current and desired position ($\mathbf{x}$, $\mathbf{x}_d \in \mathbb{R}^{3\times1}$). This controller can be physically represented as a spring with stiffness (K) that is connected to the current and desired position of the fingertips.

$$\mathbf{F}_f = K(\mathbf{x}_d - \mathbf{x}) \tag{6.13}$$

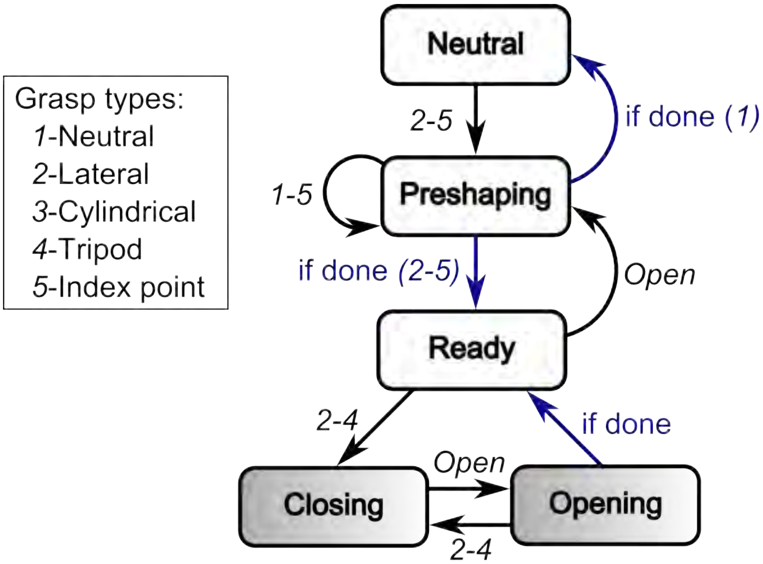

Figure 6.24: The high-level control state machine. States are changed by receiving either a grasp selection signal (*1* through *5*) or an *Open* signal from EMG sensing (blue state changes are automatic). The shaded states indicate variable speed/force depending on EMG signal intensity.

This proportional control can also be applied to the motor directly, using current control to determine the torque at the motor (τ). This controller relates the desired motor torque (τ_d) to the current and desired motor position (x_m and x_{md}) by a gain (K).

$$\tau_d = K(x_{md} - x_m) \tag{6.14}$$

If τ and x_m are known, the amount of energy injected into the system by the motor during a grasp can be calculated. x_{md} is fixed based on the grasp type, so using (6.14) the grasp energy (E_g) can be directly related to K as follows:

$$E_g = \frac{1}{2}K(x_{md} - x_m)^2 \tag{6.15}$$

By ensuring that the injected energy is limited to that of the system's desired physical equivalent (the elastic element represented by K), the system can be made inherently passive and stable [110**?**]. This is accomplished by implementing an 'energy tank' (E_t) which contains the maximum amount of energy available to the grasp. A control law limits τ depending on τ_d, the minimal energy level in the tank (a) and the angular velocity of the motor ($\dot{q}$):

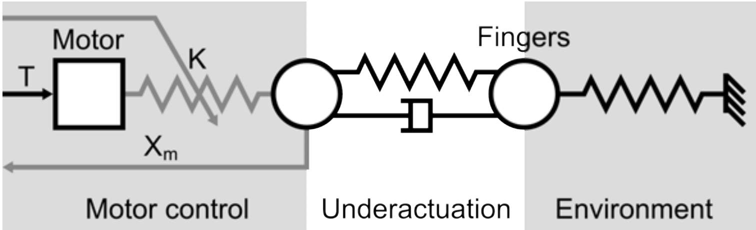

Figure 6.25: A simplified one-dimensional diagram of the grasp energy low-level control system, the hand, and its environment. The control action is represented by the virtual stiffness (K) in gray.

$$\tau = \begin{cases} \tau_d & \text{if } E_t \geq a \vee (\tau_d \dot{q} < 0) \\ 0 & \text{if } E_t < a \wedge (\tau_d \dot{q} > 0) \end{cases} \tag{6.16}$$

To ensure passivity, a is adjusted according to the controller's sample time and the rate of energy transfer to the grasp. Ideally, the user's control over the hand's grasping behavior is implemented by changing the desired elasticity of the grasp. By rewriting (6.15), K can be derived from E_g. By scaling the flow of energy from E_t to E_g with the intensity of the EMG signal, the user is able to directly control the energy of the grasp while maintaining passivity and stability. A diagram of the resulting control system is shown in Figure 6.25.

The example above illustrates the effect of the grasp energy controller in a 1D situation. Although the fingers' underactuation and joint locks lead to a variable number of DOF, the basic structure of the control system remains valid. With this system, the user is capable of controlling both force and speed by adjusting the grasp energy, which has the advantage of being a scalar and intuitively interpretable measure.

6.3.4 Grasping experiments

EMG input

A real-time EMG sensing algorithm has been developed, based on multichannel surface myoelectric signals and pattern recognition. Its structure resembles that of most pattern-recognition-based myoelectric control systems [47, 1] and is shown in Figure 6.26.

A reference amplifier (REFA 72, TMSi, Oldenzaal, the Netherlands) with a sample frequency of 2048 Hz is used to record signals from a grid of monopolar Ag/AgCl electrodes (BRS-50-K, Ambu, Ballerup, Denmark) evenly distributed

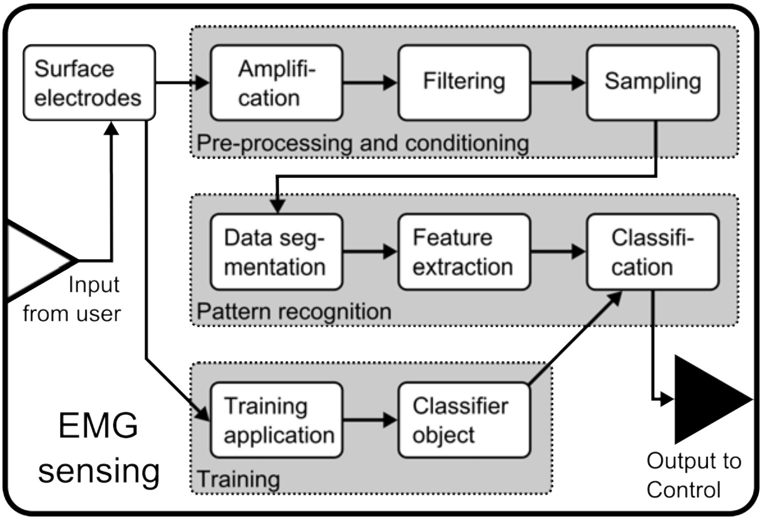

Figure 6.26: A diagram of the real-time sensing algorithm's substructure. First, myoelectric signals of residual forearm muscles are collected using surface electrodes. The myoelectric signals are then amplified, digitized and filtered. The resulting data is broken into small segments, from which characteristic information is extracted. Finally, for each segment, a decision on user intent is made by classification.

around the proximal part of the forearm. After amplification and digitization, the signal samples are filtered with a second-order Butterworth band-pass filter of 10 – 350 Hz to eliminate DC offset and artifacts. An average reference derivation (ARD) [122] is made of every recording, to maintain as many channels and therefore as much information as possible. The multichannel grid enables the creation of spatial distribution maps of muscle activity, rather than picking up the activity of specific muscles. A geometrical configuration is a clinically practical way of electrode placement and does not substantially affect classification accuracy in comparison to other configurations [123, 124, 125, 126].

To identify the intended motions, RMS values are used as features and the Nearest Neighbor technique as a classifier. The latter is chosen because of its simplicity, though retaining the ability to create non-linear class boundaries. RMS values are calculated per electrode channel over 150 ms analysis windows with a 50 ms sliding window, as recommended in Englehart and Hudgins [127], Farrel and Weir [128], and Smith et al. [129]. The average amplitude of all electrodes' myoelectric activity is used as a measure of the intensity of the grasp [14].

After a session of collecting steady-state myoelectric signals in a training application (see Figure 10), subject-specific classifiers are trained to identify the various hand motions (grasp types *1-5* and *Open*). The classifier object is made

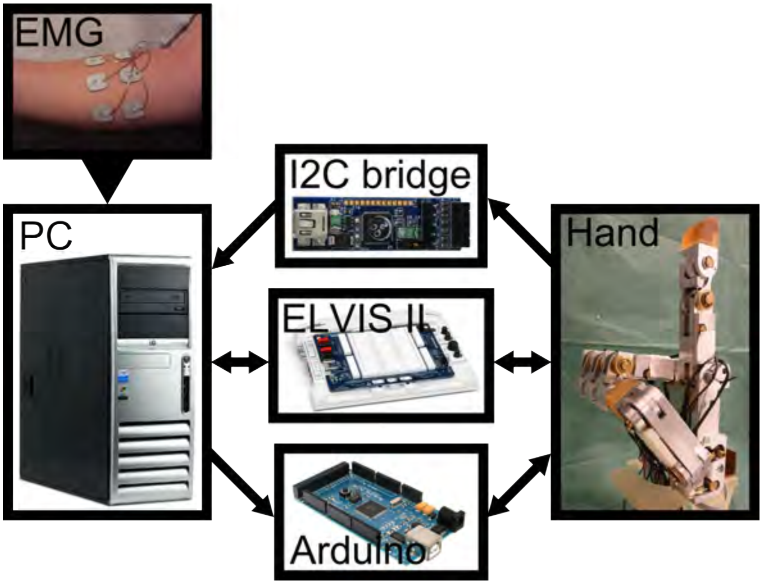

Figure 6.27: A diagram showing the various hardware components of the test setup: the EMG sensing system; a PC, running the high-level control system in Matlab (The Mathworks, Inc., Natick, MA, USA); an I2C bridge for communication with the tactile sensors; an ELVIS II digital acquisition device and breadboard (National Instruments Corporation, Austin, TX, USA); an Arduino Mega microcontroller, on which the low-level controller is programmed; and the UT Hand-I prosthesis prototype. The arrows indicate the signal flow between the components.

available to the real-time sensing algorithm, allowing the EMG sensing system to determine user intent. The resulting class decisions are supplied to the high-level controller PC via a local network connection.

Experimental setup

The components of the experimental setup are described here. A diagram of the system's hardware components is shown in Figure 6.27.

Software The high-level controller is implemented in Matlab. The low-level controller is programmed onto the Arduino Mega microcontroller via Simulink (The Mathworks, Inc., Natick, MA, USA). The Arduino provides pulse-width modulation (PWM) motor control based on processed force, position and EMG data.

Test protocol The test protocol will consist of evaluating the functionality of the high-level state machine with EMG input, and the effectiveness of the low-level grasp energy controller.

High-level control The three grasp types are each executed on a relevant object: a small block for the lateral grasp, a bottle for the cylindrical grasp, and an eraser for the tripod grasp. The high-level controller is navigated by EMG signals from an able-bodied test subject. For each grasp, preshaping is initiated by giving the appropriate grasp type selection signal (*2-4*, see Figure 6.24). The grasp is closed by maintaining this grasp type signal, then opened by an *Open* signal. These grasps are executed with the proportional low-level controller; high-level state changes and finger joint angles are recorded.

Low-level control The grasp energy controller is tested by executing a lateral grasp on the small block object. The first test is performed by starting with a fixed amount of grasp energy, and in the second test an incremental amount of energy is added to the grasp. The thumb MCP joint angle, motor current and external force on the fingertip are measured.

Results

The results of these experiments are shown in the following section. Please refer to the accompanying video that demonstrates the three grasp types. First, the functionality of the EMG-based high-level controller is demonstrated by performing all three grasp types on various objects with proportional low-level control. The grasp energy controller will then be demonstrated separately, using a lateral grasp.

Object grasping with proportional control The results of an object grasp for each grasp type are shown in Figures 6.28, 6.29, and 6.30. These grasps have been performed using the low-level proportional controller.

Lateral grasp For the lateral grasp, preshaping is done only by flexion of the four fingers. After preshaping, the grasp is closed and opened by flexing and extending the thumb.

Cylindrical grasp Preshaping of the cylindrical grasp consists of minor thumb opposition, and grasping consists of flexion of the four fingers, followed by the thumb once the fingers are sufficiently flexed. Opening the grasp similarly extends the thumb before the other fingers.

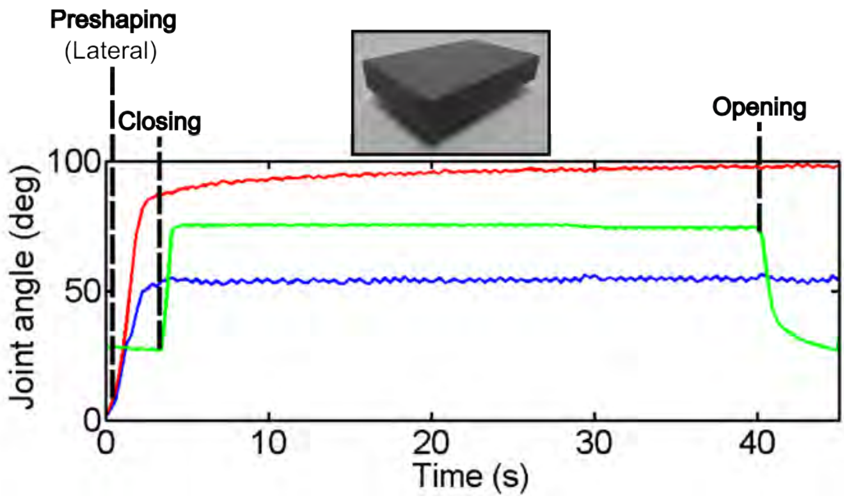

Figure 6.28: Flexion angles of the index proximal interphalangeal (PIP, blue), index metacarpophalangeal (MCP, red), and thumb interphalangeal (IP, green) joints during lateral grasping of a small block. The dashed lines indicate state changes in the high-level controller.

Tripod grasp The tripod grasp is preshaped by fully opposing the thumb, combined with full flexion of the ring and little fingers and thumb flexion to around 30 degrees. The grasp is closed by flexing the four fingers. The DIP and PIP joints of the index and middle fingers are locked, which causes them to contact the thumb in a precision grasp. The ring and little fingers remain fully flexed and take no part in the grasp.

Object grasping with grasp energy control The following grasps have been performed using the low-level grasp energy controller. In Figure 6.31, a lateral grasp is performed with a fixed initial amount of grasp energy. In Figure 6.32, the grasp energy starts at 0 and is increased over time.

Discussion The subsections of the control system are evaluated based on the experimental results.

EMG input The input from the EMG sensing system provides an accurate representation of the user's intent. Erroneous classifications do occur, mostly when switching between grasp types. Since EMG data is transmitted every 50 ms, the addition of an input filter eliminates any problems due to these errors before they become noticeable to the user.

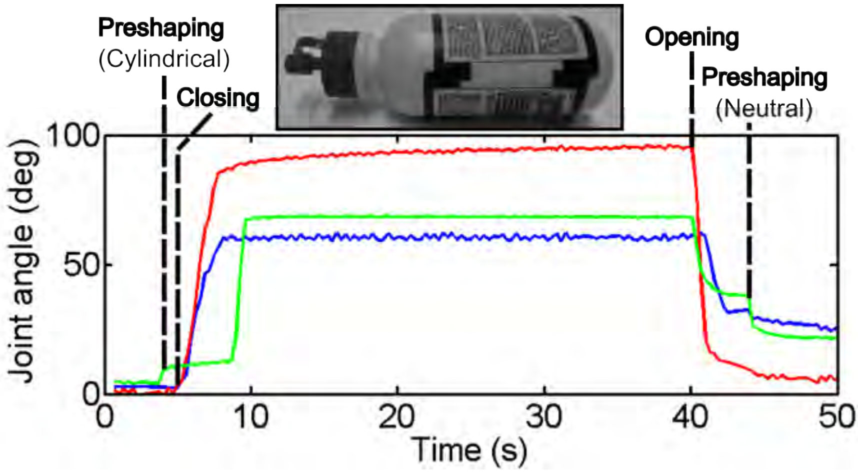

Figure 6.29: Flexion angles of the index proximal interphalangeal (PIP, blue), index metacarpophalangeal (MCP, red), and thumb interphalangeal (IP, green) joints during cylindrical grasping of a bottle. The dashed lines indicate state changes in the high-level controller.

High-level state machine The structure of the state machine allows the user to start and finish a grasp by giving only the relevant grasp type and hand open commands. The grasp can also be interrupted at any time, giving the user the option to adjust or retry a failed grasp. This combination provides both ease of use and flexibility.

Low-level controller Automatic execution of grasps reduces the amount of effort and concentration required to execute a grasp. Directly controlling the amount of energy available to the grasp is a natural method of ensuring its intuitive operation, which is an important factor in interaction with the external world. This also allows the user to influence the speed and force of the grasp in a physically intuitive way, providing a greater deal of control if desired. Variations in the intensity signal have been observed for different users and grasp types, making accurate control over the grasp energy level more difficult. However, this addition remains entirely optional, and can therefore be ignored until the user becomes more experienced with the system.

6.3.5 Conclusion

In this paper, the development of a novel EMG-based control system for the UT Hand-I is described. The UT Hand-I is an anthropomorphic hand prosthesis pro-

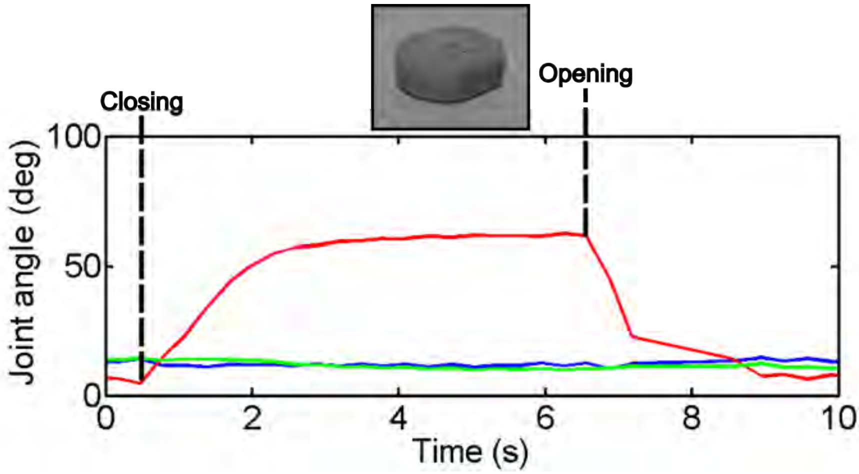

Figure 6.30: Flexion angles of the index proximal interphalangeal (PIP, blue), index metacarpophalangeal (MCP, red), and thumb interphalangeal (IP, green) joints during tripod grasping of an eraser. The dashed lines indicate state changes in the high-level controller.

totype with 15 DOF and 3 DC motor actuators. The inclusion of joint locking systems allows various grasping motions to be executed despite this significant underactuation. The hand also features flexible angle sensors on its joints, and tactile sensor arrays embedded in the rubber fingertips.

The EMG sensing system used here enables the classification of up to 8 muscle activation patterns, compared to the 2 of most commercial prostheses. However, the control of a multifunctional prosthesis should still be intuitive and require little continuous effort. To this end, a two-tiered control system has been developed, based on the aforementioned EMG input. A user-controlled high-level state machine can be navigated to determine a desired grasping behavior, and an automatic low-level controller executes the desired grasp and handles interaction with the environment. The performance of the low-level controller can be influenced in a physically consistent way by modulating the total energy available to the grasp. This method provides an intuitive and stable way of adding user control to an automatic grasp.

After evaluating the control system in a series of tests with three different grasp types on various appropriate objects, the results show the EMG signals are interpreted correctly by the high-level state machine. Any grasping action can be performed using only 2 control signals; however, the high- and low-level controllers both give the user additional options to adjust or retry a grasp if necessary.

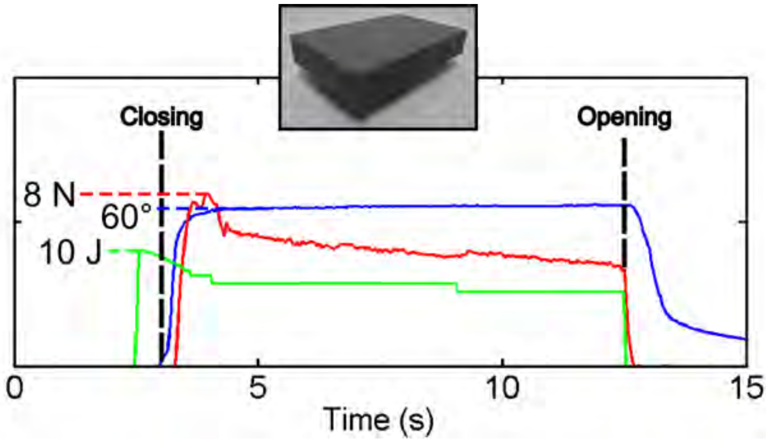

Figure 6.31: Thumb MCP flexion angle (blue), fingertip force (red), and motor current (green) during lateral grasping of a small block with fixed grasp energy. The dashed black lines indicate state changes in the high-level controller.

Future work

Future work on the UT Hand-I system can be divided into improvements to the prosthesis design and control system.

Prosthesis design The current prosthesis design actuates the fingers with a single DC motor, using extension springs to provide a return force. Adding a second actuator for extension would not only eliminate the need for the springs, increasing the force of the grasp, but also allow control over the finger's stiffness. With a non-linear compliance between each actuator and the fingers, the difference between the two actuators' torques would provide a net actuation force, and the level of opposing force would increase the fingers' stiffness. Stiffness control would allow the hand to remain compliant when not in use or in interaction with humans, but become more rigid when performing fine manipulation or strong grasping.

Control system Adding the ability to change the fingers' stiffness requires a new method of control. A possible implementation in the current system could be coupling stiffness to the EMG intensity, or assigning a certain fixed stiffness for each grasp type. Co-contraction in the forearm would be a more natural way to control joint stiffness, if made available to the high-level controller. Integration of the control system with a user feedback system would further enhance the intuitiveness and usability of the system in situations where visual feedback is

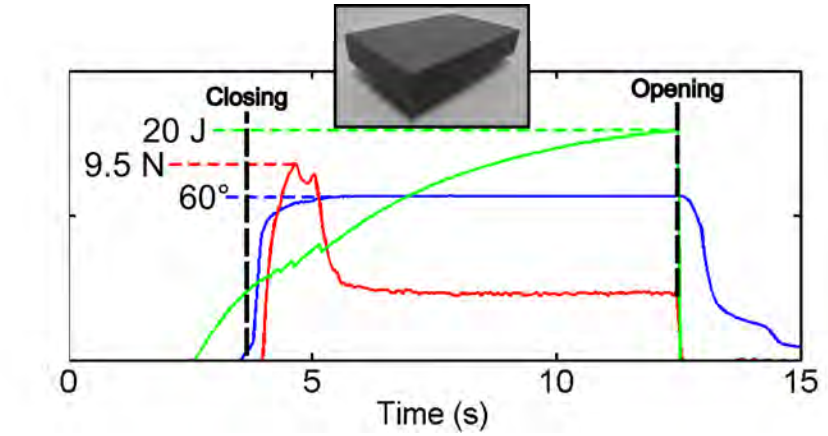

Figure 6.32: Thumb MCP flexion angle (blue), fingertip force (red), and motor current (green) during lateral grasping of a small block with increasing grasp energy. The dashed black lines indicate state changes in the high-level controller.

unavailable [130].

Chapter 7

Discussion

In this chapter, the performance of the UT Hand I prototype and its control system are evaluated with regard to the requirements put forth in Section 1.3. Possible paths for future research in hand prostheses are also laid out, as well as recommendations for the development of a future version of the UT Hand based on experiences with the first prototype.

7.1 Requirements

The list of requirements that followed from the Myopro workshop and literature review are repeated here. The way the UT Hand I fulfills these requirements, or demonstrates a concept able to fulfill them, is described for each of them.

Requirement 1: the design should resemble the human hand.

The UT Hand I has an anthropomorphic design containing 15 DOFs for finger flexion, thumb flexion, and thumb opposition. Additionally, the UT Hand's mechanisms have been designed to not just resemble the human hand at rest, but to also imitate its motion. Using tendon-pulley underactuation for finger flexion causes the finger to move in a similar way to the human finger, even when obstructed. Although minor inaccuracies remain, such as the identical finger sizes and lack of abduction DOFs, these can easily be improved upon in redesigns of the prototype.

Requirement 2: the size and weight of the hand should be minimized.

Reducing the hand's actuation is the most effective way to decrease the size and weight of current hand prostheses. The application of minimal actuation to the fingers of the UT Hand I provides a proof of concept for single-actuator prostheses with a human-like number of DOFs. The use of tendon-pulley underactuation also enables easy implementation of alternative methods of actuation, such as pneumatic cylinders. Although the current size and weight of the UT Hand I are still above that of an average human hand, the mechanisms used in its construction allow for a multifunctional hand to be designed that can meet the requirements for a comfortably wearable hand prosthesis.

Requirement 3: the cylindrical, tripod, and lateral grasp types should be available.

The UT Hand I's joint locking capability not only allows for fingers to be excluded from precision grasps, but also for different finger motion profiles to be associated with each grasp type. Combined with actuated thumb opposition, this provides the user with three truly different grasp configurations, optimized for most activities of daily living.

The control system also allows the three main grasp types to be accessed by classification of different EMG control signals. This makes the different grasps more intuitively accessible to the user.

Requirement 4: the grasp execution time should not disturb the user.

With the current quality of DC motor actuation at sizes fit for hand prosthesis use, the duration of grasp execution is significantly higher than recommended for intuitive grasping. However, experiments with pneumatic cylinder actuation resulted in a flexion time under half that of comparably much larger DC motor actuators.

The control system is currently run on an Arduino microcontroller board, and is capable of responding to new EMG input signals within the 50 ms delay between them. However, the EMG signals are filtered by the high-level controller to prevent erroneous classifications from EMG noise. This causes an additional 100 ms delay before confirmation of a new grasp type, but the total computation time does not exceed the 300 ms that can be considered acceptable [48].

Requirement 5: the hand's pose and external forces should be measured.

The sensor suite of the UT Hand I focuses on measuring joint angles and fingertip contact pressure. The joint angle data is then sent to a kinematics algorithm which calculates the exact pose of the fingers, and the pressure data is used to determine the magnitude (and an approximation of the direction) of external forces. This information is used by the control system, but the degree of hand opening and magnitude of external force can also be supplied to the user through a feedback system [130].

Motor torque and position information is also available to the control system, in order to determine the amount of energy injected into the grasp by the actuator.

Requirement 6: the user should be able to directly control the speed and force of grasping.

The EMG signal's RMS amplitude is used to control the intensity of the grasp. However, either force or velocity control alone is not sufficient to guarantee compliant interaction with the environment. Therefore, the control system of the UT Hand I uses grasp energy as a method of controlling the speed and force of the grasp simultaneously. This method is more intuitive, as the physical relation between speed and force of the hand is properly defined.

Requirement 7: the prosthesis should automatically continue holding a grasped object.

With the interaction control systems implemented on both the UB Hand IV and UT Hand I, any object obstructing the movement of the fingers will have a continuous force applied to it based on the desired grasp energy and the distance between the fingers and their intended target. The high-level control system implements holding behavior by automatically maintaining the grasp as long as no opening signal is received.

7.2 Recommendations

This section provides possible options for further developments of hand prostheses, as well as several adjustments which would improve the performance of the current UT Hand I design.

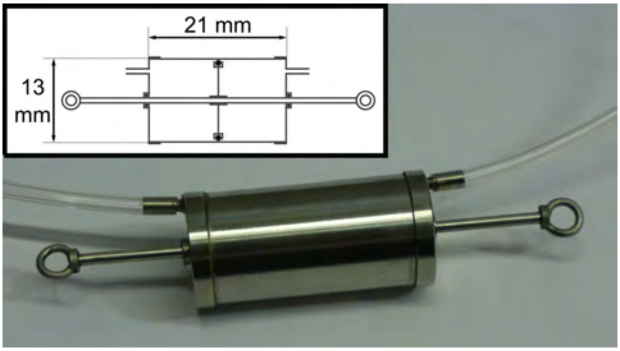

Figure 7.1: The redesigned bidirectional pneumatic cylinder. A design drawing is shown in the top left corner.

7.2.1 Pneumatic actuation

Investigation into alternative methods of actuation has led to additional research into the application of pneumatic cylinder actuators. The pneumatic cylinder of Section 3.2 was redesigned to allow for bidirectional actuation (shown in Figure 7.1). The pneumatic actuation system as a whole was also redesigned, to allow either side of the cylinder to be pressurized separately. This addresses the problems encountered in earlier research, such as delayed CO_2 venting and the necessity of a return force. The UT Hand I does not implement pneumatic actuation by default; however, the current design does allow for alternative actuation methods to be connected to the finger actuation linkage for experiments.

Because of the lower extension spring stiffness of the UT Hand I, the finger flexion time was decreased to approximately 200 ms. However, the valves used in these experiments were not capable of adjusting the pressure in the cylinder, so only full flexion or extension were available. If a set of valves can be customized to vary the pressure and be made small enough to fit in the palm of the hand (see Figure 7.2), the resulting actuation system would be significantly faster than a DC motor, and at least as powerful.

7.2.2 Stiffness control

Interaction with the environment could be improved even further by enabling control of the stiffness of the hand. Such systems would require a reworking of the hardware, replacing the extension springs in the fingers by a second actuator and underactuation linkage. By adding non-linear springs in series with both actuators, the fingers' stiffness can be increased by moving both actuators in opposite

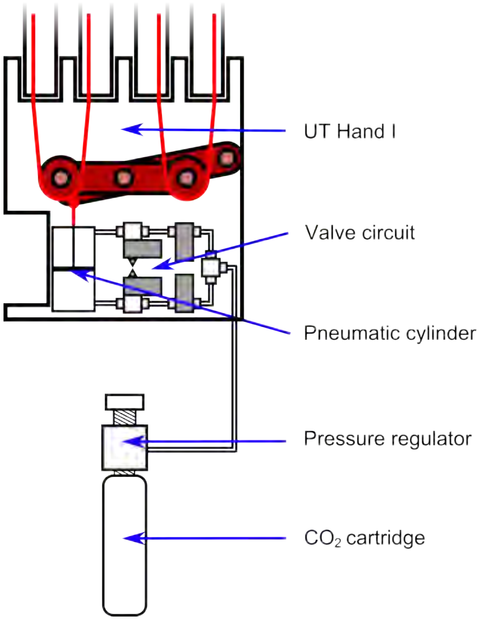

Figure 7.2: A diagram of a complete pneumatic actuation system actuating the UT Hand I. The cylinder and pressure regulator replace the conventional prosthesis battery.

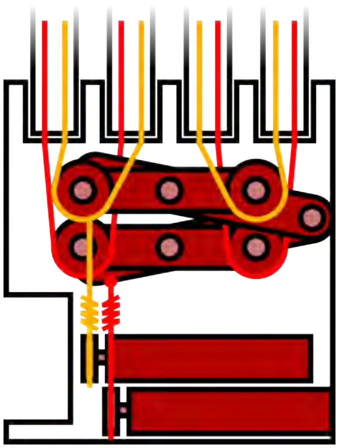

Figure 7.3: A diagram of a stiffness control system implemented on the UT Hand I. The springs represent non-linear compliant elements.

directions [131]. The principle is illustrated in Figure 7.3. This system would require some adjustments to the actuation system: the underactuation linkage would need to be made thinner in order to house two of the mechanisms in the palm, and thumb flexion would need to be coupled to the fingers to make room for the additional actuator.

Control of the adjustable stiffness of the hand would need to be linked to the user's EMG signal. In the able hand, stiffness is increased by co-contraction of the flexor and extensor muscles. Isolating the degree of co-contraction by means of EMG sensing would be an intuitive way to adjust the stiffness of the prosthesis as well.

7.2.3 Mechanical design

To improve the effectiveness of the prototype, several changes can be made to its mechanical design.

Bidirectional joint locks The current implementation of the joint locking mechanisms is unidirectional, which limits their application outside of the three main grasp types. If a secondary pawl were added to the locking mechanisms, any desired combination of finger motions can be added to the control system by changes in software alone, giving the system significant versatility.

Compliant distal finger joint linkage The distal joint of each of the UT Hand's fingers is linked rigidly in a manner similar to the flexion of the human hand. This similarity is limited to an unobstructed movement, however, as the human distal finger joint is compliant to external forces. This compliance is already present in the UT Hand's thumb (due to its larger size allowing a tendon coupling), but it could also be achieved by replacing the distal finger joints' linkage bars with a compliant version.

Thumb opposition transmission Because the opposition of the thumb takes no part in active grasping, the implementation of a nonbackdrivable worm wheel transmission has been effective: a relatively small actuator is sufficient, and the impact of external forces and thumb flexion on the degree of opposition is strongly reduced. However, the system's performance can still be improved by a stiffer and closer connection between the motor and thumb opposition axes, as the current amount of play can lead to inaccuracies in positioning and small shifts of the thumb during grasping.

Takktile sensors The most significant improvements to the sensor suite can be made with the tactile sensors, which can be applied to the palm of the hand as well to improve force detection during cylinder grasps. The flexibility of the Takktile system makes this possible with minimal additional space requirements.

Underactuation linkage The underactuation linkage serves to distribute the actuator force equally over all four fingers. Therefore, the friction in the linkage should be as low as possible. The current linkage is optimized for robustness; additional bearings would improve its functioning. Also, the tendons connecting the linkage to the actuator and those connected to the fingers are slightly misaligned. An additional pulley between the actuator and linkage should prevent this. Finally, the maximum stroke of the linkage is limited by the current size of the mechanism. A compacter redesign of the linkage could free up precious space in the palm.

Slip detection With the BioTac sensor system, the high-frequency vibrations caused by an object slipping past the fingertips can be detected. Reacting to these signals by applying additional force could further improve automated object holding. Alternative methods of detecting slip are also possible: for example, a similar system has been implemented on the Southampton Remedi hand [41] by means of an integrated microphone.

7.3 Conclusion

In this thesis the development of a new hand prosthesis system is described, with the goal of increasing user acceptance via a multifunctional mechanical design and a control system with EMG sensing input. After determining a set of requirements based on the needs of prosthesis users, the current state of the art was reviewed with regard to fulfilling these needs. To address some of the limitations found in modern hand prostheses, several systems were developed: A joint locking system to enhance the controllability of underactuated DOFs, a pneumatic cylinder to reduce actuator size and weight, and a grasp control system capable of stable interaction with the environment. Subsequently, the UT Hand I prototype was designed to demonstrate the feasibility of incorporating these systems in a modern anthropomorphic hand prosthesis. The UT Hand I provides a proof of concept for the implementation of minimal actuation in myoelectric hand prostheses, while maintaining controllability of its DOFs. It also functions as a testbed for the development of a two-tiered control system, consisting of intuitive user control of the general grasping behavior and compliant automated control of the grasp. Combined with an advanced EMG sensing system and user feedback, it forms the basis of a prosthetic solution that is able to restore both functionality and controllability to the user.

Appendices

Appendix 1 - Variables and constants

The symbolic conventions adopted in Chapter 5 are made explicit here:

x- Scalar values

X - Points

$\mathbf{x}$- Vectors

$\mathbf{X}$- Matrices

The nomenclature used to express lengths between points in the kinematic equations (e.g. b_{XY} and l_{ZW}), is given by:

$$b_{XY} = |X - Y|\,, \qquad l_{ZW} = |Z - W| \tag{7.1}$$

Table 7.1: Geometric values of the underactuation mechanisms in the palm, thumb and fingers.

Label	Value	Description
b_{PO_1}	20 mm	Length of one of the bars in the fingers' four-bar mechanism
b_{PQ}	6.25 mm	Length of one of the bars in the fingers' four-bar mechanism
b_{QO_2}	20.91 mm	Length of one of the bars in the fingers' four-bar mechanism
b_{OH}	41 mm	Length of one of the bars in the palm pulley linkage
b_{HS_2}	19 mm	Length of one of the bars in the palm pulley linkage
b_{OF}	57.5 mm	Length of one of the bars in the palm pulley linkage
A	$\begin{bmatrix} -71.65 \\ 15.5 \end{bmatrix}$ mm	Position of a finger alignment pulley at the top of the palm
B	$\begin{bmatrix} -53.15 \\ 15.5 \end{bmatrix}$ mm	Position of a finger alignment pulley at the top of the palm
C	$\begin{bmatrix} -30.75 \\ 15.5 \end{bmatrix}$ mm	Position of a finger alignment pulley at the top of the palm
D	$\begin{bmatrix} -12.35 \\ 15.5 \end{bmatrix}$ mm	Position of a finger alignment pulley at the top of the palm
r_L	4.25 mm	Radius of the two pulleys in the palm pulley linkage
r_J	4.85 mm	Radius of the pulleys in the joints of the four fingers
$r_{r_{4f}}$	5 mm	Radius of the reel connected to the finger flexion motor
r_{J_t}	6.75 mm	Radius of the pulley in the MCP joint of the thumb
r_{S_t}	6.5 mm	Radius of the pulley on the opposition shaft of the thumb
r_{r_t}	4 mm	Radius of the reel connected to the thumb flexion motor
l_D	45 mm	Length of the fingers' distal phalanx
l_I	20 mm	Length of the fingers' intermediate phalanx
l_P	30 mm	Length of the fingers' proximal phalanx
l_{D_t}	30 mm	Length of the thumb's distal phalanx
l_{P_t}	36.7 mm	Length of the thumb's proximal phalanx

Table 7.2: Mathematical constants used in the linear approximation of the palm pulley linkage kinematics.

Label	Value
a_1	76.3819 mm
a_2	34.9877 mm
a_3	-192.754 mm
b_1	66.4568 mm
b_2	-30.5868 mm
b_3	-153.817 mm
c_1	$6.56165 \times 10^{-3}\,\mathrm{mm}^{-1}$
c_2	$7.50576 \times 10^{-3}\,\mathrm{mm}^{-1}$
c_3	2.41930

Table 7.3: Variables used in the kinematic calculations of the palm.

Label	Description
θ_D	Angle of the finger's distal phalanx with respect to its proximal phalanx
θ_I	Angle of the finger's intermediate phalanx with respect to its proximal phalanx (= θ_{PIP})
$\theta_{PIP_1}, ...\theta_{PIP_4}$	PIP joint angles of the four fingers
$\theta_{MCP_1}, ...\theta_{MCP_4}$	MCP joint angles of the four fingers
O_1, O_2, P, Q	Joints of the finger four-bar linkage
S_1, S_2	Central points of the palm linkage pulleys
T_A, T_B, T_C, T_D	Tangent points on the palm linkage pulleys
α, β	Lagrangian parameters of the palm pulley linkage
ψ_1, ψ_2	The tendon arc angles of the two palm linkage pulleys
l_{AT_A}, l_{BT_B}, l_{CT_C}, l_{DT_D}	Tangent parts of the tendon control lengths
ϕ_A, ϕ_B, ϕ_C, ϕ_D	Angles of the tangent parts with respect to the line AD
l_1, l_2	Total length of the finger tendons
$\widetilde{\alpha}$	Approximated linkage angle α, as per Equation 5.12
$\varphi_{m_{4f}}$	Rotation angle of the finger flexion motor shaft
$\mathbf{J}_l^\theta$	Jacobian matrix relating the angle of the finger joints to the tendon control lengths
$\mathbf{J}_\alpha^l$	Jacobian matrix relating the tendon control lengths to the palm linkage angle α
$\nu_{m_{4f}}^\alpha$	Transmission ratio between α and the finger flexion motor
$\mathbf{J}_{m_{4f}}^{\theta_f}$	Inverse Jacobian matrix for the four fingers
$\mathbf{J}_{\theta_f}^{m_{4f}}$	Forward Jacobian matrix for the four fingers
$\mathbf{J}_{m_t}^{\theta_t}$	Inverse Jacobian matrix for the thumb
f_1, f_2	Number of unlocked joints for each tendon
l_u	Variation in palm control length for each of the unlocked finger joints
$\mathbf{d}$	Vector of the joints' lock status (0 if locked, 1 if unlocked)
$\dot{\boldsymbol{\theta}}_f$	Vector of the fingers' PIP and MCP joint velocities
$\dot{\theta}_{MCP_t}$	Flexion velocity of the thumb MCP joint
$\dot{\theta}_{OPP_t}$	Opposition velocity of the thumb
ω_{4f}	Rotational velocity of the finger flexion motor
ω_{f_t}	Rotational velocity of the thumb flexion motor
ω_{o_t}	Rotational velocity of the thumb opposition motor

Bibliography

[1] B. Peerdeman, D. Boere, H. Witteveen, R. Huis in 't Veld, H. Hermens, S. Stramigioli, J. Rietman, P. Veltink, and S. Misra, "Myoelectric forearm prostheses: State of the art from a user requirements perspective," *Journal of Rehabilitation Research & Development (JRRD)*, vol. 48, no. 6, pp. 719–738, July 2011.

[2] P. Finer, *Antique Arms and Armour 1999*.

[3] D. S. Childress, "Historical aspects of powered limb prostheses," *Clinical Prosthetics & Orthotics*, vol. 9 (1), pp. 2–13, 1985.

[4] www.ottobock.com/cps/rde/xchg/ob_com_en/hs.xsl/19932.html.

[5] D. J. Atkins, D. C. Y. Heard, and W. H. Donovan, "Epidemiologic overview of individuals with upper-limb loss and their reported research priorities," *Journal of Prosthetics and Orthotics*, vol. 8, no. 1, pp. 2–11, 1996.

[6] E. Biddiss and T. Chau, "Upper-limb prosthetics: Critical factors in device abandonment," *American Journal of Physical Medicine and Rehabilitation*, vol. 86, no. 12, pp. 977–987, 2007.

[7] J. L. Pons, R. Ceres, E. Rocon, D. Reynaerts, B. Saro, S. Levin, and W. Van Moorleghem, "Objectives and technological approach to the development of the multifunctional manus upper limb prosthesis," *Robotica*, vol. 23, pp. 301–310, 2005.

[8] P. E. Klopsteg and P. D. Wilson, *Human limbs and their substitutes*. Hafner, New York, 1954.

[9] R. Huis in 't Veld, I. Widya, R. Bults, L. Sandsjo, H. Hermens, and M. Vollenbroek-Hutten, "A scenario guideline for designing new teletreatments: a multidisciplinary approach," *J Telemed Telecare*, vol. 16, no. 6, pp. 302–307, 2010.

[10] P. Beynon-Davies and S. Holmes, “Design breakdowns, scenarios and rapid application development,” *Information & Software Technology*, vol. 44, no. 10, pp. 579–592, 2002.

[11] A. Bookman, M. Harrington, L. Pass, and E. Reisner, *Family Caregiver Handbook*. Massachusetts Institute of Technology, 2007.

[12] R. F. Chandler, C. E. Clauser, J. T. McConville, H. M. Reynolds, and J. W. Young, “Investigation of inertial properties of the human body,” 1975.

[13] J. Lin, Y. Wu, and T. S. Huang, “Modeling the constraints of human hand motion,” in *Proceedings of Workshop on Human Motion (HUMO)*, Austin, USA, 2000, pp. 121–126.

[14] D. Staudenmann, I. Kingma, A. Daffertshofer, D. F. Stegeman, and J. H. Van Dieën, “Improving EMG-based muscle force estimation by using a high-density EMG grid and principal component analysis,” *IEEE Transactions on Biomedical Engineering*, vol. 53, no. 4, pp. 712–719, 2006.

[15] B. Peerdeman, D. Boere, L. Kallenberg, S. Stramigioli, and S. Misra, “A modeling framework for control of myoelectric hand prostheses,” in *Proceedings of the 32rd Annual International Conference of the IEEE Engineering in Medicine and Biology Society (EMBC)*, Buenos Aires, Argentina, September 2010, (Accepted).

[16] B. Peerdeman, G. J. Pieterse, S. Stramigioli, J. S. Rietman, E. E. G. Hekman, D. M. Brouwer, and S. Misra, “Design of joint locks for underactuated fingers,” in *Proceedings of the IEEE International Conference on Biomedical Robotics and Biomechatronics (BioRob)*, Rome, Italy, July 2012, pp. 488–493.

[17] B. Peerdeman, U. Fabrizi, G. Palli, C. Melchiorri, S. Stramigioli, and S. Misra, “Development of prosthesis grasp control systems on a robotic testbed,” in *Proceedings of the IEEE International Conference on Biomedical Robotics and Biomechatronics (BioRob)*, Rome, Italy, July 2012, pp. 1110–1115.

[18] B. Peerdeman, G. Smit, D. Plettenburg, S. Stramigioli, and S. Misra, “Evaluation of pneumatic cylinder actuators for hand prostheses,” in *Proceedings of the IEEE International Conference on Biomedical Robotics and Biomechatronics (BioRob)*, Rome, Italy, July 2012, pp. 1105–1109.

[19] B. Peerdeman, S. Stramigioli, E. Hekman, D. Brouwer, and S. Misra, "Development of underactuated prosthetic fingers with joint locking and electromyographic control," *Mechanical Engineering Research*, vol. 3 (1), pp. 130–142, 2013.

[20] B. Peerdeman, M. Valori, D. M. Brouwer, E. E. G. Hekman, S. Misra, and S. Stramigioli, "Ut hand i: A lock-based underactuated hand prosthesis," *Mechanism and Machine Theory*, vol. Accepted, no. 6, July 2014.

[21] B. Peerdeman, D. Boere, M. Valori, S. Misra, and S. Stramigioli, "Emg-based grasp control of the ut hand-i," *Bionic Engineering*, vol. Submitted, no. 6, July 2014.

[22] M. Carrozza, G. Cappiello, S. Micera, B. B. Edin, L. Beccai, and C. Cipriani, "Design of a cybernetic hand for perception and action," *Biological Cybernetics*, vol. 95, no. 6, pp. 629–644, 2006.

[23] C. Light and P. Chappell, "Development of a lightweight and adaptable multiple-axis hand prosthesis," *Medical Engineering and Physics*, vol. 22, pp. 679–684, 2000.

[24] J. Pons, E. Rocon, R. Ceres, D. Reynaerts, B. Saro, S. Levin, and W. van Moorleghem, "The MANUS-HAND dextrous robotics upper limb prosthesis: Mechanical and manipulation aspects," *Autonomous Robots*, vol. 16, no. 2, pp. 143–163, 2004.

[25] D. H. Plettenburg, "Electric versus pneumatic power in hand prostheses for children," *Journal of Medical Engineering & Technology*, vol. 13, no. 1-2, pp. 124–128, 1989.

[26] F. Daerden and D. Lefeber, "Pneumatic artificial muscles: actuators for robotics and automation," *European journal of Mechanical and Environmental Engineering*, vol. 47, pp. 10–21, 2000.

[27] Y. Lee and I. Shimoyama, "A skeletal framework artificial hand actuated by pneumatic artificial muscles," in *Proceedings of the IEEE International Conference on Robotics and Automation (ICRA)*, vol. 2, 1999, pp. 926–931 vol.2.

[28] T. Noritsugu, D. Sasaki, and M. Takaiwa, "Application of artificial pneumatic rubber muscles to a human friendly robot," in *Proceedings of the IEEE International Conference on Robotics and Automation (ICRA)*, vol. 2, September 2003, pp. 2188–2193, vol.2.

[29] H. Takeda, N. Tsujiuchi, T. Koizumi, H. Kan, M. Hirano, and Y. Nakamura, *Development of prosthetic arm with pneumatic prosthetic hand and tendon-driven wrist*, 2009, vol. 1.

[30] Shadow Robot Company. Shadow dextrous hand, featuring air muscles. [Online]. Available: http://www.shadowrobot.com/hand/

[31] D. Plettenburg, "Pneumatic actuators: a comparison of energy-to-mass ratio's," in *Proceedings of the International Conference on Rehabilitation Robotics (ICORR)*, Chicago, USA, July 2005, pp. 545–549.

[32] S. Schulz, C. Pylatiuk, M. Reischl, J. Martin, R. Mikut, and G. Bretthauer, "A hydraulically driven multifunctional prosthetic hand," *Robotica*, vol. 23, no. 3, pp. 293–299, 2005.

[33] D. Yang, J. Zhao, Y. Gu, X. Wang, N. Li, L. Jiang, H. Liu, H. Huang, and D. Zhao, "An anthropomorphic robot hand developed based on underactuated mechanism and controlled by EMG signals," *Journal of Bionic Engineering*, vol. 6, pp. 255–263, 2009.

[34] S. Hirose, "Connected differential mechanism and its applications," in *Proceedings of the International Conference on Advanced Robotics*, 1985, pp. 319–326.

[35] G. Borghesan, G. Palli, and C. Melchiorri, "Design of tendon-driven robotic fingers: Modeling and control issues," in *Proceedings of the IEEE International Conference on Robotics and Automation (ICRA)*, Anchorage, Alaska, USA, May 2010.

[36] S. A. Dalley *et al.*, "Design of a multifunctional anthropomorphic prosthetic hand with extrinsic actuation," *IEEE/ASME Transactions on Mechatronics*, vol. 14, no. 6, pp. 699–706, 2009.

[37] D. Bennett, S. Dalley, and M. Goldfarb, "Design of a hand prosthesis with precision and conformal grasp capability," in *Proceedings of the Annual International Conference of the IEEE Engineering in Medicine and Biology Society (EMBC)*, August 2012, pp. 3044–3047.

[38] N. Dechev, W. L. Cleghorn, and S. Naumann, "Multiple finger, passive adaptive grasp prosthetic hand," *Mechanism and Machine Theory*, vol. 36, no. 10, pp. 1157–1173, 2001.

[39] http://www.touchbionics.com/.

[40] J. L. Pons, R. Ceres, E. Rocon, S. Levin, I. Markovitz, B. Saro, D. Reynaerts, W. Van Moorleghem, and L. Bueno, "Virtual reality training and EMG control of the MANUS hand prosthesis," *Robotica*, vol. 23, no. 03, pp. 311–317, 2005.

[41] C. M. Light, P. H. Chappell, B. Hudgins, and K. Engelhart, "Intelligent multifunction myoelectric control of hand prostheses," *Journal of Medical Engineering and Technology*, vol. 26, no. 4, pp. 139–146, 2002.

[42] M. Santello, M. Flanders, and J. F. Soechting, "Postural hand synergies for tool use," *Journal of Neuroscience*, vol. 18, no. 23, pp. 10 105–10 115, 1998.

[43] L. Zollo, S. Roccella, E. Guglielmelli, M. C. Carrozza, and P. Dario, "Biomechatronic design and control of an anthropomorphic artificial hand for prosthetic and robotic applications," *Mechatronics, IEEE/ASME Transactions on*, vol. 12, no. 4, pp. 418–429, 2007.

[44] C. J. De Luca, *Encyclopedia of medical devices and instrumentation*, J. G. Webster, Ed. Boston, Massachusetts: John Wiley & Sons, Inc., 2006.

[45] J. G. Webster, W. H. Olson, R. A. Peura, J. W. Clark, and M. R. Neuman, *Medical instrumentation: application and design*. Hoboken, New Jersey: John Wiley & Sons Inc., 1998.

[46] M. Zecca, S. Micera, M. C. Carrozza, and P. Dario, "Control of multifunctional prosthetic hands by processing the electromyographic signal," *Critical Reviews in Biomedical Engineering*, vol. 30, no. 4-6, pp. 459–485, 2002.

[47] M. A. Oskoei and H. Hu, "Myoelectric control systems–a survey," *Biomedical Signal Processing and Control*, vol. 2, no. 4, pp. 275–294, 2007.

[48] B. Hudgins, P. Parker, and R. N. Scott, "A new strategy for multifunction myoelectric control," *IEEE Transactions on Biomedical Engineering*, vol. 40, no. 1, pp. 82–94, 1993.

[49] K. Englehart, B. Hudgins, and P. A. Parker, "A wavelet-based continuous classification scheme for multifunction myoelectric control," *IEEE Transactions on Biomedical Engineering*, vol. 48, no. 3, p. 302, 2001.

[50] F. C. P. Sebelius, B. N. Rosén, and G. N. Lundborg, "Refined myoelectric control in below-elbow amputees using artificial neural networks and a data glove," *Journal of Hand Surgery*, vol. 30, no. 4, pp. 780–789, 2005.

[51] RSLSteeper. The bebionic Hand. http://www.bebionic.com/.

[52] Touch Bionics Inc. i-LIMB Hand. http://www.touchbionics.com/i-LIMB.

[53] Otto Bock. Michelangelo Hand. http://www.ottobock.com/.

[54] M. Saliba and C. de Silva, "An innovative robotic gripper for grasping and handling research," in *Proceedings of the International Conference on Industrial Electronics, Control and Instrumentation (IECON)*, vol. 2, 1991, pp. 975–979.

[55] N. Ulrich, V. Kumar, R. Paul, and R. Bajcsy, *Grasping with mechanical intelligence*. Warsaw, Poland: School of Engineering and Applied Science, University of Pennsylvania, 1989.

[56] J. U. Chu, D. H. Jung, and Y. J. Lee, "Design and control of a multifunction myoelectric hand with new adaptive grasping and self-locking mechanisms," in *Proceedings of the IEEE International Conference on Robotics and Automation*, 2008, pp. 743–748.

[57] B. Buchholz and T. J. Armstrong, "An ellipsoidal representation of human hand anthropometry," *Human Factors: The Journal of the Human Factors and Ergonomics Society*, vol. 33, pp. 429–441, 1991.

[58] T. J. Armstrong, C. Best, S. Bae, J. Choi, D. C. Grieshaber, D. Park, C. Woolley, and W. Zhou, "Development of a kinematic hand model for study and design of hose installation," pp. 85–94, 2009.

[59] B. Dizioglu and K. Lakshiminarayana, "Mechanics of form closure," *Acta Mechanica*, vol. 52, pp. 107–118, 1984.

[60] B. Hamrock, S. Schmid, and B. Jacobson, *Fundamentals of machine elements*, ser. McGraw-Hill series in mechanical engineering. McGraw-Hill Higher Education, 2004.

[61] K. Johnson, *Contact mechanics*. Cambridge University Press, 1987.

[62] Piezo Systems, Inc. Piezo Stack Actuators. http://www.piezo.com/prodstacks1.html.

[63] ——. Piezo Bending Actuators. http://www.piezo.com/prodbm64l.html.

[64] P. Potapov and E. P. da Silva, "Time response of shape memory alloy actuators," *Journal of Intelligent Material Systems and Structures*, vol. 11, pp. 125–134, February 2000.

[65] W. J. Buehler and F. E. Wang, “A summary of recent research on the nitinol alloys and their potential application in ocean engineering,” *Ocean Engineering*, vol. 1, no. 1, pp. 105–120, 1968.

[66] Geeplus Europe Ltd. C110 small push pull solenoid. [Online]. Available: http://www.geeplus.biz

[67] Delft Prosthetics. Wilmer quick exchangeable hand prosthesis. [Online]. Available: http://www.delftprosthetics.com/en/products/exchangeable-hand-prosthesis

[68] HBM. C9b force transducer. [Online]. Available: http://www.hbm.com/

[69] Allegro MicroSystems, Inc. A1301 continuous-time ratiometric linear hall effect sensor ic. [Online]. Available: http://www.allegromicro.com

[70] M. Carrozza, C. Suppo, F. Sebastiani, B. Massa, F. Vecchi, R. Lazzarini, M. Cutkosky, and P. Dario, “The SPRING hand: Development of a self-adaptive prosthesis for restoring natural grasping,” *Autonomous Robots*, vol. 16, pp. 125–141, 2004.

[71] Maxon Motor. Ec-max 22 dc motor. http://www.maxonmotor.com/2988.html.

[72] Otto Bock. Otto bock energypack 757b20. [Online]. Available: http://www.ottobock.com

[73] D. H. Plettenburg, “A sizzling hand prosthesis. on the design and development of a pneumatically powered hand prosthesis for children,” Ph.D. dissertation, Delft University of Technology, The Netherlands, 2002.

[74] LabVIEW, *2011*. National Instruments: Austin, Texas, 2011.

[75] National Instruments. ELVIS II Instrumentation, Design, and Prototyping Platform. [Online]. Available: http://sine.ni.com/nips/cds/view/p/lang/en/nid/13137

[76] *Design response of weighting networks for acoustical measurements*, ANSI S1.42-2001 Std.

[77] N. Crone, “A comparison of myo-electric and standard prostheses: A case study of a preschool aged congenital amputee,” *Canadian Journal of Occupational Therapy*, vol. 53, pp. 217–222, 1986.

[78] D. Aukes, S. Kim, P. Garcia, A. Edsinger, and M. Cutkosky, “Selectively compliant underactuated hand for mobile manipulation,” in *Proceedings of the 2012 IEEE International Conference on Robotics and Automation (ICRA)*, May 2012, pp. 2824–2829.

[79] N. Wettels, *Biomimetic Tactile Sensor for Object Identification and Grip Control: A Multi-modal Sensor Mimicking the Human Digit*. LAP Lambert Acad. Publ., 2011.

[80] D. Boere, L. Kallenberg, H. Witteveen, H. Hermens, and J. Rietman, “A multichannel semg method for myoelectric control of a forearm prosthesis,” in *International Society of Electrophysiology and Kinesiology (ISEK)*. Aalborg, Denmark: University of Twente, June 2010.

[81] N. Hogan, “Impedance control: an approach to manipulation,” *Journal of Dynamic Systems Measurement and Control*, vol. 107, pp. 1–24, 1985.

[82] R. Weir, M. Mitchell, S. Clark, G. Puchhammer, M. Haslinger, R. Grausenburger, N. Kumar, R. Hofbauer, P. Kushnigg, M. E. V. Cornelius and, H. Eaton, and D. Wenstrand, “The intrinsic hand - a 22 degree-of-freedom artificial hand-wrist replacement,” in *Proceedings of the MyoElectric Controls/Powered Prosthetics Symposium*, Fredericton, Canada, August 2008.

[83] C. Cipriani, M. Controzzi, and M. C. Carrozza, “The smarthand transradial prosthesis,” *Journal of neuroengineering and rehabilitation*, vol. 8:29, pp. 1–14, 2011.

[84] M. C. Carrozza, G. Cappiello, G. Stellin, F. Zaccone, F. Vecchi, S. Micera, and P. Dario, “A cosmetic prosthetic hand with tendon driven underactuated mechanism and compliant joints: Ongoing research and preliminary results,” in *Proceedings of the 2005 IEEE International Conference on Robotics and Automation (ICRA)*, 2005.

[85] H. Huang, L. Jiang, D. Zhao, J. Zhao, H. Cai, H. Liu, P. Meusel, B. Willberg, and G. Hirzinger, “The development on a new biomechatronic prosthetic hand based on under-actuated mechanism,” in *Proceedings of the 2006 IEEE/RSJ International Conference on Intelligent Robots and Systems*, Beijing, China, October 2006.

[86] M. Wassink, R. Carloni, and S. Stramigioli, “Port-hamiltonian analysis of a novel robotic finger concept for minimal actuation variable impedance grasping,” in *Proceedings of the IEEE International Conference on Robotics and Automation (ICRA)*, Anchorage, Alaska, USA, 2010, pp. 771–776.

[87] S. yoon Jung and I. Moon, “Grip force modeling of a tendon-driven prosthetic hand,” in *International Conference on Control, Automation and Systems (ICCAS)*, Oct 2008, pp. 2006–2009.

[88] E. N. Haulin, A. A. Lakis, and R. Vinet, “Optimal syntesis of a planar four-link mechanism used in hand prosthesis,” *Mechanism and Machine Theory*, vol. 36, no. 11-12, pp. 1203–1214, 2001.

[89] Y. Tenzer, L. P. Jentoft, and R. D. Howe, “Inexpensive and easily customized tactile array sensors using mems barometers chips,” *IEEE (conditionally accepted)*, 2012.

[90] H.-T. Lin, L.-C. Kuo, H.-Y. Liu, W.-L. Wu, and F.-C. Su, “"the three-dimensional analysis of three thumb joints coordination in activities of daily living",” *Clinical Biomechanics*, pp. 371–376, 2011.

[91] N. A. Andrade, G. A. Borges, F. A. de O. Nascimento, A. R. S. Romariz, and A. F. da Rocha, “A new biomechanical hand prosthesis controlled by surface electromyographic signals,” in *Proceedings of the 29th Annual International Conference of the IEEE EMBS*, Lyon, France, August 2007.

[92] C. Pylatiuk, S. Mounier, A. Kargov, S. Schulz, and G. Bretthauer, “Progress in the development of a multifunctional hand prosthesis,” in *Proceedings of the Annual International Conference of the IEEE Engineering in Medicine and Biology Society (EMBS)*, San Francisco, USA, 2004, pp. 4260–4263.

[93] K. T. OToole and M. M. McGrath, “Mechanical design and theoretical analysis of a four fingered prosthetic hand incorporating embedded SMA bundle actuators,” 2007.

[94] B. Buchholz, T. J. Armstrong, and S. A. Goldstein, “Anthropometric data for describing the kinematics of the human hand,” *Ergonomics*, vol. 35, no. 3, pp. 261–273, 1991.

[95] J. L. Sancho-Bru, A. Perez-Gonzalez, M. Vergara, and D. J. Giurintano, “A 3D biomechanical model of the hand for power grip,” *Journal of Biomechanical Engineering*, vol. 125, no. 1, pp. 78–83, 2003.

[96] J. Kuch and T. Huang, “Human computer interaction via the human hand: a hand model,” in *Proceedings of the Twenty-Eighth Asilomar Conference on Signals, Systems and Computers*, Pacific Grove, USA, October-November 1994, pp. 1252–1256.

[97] G. ElKoura and K. Singh, “Handrix: animating the human hand,” in *Proceedings of the ACM SIGGRAPH/Eurographics symposium on Computer Animation (SCA)*. Aire-la-Ville, Switzerland: Eurographics Association, 2003, pp. 110–119.

[98] D. Dragulescu and L. Ungureanu, “The modeling process of a human hand prosthesis,” in *Proceedings of the 4th International Symposium on Applied Computational Intelligence and Informatics (SACI)*, Timisoara, Romania, 2007, pp. 263–268.

[99] V. Duindam and S. Stramigioli, “Modeling the kinematics and dynamics of compliant contact,” in *Proceedings of the IEEE International Conference on Robotics and Automation (ICRA)*, Taipei, Taiwan, September 2003, pp. 4029–4034.

[100] M. Zecca, S. Micera, M. C. Carrozza, and P. Dario, “Control of multifunctional prosthetic hands by processing the electromyographic signal,” in *Critical Reviews in Biomedical Engineering*, 2002, pp. 459–485.

[101] M. R. Cutkosky, “On grasp choice, grasp models, and the design of hands for manufacturing tasks,” *Robotics and Automation, IEEE Transactions on*, vol. 5, no. 3, pp. 269–279, 1989.

[102] P. Kyberd and P. H. Chappell, “The southampton hand: An intelligent myoelectric prosthesis,” *Journal of Rehabilitation Research and Development*, vol. 31, no. 4, pp. 326–334, 1994.

[103] C. Cipriani, M. Controzzi, and M. C. Carrozza, “Progress towards the development of the smarthand transradial prosthesis,” in *Rehabilitation Robotics, 2009. ICORR 2009. IEEE International Conference on*, 2009, pp. 682–687.

[104] P. C. Breedveld, *Modeling and simulation of dynamic systems using bond graphs*, H. Unbehauen, Ed. Oxford, UK: Eolss Publishers, 2008.

[105] E. Dionysian, J. Kabo, and R. Meals, “Determination of joint stiffness of the human proximal interphalangeal joints: Development and clinical evaluation of a new device,” in *Proceedings of the Annual International Conference of the IEEE Engineering in Medicine and Biology Society (EMBC)*, vol. 4, October-November 1992, pp. 1546–1547.

[106] E. Dionysian, J. M. Kabo, F. J. Dorey, and R. A. Meals, “Proximal interphalangeal joint stiffness: Measurement and analysis,” *The Journal of Hand Surgery*, vol. 30, no. 3, pp. 573–579, 2005.

[107] D. J. Giurintano, A. M. Hollister, W. L. Buford, D. E. Thompson, and L. M. Myers, “A virtual five-link model of the thumb,” *Medical Engineering and Physics*, vol. 17, no. 4, pp. 297–303, 1995.

[108] J. N. Goubier, L. Devun, D. Mitton, F. Lavaste, and E. Papadogeorgou, “Normal range-of-motion of trapeziometacarpal joint,” *Chirurgie de la Main*, vol. 28, no. 5, pp. 297–300, 2009.

[109] V. Duindam, “Port-based modeling and control for efficient bipedal walking robots,” Ph.D. dissertation, University of Twente, Enschede, 2006.

[110] S. Stramigioli, *Modeling and IPC Control of Interactive Mechanical Systems: A Coordinate-Free Approach*. Springer-Verlag New York, Inc., 2001.

[111] “DEXMART Project website,” http://www.dexmart.eu/.

[112] L. Biagiotti, F. Lotti, C. Melchiorri, G. Palli, P. Tiezzi, and G. Vassura, “Development of UB Hand 3: Early results,” in *Proceedings of the IEEE International Conference on Robotics and Automation (ICRA)*, Barcelona, Spain, April 2005, pp. 4488–4493.

[113] A. Bicchi and D. Prattichizzo, “Analysis and optimization of tendineous actuation for biomorphically designed robotic systems,” *Robotica*, vol. 18, pp. 23–31, 2000.

[114] L. Barbieri and M. Bergamasco, “Nets of tendons and actuators: an anthropomorphic model for the actuation system of dexterous robot hands,” in *Proceedings of the International Conference on Advanced Robotics (ICAR)*, Pisa, Italy, June 1991, pp. 357–362.

[115] M. Kaneko, M. Wada, H. Maekawa, and K. Tanie, “A new consideration on tendon-tension control system of robot hands,” in *Proceedings of the IEEE International Conference on Robotics and Automation (ICRA)*, Sacramento, USA, April 1991, pp. 1028–1033.

[116] G. Palli, G. Borghesan, and C. Melchiorri, “Tendon-based transmission systems for robotic devices: Models and control algorithms,” in *Proceedings of the IEEE International Conference on Robotics and Automation (ICRA)*, Kobe, Japan, May 2009, pp. 4063–4068.

[117] MATLAB, *version 7.10.0 (R2010a)*. The MathWorks Inc.: Natick, Massachusetts, 2010.

[118] L. Biagiotti, H. Liu, G. Hirzinger, and C. Melchiorri, "Cartesian impedance control for dexterous manipulation," in *Proceedings of the IEEE/RSJ International Conference on Intelligent Robots and Systems (IROS)*, vol. 4, 27-31 2003, pp. 3270 – 3275.

[119] C. Secchi, S. Stramigioli, and C. Melchiorri, "Geometric grasping and telemanipulation," in *Proceedings of the IEEE/RSJ International Conference on Intelligent Robots and Systems*, Maui, USA, 2001, pp. 1763–1768.

[120] E. Engeberg, S. Meek, and M. Minor, "Hybrid force-velocity sliding mode control of a prosthetic hand," *Biomedical Engineering, IEEE Transactions on*, vol. 55, no. 5, pp. 1572–1581, 2008.

[121] T. Wimböck, C. Ott, and G. Hirzinger, "Analysis and experimental evaluation of the intrinsically passive controller (ipc) for multifingered hands," in *Proceedings of the IEEE International Conference on Robotics and Automation*, 2008, pp. 278–284.

[122] E. Niedermeyer and F. Lopes da Silva, *Electroencephalography: Basic Principles, Clinical Applications, and Related Fields*. Baltimore: Lippincott Williams & Wilkins, 2004.

[123] D. W. Boere, H. J. B. Witteveen, H. J. Hermens, and J. S. Rietman, "Searching for optimal electrode number and configuration in multichannel myoelectric prosthesis control," in *ISPO World Congress*, Hyderabad, India, 2013.

[124] H. Daley, K. Englehart, L. Hargrove, and U. Kuruganti, "High density electromyography data of normally limbed and transradial amputee subjects for multifunction prosthetic control," *Journal of Electromyography and Kinesiology*, vol. 22, no. 3, pp. 478–484, 2012.

[125] T. R. Farrell and R. F. Weir, "A comparison of the effects of electrode implantation and targeting on pattern classification accuracy for prosthesis control," *IEEE Transactions on Biomedical Engineering*, vol. 55 (9), pp. 2198–2211, 2008.

[126] L. J. Hargrove, K. Englehart, and B. Hudgins, "A comparison of surface and intramuscular myoelectric signal classification," *IEEE Transactions on Biomedical Engineering*, vol. 54, pp. 847–853, 2007.

[127] K. Englehart and B. Hudgins, "A robust, real-time control scheme for multifunction myoelectric control," *IEEE transactions on bio-medical engineering*, vol. 50, no. 7, p. 848, 2003.

[128] T. R. Farrell and R. F. Weir, "The optimal controller delay for myoelectric prostheses," *IEEE Transactions on Neural Systems and Rehabilitation Engineering*, vol. 15, no. 1, pp. 111–118, 2007.

[129] L. Smith, L. Hargrove, B. Lock, and T. Kuiken, "Determining the optimal window length for pattern recognition-based myoelectric control: Balancing the competing effects of classification error and controller delay," *IEEE Transactions on Neural Systems and Rehabilitation Engineering*, vol. 19, no. 2, pp. 186–192, 2011.

[130] H. Witteveen, F. Luft, J. Rietman, and P. Veltink, "Stiffness feedback for myoelectric forearm prostheses using vibrotactile stimulation," *IEEE transactions on neural systems and rehabilitation engineering*, vol. Online prepublication, pp. 1–9, 2013.

[131] M. Wassink, R. Carloni, D. Brouwer, and S. Stramigioli, "Novel dexterous robotic finger concept with controlled stiffness," in *28th Benelux Meeting on Systems and Control : book of abstracts*. Delft: DISC, March 2009, p. 115.

Acknowledgements

During the four years of work that led to this thesis, I have been fortunate enough to be supported by dozens of people in one way or another, and taking the time to sincerely thank each of them is the least I can do. So, here we go!

I should start with the people that made it possible for me to write this in the first place. Stefano, ever since you helped me get that internship in the USA years ago, you've been a great inspiration, motivation and support. Thank you for giving me the opportunity to get started on this journey, and finding the time to help me out when I needed it most. Sarthak, I feel like I've made great improvements to the way I work since I started here fresh off my MSc, and I have you to thank for most of it. Thanks for helping me stay focused and motivated enough to get this project done one step at a time, which has given me the confidence to take on anything I set my mind to.

The Myopro project has been a wonderful opportunity to cooperate with people from very different backgrounds to my own. Thanks to all my Myopro project partners for the work we did together, and especially my fellow Myopro PhDs Daphne and Heidi. I think we made a great team together, and our meetings, experiments, and lunches together were always a lot of fun :)

During my PhD I've also had the pleasure of collaborating with many researchers, both from other universities and my own, who have provided me with valuable insights, advice and assistance. Thank you Dannis, Edsko, Dick, Gerwin, Gianluca, Gianni and Claudio, for all the great research we did together!

A lot has changed in our group during my stay there, such as going from Hogekamp to Carré and from CE to RAM, but I'm glad to see the most important things have remained the same. The team spirit and willingness to cooperate and share makes this a great group to be a part of, and I will always fondly remember our brainstorm sessions and other group activities. To Alfred, Gerben, en Marcel, thank you very much for always being there to teach me about all of the cool stuff I got to play with; and Jolanda en Carla, thanks so much for helping me get things done at the university and helping me get in touch with the right people. I'm sure I would be lost without your help!

I'd also especially like to thank my office-mates, who always managed to brighten up the workday :) I'm very happy we could have such a nice time together, not just during our discussions at work, but also at board game nights, parties, and even trips abroad! Abeje, Bayan, Douwe, Oguzcan, Yunyun, Yury, and of course your lovely +1s, thank you! I hope we can continue to meet up often :)

During my research I've also been assisted by BSc, MSc, Saxion and PhD students, who've helped me with all aspects of my project. Arnoud, Gert Jan, Giovanni, Marcello, Peter, and Ugo, thank you for your contributions!

Thanks to all the housemates who have kept me company at Matenweg 32 over the years. I consider myself very lucky to have ended up in such a nice and varied group of people, who were always super gezellig to hang out with :)

Of course also thanks to all of my friends, for making sure I could recharge my batteries in between doing Science! Hjalmar, Enne, Niels, Dirk, Jet, Kasper, Gerwin, Jasper, Ruud, Sven, and everyone else: from regular hanging out to entire Sleep Deprivation Weekends, thanks for the great times we had, and will have!

Special thanks to my family, for always having the utmost confidence in me and supporting me in everything I do. Mam & Pap, Kees & Merel, and Rick & Femke, thank you very much! Kees and Rick of course get double thanks for being there with me on the big day!

Finally I want to thank my dear Chen; of all the great things that have happened to me in the last four years, meeting you was easily the best! Thank you so much for always being there with me, even when working late hours, weekends, or worse :) The last few months have been pretty tough on both of us, but knowing you'd be joining me afterward has always been enough to keep me going. Let's have a wonderful time together!

About the author

Bart Peerdeman was born in Venhuizen, the Netherlands, on September 21st, 1984. He finished his BSc study in Electrical Engineering at the University of Twente in 2002. This was followed by a MSc study in Mechatronics, during which he traveled to the USA for a 9-month internship at JADI Inc., a Michigan-based robotics company.

After obtaining his MSc degree for his work on the TUlip soccer robot's world modeling system, he took a PhD position on the Myopro project. His assignment in this project is to develop a control system and mechanical prototype for a new type of prosthetic hand.

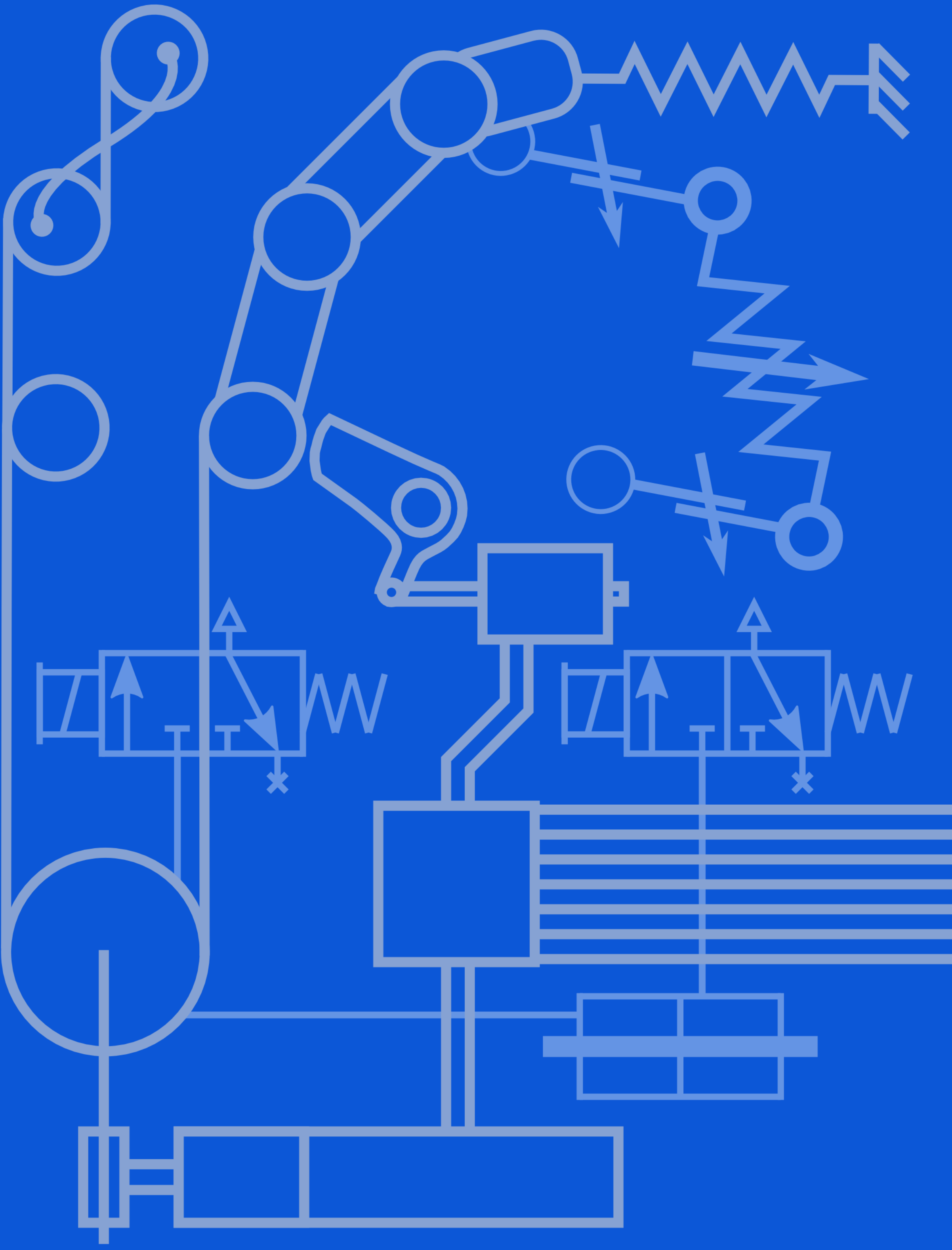

ISBN: 978-90-9028264-0